DEVELOPMENT OF COMPUTER CODE FOR STABILITY ANALYSIS OF MOLTEN SALT NATURAL CIRCULATION LOOP WITH AND WITHOUT INTERNAL HEAT GENERATION

By

NADELLA SAIKRISHNA
Enrolment No.: ENGG01201501082

Bhabha Atomic Research Centre, Mumbai

A thesis submitted to the

Board of Studies in Engineering Sciences

In partial fulfilment of requirements

for the Degree of

MASTER OF TECHNOLOGY

of

HOMI BHABHA NATIONAL INSTITUTE

December, 2017

Homi Bhabha National Institute

Recommendations of the Thesis Examining Committee

As members of the Thesis examining Committee, we recommend that the thesis prepared by **Shri Nadella Saikrishna** entitled "**Development of computer codes for stability analysis of molten salt natural circulation loop with and without internal heat generation**" be accepted as fulfilling the thesis requirement for the Degree of Master of Technology.

	Name	Signature
Member – 1	Shri K. Madhusoodanan	
Member – 2	Shri P. V. Durgaprasad	
Member – 3	Shri P. Majumdar	
Member – 4	Dr R. R. Rakesh	
Member – 5	Dr K. Bhargava	
Technical Adviser	Shri A. K. Srivastava	
Examiner		
Guide & Convener	Dr N. K. Maheshwari	
Chairman	Dr G. Ramireddy	

Final approval and acceptance of this thesis is contingent upon the candidate's submission of the final copies of the thesis to HBNI.

I hereby certify that I have read this thesis prepared under my direction and recommend that it may be accepted as fulfilling the thesis requirement.

Date:

Place:

Signature of the Guide

Name of the Guide: Dr N K Maheshwari

DECLARATION

I, hereby declare that the investigation presented in the thesis has been carried out by me. The work is original and has not been submitted earlier as a whole or in part for a degree/diploma at this or any other Institution / University.

(Nadella Saikrishna)

DEDICATION

I would like to dedicate this thesis work to those who toil day and night in the quest of understanding Mother Nature, savouring the immense pleasure it gives, thereby directly or indirectly help uplifting the lives of Mankind

and

To my dear parents and teachers who gave me a chance to be one

ACKNOWLEDGEMENT

On this platform, with an escalation of taking a step forward in understanding Mother Nature, I would like to express my appreciation to the divine energy which is present in every soul on the Earth.

I would like to pay my sincere gratitude to Dr Naresh Kumar Maheshwari, Head, PS&SS, for guiding me throughout the tenure with valuable and encouraging suggestions and giving sufficient time for this work amid the challenging commitments of the section; to Shri Abhishek Kumar Srivastava for helping me in conducting the experiments and giving valuable suggestions; to Shri S. S. Jana, RED for helping me with the instrumentation and control part of MSNCL; to Dr P. K. Vijayan, RR fellow, BARC, for the knowledge and experience he shared with me regarding natural circulation loops. Prolonged discussion with them, despite their busy schedules, helped me in invaluable way.

I would like to thank Shri A. Rama Rao, former Associate Director, RDDG, Shri Avaneesh Sharma, Head, AHWRD and Dr D. N. Badodkar, Director, RDDG for giving an opportunity to pursue this academic work.

I would like to thank the Chairman and members of M.Tech monitoring committee for reviewing my work and giving suggestions.

I am very much grateful to my parents Shri Nadella Venkata Rao, Smt. Padmavathi, my sister Kum. Anusha and my colleagues and friends for sharing smiles on my achievements and giving emotional strength during difficult times. They gave me the most essential tools, confidence and assurance, for my accomplishment today. I would like to thank Kum. Shalini, SO/C, RED for suggesting a nice name for the computer code package, SiPhN (**Si**ngle **Ph**ase **N**atural circulation, pronounced as siphon).

Thank you all once again.

(Nadella Saikrishna)

CONTENTS

SYNOPSIS

Stability analysis of molten salt based natural circulation loops has been pursued in the current project work for two cases of heat addition to working fluid *viz.* localized surface heating (SHF/LH) and distributed internal heat generation (IHG/DH).

As for the former case of heat addition through localized surface heat flux, two phases of experiments have been performed on MSNCL facility, Hall 7 at different power levels and cooling rates for Horizontal Heater Horizontal Cooler (HHHC), Vertical Heater and Horizontal Cooler (VHHC), Horizontal Heater and Vertical Cooler (HHVC) and Vertical Heater and Vertical Cooler (VHVC) orientations. All the operating conditions for which experiments were performed have been found to be stable.

Existing formulation for linear stability analysis has been applied to all four orientations of MSNCL geometry with suitable modification for the tilt on top and bottom legs. It has been found that the predictions are so conservative that even stable operating conditions are predicted as unstable. Consideration of the local pressure losses in the calculations, improved the accuracy of predictions in all orientations except in HHHC.

An improved model has been derived in dimensionless form incorporating some phenomena like wall thermal inertia, heat exchange effect and heat losses. A new parameter space Gr_m – $St_{mo,c}$ has been adopted for better representation and intuitive usage of stability maps. A new computer code for linear stability analysis has been developed with the capabilities of studying individual effect of these phenomena. This code has been successfully applied to two water based NCLs in HHHC orientation. This model has been found to predict the loop stability behaviour correctly. Effects of wall thermal inertia and local pressure losses are clearly evident from the predictions. The model has been applied to MSNCL in HHHC

orientation and prediction of stability behaviour has been found to be more accurate as per the experimental data available.

Coming to the latter case of heat addition through distributed internal heat generation, which is relevant to main heat transport in Molten Salt Reactors (MSR), theoretical investigations have been pursued on stability behaviour. A formulation for linear stability analysis in dimensionless form has been derived considering the internal heat generation (IHG) outside the main heater which is representative of decay heat in MSR main heat transport loop. This formulation has been implemented in a computer code and validated against the theoretical predictions available in literature. Studies on effect of IHG outside the main heater on stability behaviour have been performed with and without considering wall thermal inertia. MSNCL has been considered for this analysis and all the stability maps have been represented in Gr_m – $St_{mo,c}$ space. A range of 0 to 10% IHG (% in terms of IHG in heater) has been considered outside the heater portion for current study. When wall thermal inertia is not considered, stability of MSNCL is found to be lower at higher IHG outside heater portion. However, when actual loop was studied including wall, it has been found to be stable for the total study range.

To help in understanding the phenomenon of stabilization due to wall in case of MSNCL and an SS/water loop studied and to validate the linear stability analysis predictions in detail, a transient computer code has been developed with capability of simulating both cases of heat addition as mentioned earlier. This analysis, since the full governing equations are solved, is called non-linear analysis for stability. Welander's warm pocket theory for instability in single phase natural circulation loops has been verified. By simulating MSNCL with different wall thickness values in SHF/LH case, it has been found that by heat exchange with thermal anomalies in the fluid, wall plays an important role in stabilizing the NCLs. Later, numerous simulations have been performed at various operating conditions to generate stability data for

validation of stability maps predicted by linear stability analysis codes for both cases of heat addition. It has been found that despite the assumption involved, linear stability analysis is able to predict the stability behaviour sufficiently accurate.

All three computer codes have been carefully integrated into a single package called SiPhN (**Si**ngle **Ph**ase **N**atural circulation) with a user-friendly input-output format.

LIST OF FIGURES

LIST OF TABLES

LIST OF SYMBOLS

A, A_1, A_2	Cross section area of working fluid, inner shell and outer shell of wall respectively (m^2)
B	Heat exchange parameter (no units) (Eq. 2.9)
b	Friction parameter (Eq. 4.16)
C_i	Concentration of nuclide *i*
C_p, C_{pw}	Specific heat capacity of working fluid and wall (J/kg.K)
D_i	Molecular diffusivity of nuclide *i*
D, D_1, D_2	Inner diameter, inner shell outer diameter, outer shell outer diameter of NCL piping (m)
E	Energy (J)
f	Darcy friction factor (no units)
g	Gravitational acceleration = 9.81 m^2/s
Gr_m	Modified Grashof number (Eq. 3.7)
H	Height of NCL (m)
h	Convective heat transfer coefficient ($W/m^2.K$)
i	$=\sqrt{-1}$
$I_{ss}, \bar{I}$	Temperature integrals in steady state and perturbed state
j	Node
K	Local pressure loss coefficient
K_i	Local pressure loss per unit length
k, k_w	Thermal conductivity of fluid and wall (W/m.K)
L	Length scale (see subscripts)
Nu	Nusselt number (no units)
n	Complex frequency
Pr	Prandtl number (no units)
p	Pressure (Pa), friction parameter in Eq. 4.16 (no units)
Q, Q_b	Heat input (W), boundary heat transfer (W/m)
q or q'', q'''	Surface heat flux (W/m^2), internal heat generation (W/m^3)
Re	Reynolds number (no units)
R_w	Thermal resistance of wall per unit length in radial direction (K.m/W)
$St_{mi,j}$	Modified Stanton number based on internal heat transfer coefficient in section j (no units)
$St_{m,j}$	Modified Stanton number based on overall heat transfer coefficient in section *j* (no units)
St_m	Same as $St_{m,c}$
$St_{mo,j}$	Modified Stanton number based on external heat transfer coefficient in section j (no units)
S, s	Spatial coordinate along the length of NCL
T	Temperature (°C)
t	Time (s)
t_w	Thickness of NCL wall (m)
U	Overall heat transfer coefficient (W/m^2K)
u	Velocity of working fluid (m/s)
w	Mass flow rate (kg/s)
Z, z	Coordinate in vertical direction

Greek symbols

α	Angle of inclination of bottom leg of NCL from horizontal, thermal diffusivity of working fluid (m^2/s)
α_w	Thermal diffusivity of NCL wall (m^2/s)
β	Angle of inclination of top leg of NCL from horizontal
β_f	Volumetric expansion coefficient of working fluid (1/K)
γ	Angle of inclination of arbitrary section of NCL
θ	Dimensionless temperature
λ	Decay constant (1/s)
μ	Dynamics viscosity (Pa.s)
ξ	Parameter representing wall radial thermal resistance
ρ	Density (kg/m^3)
τ	Dimensionless time
χ_j	Same as $St_{m,j}$
ω	Dimensionless mass flow rate

Subscripts

i	Internal
j	Section of NCL (h,hl,cl,c) (or)Node
h,hl,c,cl	Heater, hot leg, cooler, cold leg for length scales, end points of these sections for temperature T or θ.
f	Working fluid
w, wi, wo	Wall, wall inner shell, wall outer shell
o	External/outer
s	Secondary side
ss	Steady state
t	Total
1, 2, 3, 4	Used with length scale 'L'. defined in figs. 4.1 & 4.2 for each orientation

Superscripts and others

n	Time step
$\bar{}$ (over bar)	Dimensionless (e.g. $\bar{\rho}, \bar{C}_p, \bar{k}$ and $\bar{R}_w$)
$\hat{}$ (capped)	Shape function of perturbed variable

Abbreviations

HHHC	Horizontal Heater Horizontal Cooler
VHHC	Vertical Heater Horizontal Cooler
VHVC	Vertical Heater Vertical Cooler
HHVC	Horizontal Heater Vertical Cooler
LWR	Light Water Reactor
PHWR	Pressurized Heavy Water Reactor
AHWR	Advanced Heavy Water Reactor
CW	Clockwise
CCW	Counter clockwise
MSR	Molten Salt Reactor
IMSBR	Indian Molten Salt Breeder Reactc
MS	Molten Salt (contextually defined)
SS	Stainless Steel
IHG	Internal heat generation
SHF	Surface heat flux
DH	Distributed heating
LH	Localized heating
INPP	Indian nuclear power program
MSNCL	Molten salt natural circulation loo
NC	Natural circulation
NCL	Natural circulation loop
SM	Stability map
LSA	Linear stability analysis
NLSA	Nonlinear stability analysis
PHT	Primary Heat transport

CHAPTER 1

Introduction

1.1. Thorium and its utilization in Indian nuclear power scenario

Thorium reserves are abundant in India [1] compared to uranium. As a fuel material it has very attractive properties like

1. Higher melting point, better thermal conductivity, better capability in retention of fission gases and good dimensional stability which leads to higher possible burn-up.

2. Long lived minor actinides are generated at low level in thorium based fuel which leads to reduction in radioactivity of waste generated from nuclear reactors

3. Thorium offers greater competition to parasitic absorption in structural materials than ^{238}U due to its higher (2.47 times) capture cross section and conversion rate from fertile to fissile will be higher.

4. Having highest η value in thermal and epithermal energy range, ^{233}U results in higher conversion rates with Thorium in Th-^{233}U based reactor systems.

5. ^{233}U offers better proliferation resistance. Since, it is always accompanied with ^{232}U which is having hard gamma emitters as daughter products (^{212}Bi and ^{208}Tl).

In view of above mentioned characteristics of thorium and due to its abundance in India compared to uranium, the nuclear power program of India (INPP) aimed at best utilization of thorium for sustainable nuclear power generation in future. But, as thorium does not have any fissile isotope to start with, it has to be converted to ^{233}U by neutron irradiation before being used as fuel material. To achieve this in sequential manner with all available resources, Indian nuclear program has been designed to be in three stages. In the first stage, PHWRs are

employed to generate Plutonium using ^{238}U for further use in second stage where fast breeder technology will be utilized for transmutation of ^{232}Th to ^{233}U.

The research and development work for mining and extraction of thorium, fabrication, evaluation of various thermo-physical and irradiation properties, reprocessing and recycling of thorium based fuels has been started from initial stages of inception of three stage nuclear power program. Various advanced reactor concepts are under consideration for utilization of thorium based fuels in an efficient and safer way like Advanced Heavy Water Reactor (AHWR), Molten Salt Reactor (MSR) and some high temperature reactors. AHWR is in the advanced design stage [1] which generates around 60% of its power from thorium without external input of ^{233}U. It forms a bridge between the second and third stages of INPP from the fuel material utilization point of view. Indian Molten Salt Breeder Reactor (IMSBR) is envisaged to be deployed in third stage of INPP since it is completely self-sustainable in fissile material needs and requires only thorium feed.

1.2. Indian Molten Salt Breeder Reactor (IMSBR)

An IMSBR of 850 MWe is being designed and developed in BARC [2]. The conceptual design of IMSBR has been demonstrated by Vijayan *et al.* [3]. The following areas are being studied as part of research and development

1. Molten salt characterization studies

2. Production and purification of different molten salts in large scale

3. Thermal hydraulic studies in both forced and natural circulation with various fuel salts, blanket salts and coolant salts

4. Material development and testing for use with molten salts

5. Batch mode reprocessing methods

6. Instruments for high temperature and high irradiation environment of molten salts

7. Molten salt chemistry control techniques

8. Neutron transport coupled CFD codes for complete simulation of core thermal hydraulics along with online reprocessing

Various experimental facilities have been established for these R&D activities. Among them are the natural circulation based thermal hydraulic test facilities for fuel salt and coolant salts. Molten Active Fluoride salt Loop (MAFL) [4] is a rectangular natural circulation loop with ThF_4+LiF (77.5:22.5 wt%) as working fluid whereas Molten Salt Natural Circulation Loop (MSNCL) [5] is also a natural circulation loop with $NaNO_3$+KNO_3 (60:40 wt%) as working fluid. Both of these facilities were designed and being operated to generate data on natural circulation behaviour of molten fuel and coolant salts. They are intended to be useful in validation of thermal hydraulic system codes and theoretical stability analysis. Following section elaborates the concept of natural circulation and various aspects relevant to it.

1.3. Natural circulation

Natural circulation is a phenomenon which occurs due to differential thermal expansion of working fluid under a body force field. The loops comprising a heating section and a cooling section to facilitate the natural circulation phenomenon are called natural circulation loop (NCL). For a constant and sustained flow, heater section is placed at a lower elevation than cooler section.

A mass of fluid which is heated in the heating section (hereafter called as heater) gets expanded and its density reduces. Due to buoyancy, this hot mass of fluid tries to rise into the riser portion of the loop. Based on the compressibility of the working fluid, this upward-

moving tendency of hot mass causes movement in the whole fluid in the loop. This hot mass travels upward to the cooling section (hereafter called as cooler) and loses its heat to the secondary fluid or atmosphere. Then this mass becomes heavier and tries to come down towards the heater thus completing the cycle. In this manner flow starts and continues in an NCL.

Natural circulation phenomenon is being used successfully in steam generators of thermal power plants. Natural circulation is more attractive from the context of increased safety concerns in nuclear industry. Natural circulation can be used for core cooling as well as auxiliary heat transport in nuclear power reactors. The reliability of natural circulation is conceived from the fact that it does not require a pump. The flow is established based on the balance between buoyancy and frictional forces in the loop. However, this balance can be unstable at some operating conditions, which leads to oscillatory behaviour of flow and temperature distribution in the loop [1]. This may lead to critical heat flux and mechanical vibrations. Hence, it is of prime importance in the design of nuclear thermal hydraulics to ensure the stable operation of natural circulation and its reliability. Various theoretical methodologies are used to study stability behaviour of NCLs for which general procedures are given briefly in next section. It should be noted here that the working fluid in NCLs relevant to MSRs is intended to operate in liquid phase. So, all the methodologies concerned to thermal hydraulic analysis focus on single phase NCLs even it is not explicitly mentioned.

1.4. Stability analysis of NCLs

1.4.1. Stability – definition

A system is defined as unstable if any external perturbation in operating conditions (input conditions) of the system leads to oscillations of constant or increasing amplitude in the system output conditions.

Generally stability is discussed in feedback systems. Natural circulation loops have feedback inherently. For example, a sudden increase in the flow will cause reduction in the heater outlet temperature and hence the driving force for flow reduces. This will cause the flow to be decelerated.

1.4.2. Methodologies for stability analysis of NCLs

Stability analysis is performed in either time domain or frequency domain. Yet another method has been explored which used Lorentz's chaos theory. The former two methods are described below and for Lorentz' chaos theory based model refer [6].

Frequency domain analysis with linearized governing equations

Frequency domain analysis with linearized governing equations is generally called as linear stability analysis (LSA) in prevailing research literature. The same nomenclature is adopted in current report.

The LSA of NCLs comprises two major steps, the first step being the derivation of a characteristic equation of given NCL in frequency domain. The second step involves application of some mathematical procedure to solve the characteristic equation, for roots, to assess the stability behaviour of NCL at given operating conditions. The assessment criteria are described in detail in section 4.3.

The general methodology used to derive characteristic equation of NCLs can be summarized as follows –

1. Derive governing equations (generally PDE with 1D approximation) for NCL
    a. Continuity equation
    b. Integral momentum equation
    c. Energy conservation equation for heater, cooler and remaining piping

2. Non-dimensionalize the governing equations using suitable scales
3. Derive steady state Reynolds number by solving steady state momentum and energy equations
    a. Solve steady state energy equation for heater, cooler and remaining piping separately using temperature continuity as boundary condition and obtain temperature distribution throughout the loop
    b. Determine the closed loop temperature integral in the integral momentum equation based on orientation of heater and cooler
    c. Determine the steady state Reynolds number from momentum equation
4. Substitute perturbed temperature and mass flow rate expressions into transient form of the governing equations to obtain perturbed momentum and energy equations.
5. Determine the perturbed temperature distribution by solving perturbed energy equation in heater, cooler and remaining piping from the perturbed energy equations
6. Determine the closed loop integral of perturbed temperature in the perturbed momentum equation based on orientation of heater and cooler.
7. Substitute the integral determined in step 6, into perturbed momentum equation to obtain the characteristic equation for stability.

It is general practice to depict the results of LSA of NCLs in the form of stability maps on a chosen parameter space. So far the most used parameter space is Gr_m-St_m space the details of which can be obtained in oncoming chapters.

Time domain analysis for stability

This method involves solving a set of differential equations which governs the system behaviour using numerical solution techniques like Finite Difference or Finite volume or Finite Element methods. Initial condition for this analysis is chosen to be a perturbed value of

one or more variables from the steady state corresponding to given operating conditions. The evolution of various parameters of the system (like mass flow rate, temperature) with respect to time is determined. Based on their amplitude variation with time, stability is decided. Since total governing equations are solved, this method is also called as non-linear stability analysis (NLSA) method.

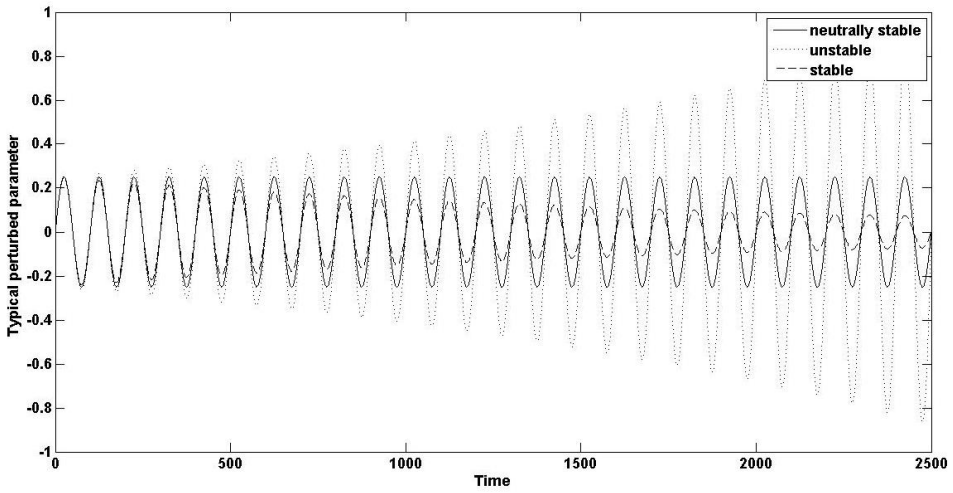

Fig 1.1 Typical transient responses of an NCL at stable, unstable and neutrally stable operating conditions

Table 1.1 Comparison of linear and non-linear stability analysis

Linear analysis	**Non-linear analysis**
Stability map is generated directly	Indirectly by trial and error or based on result of linear analysis
Tells directly whether the given condition is stable/unstable/neutrally stable	Gives transient evolution of various parameters → instability mechanism can be identified from the transient behaviour
Less computational cost for generating stability map	More computational cost
Numerical non-linear equation solvers are used	Numerical discretization schema and linear equation solvers are used
Approximate to the level of linearization and conceptual formulation	Can be accurate to the level of conceptual formulation and discretization schema

This is generally performed using transient system codes like RELAP, ATHLET etc. The characteristics, advantages and disadvantages of LSA and NLSA are summarized in Table 1.1.

1.5. Consideration on heating modes in the context of MSRs

Concerned to molten salt fuelled reactors, an important difference exists in natural circulation in the primary heat transport system compared to conventional solid fuelled reactors in terms of mode of heat input. In LWRs and PHWRs, the primary fluid (water) gains heat from the surface of the fuel elements (fuel pins or fuel rods) and carries this heat to the steam generator or steam drum. Here, the heat input to working fluid is by boundary heat flux in core. But, in molten salt reactors, the molten fuel salt is used both as fuel and coolant in the reactor core. Due to fission, the heat is generated within the fuel salt which itself is flowing through the channels provided in the core. Moreover, the internal heat generation continues to be present outside of the core due to decay of fission products within the fuel salt. This forms a distributed heat source in the working fluid. The modes of heating differentiated here may affect the thermal hydraulic performance of the primary heat transport (PHT) system, especially during natural circulation. Hence, these cases are to be studied separately in detail pertaining to natural circulation behaviour during operational transients. These cases are summarized in Table 1.2.

In the context of R & D objectives related to IMSBR program, this project aims at establishing a stability analysis methodology for molten salt based natural circulation loops for both SHF/LH and IHG/DH cases. A detailed literature review has been performed and following objectives are arrived at to be focused in current study.

Table 1.2 Cases depicting the modes of heat input to working fluid in Conventional nuclear reactors and MSRs

Case	**Short form (Abbreviation)**	**Examples (Nuclear and non-nuclear)**
Localized heat input by surface heat flux	Surface Heat Flux with Localized Heating (SHF/LH)	PHWRs, LWRs, solar heating systems with natural circulation, other NC based steam generators, decay heat removal systems etc.
Localized heat input by internal heat generation	Internal Heat Generation / Localized Heating (IHG/LH)	In some chemical reactors, due to exothermic reactions
Distributed heat input by internal heat generation	Internal Heat Generation / distributed Heating (IHG/DH)	In primary heat transport loop of MSRs

1.6. Objectives of project

1) To investigate the adequacy of existing formulation for stability analysis, and to improve them if required, in predicting stability behaviour of single phase natural circulation loops with localized external heat flux input by validation against experiments performed in MSNCL facility.
2) To formulate linear stability analysis procedure for natural circulation loops with distributed internal heat generation and predicting the stability behaviour of such a loop considering MSNCL geometry.
3) To validate the above predictions by transient system codes developed for respective purposes.

1.7. Organization of thesis

A detailed literature review has been performed and summarized in chapter 2 along with the conclusions on state-of-the-art formulations and their capabilities and issues. Chapter 3 includes the details of MSNCL facility (Hall – 7, BARC) and the experimental procedures employed along with the data generated during experiments in all four orientations. Chapter 4

and 5 deal with LSA of natural circulation loops. In chapter 4, the application of existing formulation of Vijayan *et al.* [22] to MSNCL and the need of an improved model are discussed. In Chapter 5, detailed derivation of a new improved model including wall thermal inertia, heat exchange effect and heat losses is given along with the deduction procedure for sub models to study individual effect of each phenomena. Validation studies for this model with two water-based NCLs are given. Then the validation of the same model with MSNCL experimental data is discussed. In chapter 6, derivation of an LSA model for IHG/DH case is given along with the validation studies. Few stability predictions for MSNCL are also given. Chapter 7 deals with derivation of formulation for a transient code and its validation. Then, the simulation studies on wall thermal inertia effect are discussed followed by validation of LSA predictions with NLSA. Chapter 8 summarizes the important conclusions from the current work and discusses the foreseen developments in the methodologies.

CHAPTER 2

Literature Review

2.1. Localized surface heat flux input case (SHF/LH)

Stability of natural circulation has been under investigation since early 1960s. Welander [9] proposed a simple one-dimensional theoretical model for thermal convection which consisted of a fluid filled tube heated from below and cooler from above. While experimenting with his theoretical model, he observed that convective flow in this system was undergoing oscillations before reaching steady state. So, he further experimented with the model at various operating conditions and observed that the circulation of fluid may become unstable and growing pulsations can occur in the system. He demonstrated the behaviour by numerically solving one-dimensional governing equations also. Keller [10] took up and analysed the thermal convection model of Welander to study the existence of oscillatory modes (as they called it) for the case of point heat source and sink as well as distributed heat source and sink. He mentioned that the oscillations occur in absence of inertia forces also, merely due to the interplay between buoyancy and friction by determining periodic solution for inertialess case. Welander [11] analysed the problem further with stability analysis methodology prevailing then, and constructed a neutral stability boundary in the parameter space of ϵ and q which denote friction factor and volumetric flow rate in dimensionless form. He performed several numerical experiments on the model and confirmed with acceptable accuracy the prediction of neutral stability boundary. With the observations obtained from numerical analysis he gave physical explanation for the cause of instability and also for stable behaviour at low and high ϵ values based on warm and cold pocket movement in the loop. His theory is known as Welander's warm pocket theory.

Creveling *et al.* [12] performed experiments with a toroidal free convection loop filled with water with heating section at bottom and cooling section at top. They observed unstable behaviour at medium heat flux levels whereas at low and high heat fluxes they found stable behaviour. They observed that the friction factors obtained from experimental data are significantly higher than prevailing correlations for forced flow. They performed stability analysis in frequency domain using Nyquist criteria to establish neutral stability boundary for that loop and plotted the same in E-D space where E and D are defined as follows.

$$E = \frac{Re^2 r}{Gr_m R}; D = \frac{2\pi Rh}{rCG_s}; \tag{2.1}$$

where,

r = loop piping inner radius, R = toroid radius, h = overall heat transfer coefficient at cooler, G_s = steady state mass flux, C = specific heat capacity of fluid

The prediction was reasonable for neutral boundary at high heat flux while significant deviation was observed at lower heat flux. In their stability analysis they used closure laws for friction factor and heat transfer as obtained from their experiments. They also observed that the frequency of oscillations during unstable behaviour in the loop is increasing almost linearly with increasing heat flux input. They also reported that the transition from laminar to turbulent might happen in NCLs at Reynolds numbers as low as 1500.

Gorman *et al*. [6] performed theoretical analysis of stability behaviour of toroidal natural circulation loop using Lorentz's chaos theory. They also performed experiments in the toroidal loop of Creveling *et al.* [12] and observed three different chaotic flow regimes: a globally chaotic regime whose essential features can be described by a one-dimensional cusp-shaped map, a subcritical regime in which the flow can be either chaotic or steady, and a

transient regime in which the flow remains chaotic for a time and then decays into a steady flow.

Vijayan and Date [13] performed theoretical studies on stability behaviour of figure-of-eight loop under natural circulation with through flow. They used both linear stability analysis (LSA) and nonlinear finite difference technique to study the stability behaviour. They observed that the LSA could predict only a single stability boundary which separates the unconditionally stable zone from conditionally stable zone whereas nonlinear analysis could predict existence of conditionally and unconditionally stable regimes. It was experimentally proven by them for the first time that conditionally stable regime exists in NCLs. In their analysis, they used experimentally correlated friction factor relation for figure-of-eight loop.

Vijayan and Austregesilo [14] investigated the adequacy of existing power-to-volume scaling philosophy to simulate the steady state and stability behaviour of rectangular NCLs by both experimentally and theoretically. They performed experiments with rectangular NCLs of three different diameters viz. 6 mm, 11 mm and 23.2 mm piping but same lengths for all sections. These NCLs were made of borosilicate glass tubes with water as working fluid. From the steady state flow rates they obtained from experiments, they deduced a functional relationship between *Re* and $Gr_m(D/L)$ which was observed to be same for all diameters.

$$Re = 0.3548 \left(Gr_m \frac{D}{L}\right)^{0.43} \tag{2.2}$$

From this relationship, they derived the friction factor

$$f = \frac{22.26}{Re^{0.6744}} \tag{2.3}$$

During their experiments with 23.2 mm loop, they observed unstable behaviour with repetitive flow reversals at some operating conditions and stable behaviour at others. They

performed linear stability analysis to theoretically determine the stability boundary for each loop and plotted the same in Gr_m-St_m space. It was observed that stable operating conditions were predicted as unstable theoretically. Then they repeated the experiments in different routes of achieving the same operating conditions (like power rise from a stable operating condition or power step back from an unstable operating condition) and found that those operating conditions can be unstable based on the route followed. This is called conditional stability.

Continuing their study on repetitive flow reversals shown by 23.2 mm loop at some operating conditions, Vijayan *et al.* [15] performed further experimental investigation also in the same three loops. They also performed nonlinear analysis using computer code ATHLET. Since the flow regime continuously shifts from laminar to turbulent during flow reversals, they have used a smooth switching procedure in the friction correlation to avoid artificial numerical oscillations.

$$f = \max(f_l, f_t) \tag{2.4}$$

$$f_l = \frac{16}{|Re|};\ \ (f_t)^{-1/2} = 3.48 - 4\log_{10}\left[\frac{2\varepsilon}{D} + \frac{9.35}{|Re| f_t^{\frac{1}{2}}}\right] \tag{2.5}$$

According to this friction correlation, transition from laminar to turbulent occurs around at Reynolds number of 1100 for smooth pipes. Unlike LSA performed in [14], in nonlinear analysis they considered local pressure losses and heat capacity of wall material. For heat transfer coefficient calculations they used Dittus-Boelter correlations for all *Re*. During numerical studies, they observed that with coarse nodalization, ATHLET could not predict the oscillatory behaviour whereas with refined mesh, the transient unstable behaviour could be predicted qualitatively. The switching from regular periodic oscillations to irregular chaotic behaviour was predicted at very low power than that observed from experiment. They

attributed this to the thermal stratification across cooler and heater as observed experimentally.

Misale and Frogheri [16] reported their experimental observations on the effect of local pressure drops on stability behaviour of a rectangular NCL of diameter 20 mm. They used orifices of 6 mm, 10 mm and 14 mm to vary the local pressure drop in the mid length of vertical legs of their rectangular NCL. It was observed from their experimental data that the initial oscillations during establishment of steady flow die out fast if local pressure drop is high. They observed unstable behaviour in the NCL without orifices at power level greater than 500 W while the loops with orifices did not show any unstable behaviour in the operating range of 300 to 900 W.

Misale *et al.* [17] employed a 2D axisymmetric numerical model to analyse the rectangular NCLs theoretically. The corners of the loop were not given consideration in the model, including which NCLs doesn't lend to axial symmetry. They performed transient analysis considering three different loop materials i.e. plexi glass, stainless steel and copper at power levels in the range of 100 W to 550 W. They didn't observe any instability in this operating range. In their steady state analysis, they focused on velocity profiles, friction factor and Nusselt numbers at various Gr_m values. They observed that at higher Gr_m, the velocity profiles were deviating from parabolic nature of laminar forced flow. The peak of the velocity profile was observed to be shifting towards wall from the centre of the pipe. This was due to increased difference in the temperatures of wall and fluid which in turn increases the buoyancy near the wall. This observation has been recently obtained from the CFD studies of Rakesh Chouhan *et al.* [4] also. Due to this wall peaking effect, the friction factors estimated were also higher compared to that corresponds to forced laminar flow. This conclusion was derived earlier from the experiments of Vijayan and Austregesilo [14]. They found that friction factor was following a monotonic increasing trend with respect to

increasing Gr_m. They also observed that the steady state flow rates in plexiglass loop were significantly higher with the next being steel at same power levels. They explained that the reducing thermal capacity and thermal conductivity leads to increasing wall temperatures which in turn lead to higher buoyancy and hence flow rates. Nusselt number would also be augmented due to higher velocity near the wall. They also plotted Nusselt number for different Gr_m.

Continuing their studies on effect of local pressure drops on stability behaviour of NCLs, Misale and Frogheri [18] performed further experiments in a higher diameter loop (40 mm) maintaining same length to diameter ratio. In this loop, called as LOOP#1, they used orifices of 10 mm, 22 mm, 26 mm, 30 mm and 36 mm and they operated in the power range of 500 to 3400 W. The only significant observation was that the orifice diameter (pressure drop) required to stabilize the loop is lower (higher) as the power increases.

Vijayan [19] compared the experimental data on steady state flow rates in uniform (UDL) and non-uniform (NDL) diameter loops with theoretical correlations based on fully developed forced flow friction factor correlations. They found significant deviation in the predictions by turbulent correlation for UDLs which they attributed to local friction losses. According to their formulation, including local friction losses in terms of equivalent length, they quoted that stability behaviour of NCLs can be simulated by simulating $Gr_m^{b/(3-b)}/N_G^{3/(3-b)}$ and St_m where the geometric parameter N_G is given by

$$N_G = \frac{1}{D}\sum_{i=1}^{N} L_{\text{eff},i} \tag{2.6}$$

While Misale *et al.* [17] focused on effect of wall material on steady state flow rates, Jiang and Shoji [20] experimentally and theoretically studied the effect of wall material on stability of toroidal natural circulation loop of 23 mm inner diameter filled with distilled water.

They used Lorentz chaos theory to study the stability behaviour of these loops and drew a conclusion that high thermal conductivity of wall material stabilizes the flow. This is due to higher heat transfer performance of the wall to remove any thermal disturbance in the system before leading to any apparent variation in the global flow.

They proved their theoretical conclusions by performing experiments in three loops: 1) total loop was of copper, 2) only upper half of the loop was of copper while lower half was of glass and 3) total loop was of glass. Their observations were summarized as follows.

Mono-periodic and multi-periodic flows are characterized by single and multiple frequency oscillations respectively whereas aperiodic flows show almost uniform distribution of frequencies in power spectrum. Jiang and Shoji concluded these behaviours as stable flow since all these oscillations were observed without any flow reversals. By comparing the mass flow rates obtained from heat balance and frequency of oscillations, they distinguished the local oscillations in the flow from global bulk fluid oscillations. From this they concluded that the global flow oscillation time period is related to the loop circulation time. They also explained the role of thermal conductivity of wall in leading the local flow fluctuations, as observed in loop 1, to global fluid fluctuations in loop 2 and 3. It was said that high thermal conductivity wall can remove the thermal disturbances as fast as it can introduce them and opposite is the case of low thermal conductivity wall.

In their experiments with loop 3, at higher powers they observed chaotic flow reversals which they compared with their theoretical analysis with Lorentz chaos theory and got good agreement qualitatively.

Misale *et al.* [21] took up the case of stability behaviour of single phase NCLs with various wall materials as performed by Jiang and Shoji [20], but with a rectangular NCL. They designed the loop such that it facilitated the experiments with different inclinations of the

NCL. The inclination of the loop from vertical was quoted to help simulating low gravity conditions which prevail in space applications. The heating and cooling sections are made of copper piping while the vertical sections are changeable.

They performed experimental study with glass and stainless steel as material of vertical sections. With each material they performed experiments at power levels 500, 1000, 1500, 2000 and 3000 W at inclinations of ~90^0, 60^0, 30^0 and 0^0 (vertical). They observed stable behaviour at all inclinations for the loop with stainless steel vertical sections whereas they observed unstable behaviour at all inclinations except ~90^0 (equivalent to zero gravity as mentioned in their paper) for the loop with plexi glass vertical sections. They also observed that the variation of flow rate is significant when the loop inclination changes from 60^0 to 90^0. They also compared the chaotic behaviour observed in experiments with that predicted by Lorentz theory [20] and opined that Lorentz theory could serve as a suitable model to study dynamic behaviour of rectangular NCLs.

Vijayan *et al.* [22] performed an experimental and theoretical investigation of effect of heater and cooler orientation and flow direction on the stability behaviour of rectangular NCLs with a 26.9 mm water loop. Instability was observed in only HHHC (Horizontal Heater and Horizontal Cooler) orientation. By studying the nature of instability, they established thresholds of conditional stability. They described different oscillatory modes observed viz. unidirectional, bidirectional and chaotic oscillations, and the mechanisms causing them. They also experimented on the hysteresis behaviour of NCLs with three operating procedures: 1) start up from rest 2) power rising from steady state and 3) power step back from initially unstable state. They found that NCLs show different thresholds for instability in different operating procedures. They formulated an LSA model for stability analysis of this loop. It was observed that the neutral stability boundary predicted by this formulation was too

conservative to catch the details of experimentally observed stability behaviour. In their nonlinear analysis the transient behaviour of NCL during instability could be simulated qualitatively but the thresholds and the characteristics of instability could not be predicted quantitatively. The formulations for linear stability analysis as used by them for all orientations are summarized in chapter 4. The assumptions are same as were in Vijayan and Austregesilo [14].

Misale *et al.* [23] undertook the study of effect of thermal boundary condition at cooler and heater on the steady state and stability behaviour of NCLs. They experimented with a rectangular NCL using two different working fluids viz. FC 43 and distilled water. To fulfil the aforementioned objective, they performed experiments with coolant temperature in the range of -20^0C to 30^0C and heater powers in the range of 0.1 kW to 2.5 kW. To achieve constant surface temperature condition at cooler (within 1^oC) they maintained high coolant flow. They observed both stable and unstable behaviour with both working fluids and also found that stability can be switched by solely varying the coolant temperature. They demonstrated the existence of upper threshold for instability experimentally. They observed that FC43 loop was more unstable and it was characterized by larger flow velocities than those achieved with distilled water. They found that the correlation of Vijayan *et al.* [14] for steady state flow rates was in good agreement with experimental data.

They used the formulation of Vijayan *et al.* [22] for determining the stability threshold for this loop and it was observed that this formulation gives highly conservative estimate of stability. Based on the experimental data, they constructed a stability map. They also utilized Ultrasound Pulsed Doppler Velocimetry (UPDV) technique to measure the natural circulation flow rates experimentally and to validate the frequency analysis method of determining flow velocities during instability.

Swapnalee and Vijayan [24] addressed the case when flow in one part of the loop is in transition regime while the remaining part is in either laminar or turbulent regime. They derived generalized relation for steady state flow rate for this case. They performed experiments in a rectangular NCL made of SS 347 with pressurized water (30 bar) as working fluid. This loop is of ID = 13.88 mm with a total length of 14.22 m.

In their theoretical analysis, they used forced flow friction factor correlations for laminar and turbulent regimes whereas for transition regime they correlated their experimental data to propose a friction factor for this flow regime. For switching the correlations, they used same philosophy as Vijayan *et al.* [15]. According to this methodology, the transition from laminar to turbulent flow occurs in the Reynolds number range of 898 to 3196. However, there was no physical interpretation of these ranges. With these friction factor correlations, they observed that all the experimental data of various researchers could be predicted with error less than $\pm 54\%$.

They performed linear stability analysis of their experimental loop using the methodology of Vijayan *et al.* [22], but in dimensional form. Even though, there were no unstable operating conditions during experiments, their code LISA predicted some of the experimental data as unstable. This was attributed to simplifying assumptions like neglecting wall thermal inertia etc.

Rao *et al.* [25] theoretically studied the effect of wall heat capacity on the dynamic behaviour of NCL with end heat exchangers. They considered the hot fluid and cold fluid inlet temperatures as parameters for this analysis and performed numerical start up experiments with step, ramp and exponential raise (drop) of hot (cold) fluid inlet temperature. They neglected axial heat conduction, minor losses at pipe bends, wall thermal resistance in their formulation. They observed that the model with wall heat capacity showed stable behaviour

even at the operating conditions where the model without wall heat capacity showed unstable behaviour. By this, they concluded that wall heat capacity has stabilizing effect on natural circulation loop dynamics. They constructed a stability map with the parameter space (loop Grashof number, hot fluid heat capacity rate), by solving the transient governing equations by FEM and found that the unstable zone shrinks and shifts to higher Grashof numbers.

Kudariyawar *et al.* [26] performed 3D CFD analysis on steady state and stability behaviour of rectangular NCL of Vijayan *et al.* [22]. For VHHC, VHVC and HHVC orientations they performed steady state analysis and compared with experimental data of Vijayan *et al.* [22] and correlations of Vijayan *et al.* [22], Swapnalee and Vijayan [24] and others. They found good agreement with experimental data and theoretical correlations. In the CFD analysis, they found that laminar models predicted the loop behaviour more accurately than turbulent models at Reynolds numbers 1383 and 1742 which were taken to be turbulent in the friction correlations adopted by Vijayan *et al.* [15] and Swapnalee and Vijayan [24]. For HHHC orientation, they performed transient analysis to study the stability behaviour and causes at different power levels. Using the temperature evolution along the loop with respect to time, as observed in CFD analysis, they explained the reasons for unidirectional and bidirectional oscillations in case of HHHC orientation. They verified the Welander's warm pocket theory alongside.

2.2. Internal heat generation case (IHG/DH)

Research concerning the internal heat generation and distributed heating case of natural circulation has been very recent. With the main objective of its application in MSRs and some exothermic chemical process reactors, various researchers started work in this area. Since, the attempts to improve the theoretical models for stability analysis is being performed by the same researchers simultaneously, this section introduces to the new improvements in

theoretical models of LSA, besides the observations with IHG/DH case. All of the published work is theoretical and so far no experimental investigation on this case has been published in open literature as per the knowledge of the author.

Ruiz *et al.* [27] attempted for the first time, the study of stability behaviour of NCLs with internal generation in different orientations. They derived a semi analytical linear formulation as well as a numerical non-linear formulation for this purpose. Their formulation considers that internal heat generation is uniform throughout the loop. They kept the surface heat flux at heater portion also in the formulation and hence, the formulation facilitates the parametric study between different levels of surface heat flux and internal heat generation. The assumptions taken in the formulation are same as Vijayan *et al.* [14]. For closure of friction factor, they utilized the Churchill's [7] correlation in a modified form suitable to represent as $f = a/Re^b$ (Eq. 2.7). This correlation was developed using Fermi-Dirac factor ψ as in Eq. 2.8.

$$a = 64^{\psi}0.316^{1-\psi}; b = \psi + (1-\psi) * 0.25 \tag{2.7}$$

where,

$$\psi = \frac{1}{1+\exp\left(\frac{Re-2530}{120}\right)} \tag{2.8}$$

They applied their model on the geometry of NCL of Vijayan *et al.* [22] for VHHC and VHVC orientations. In their parametric studies, they observed that internal heat generation can change the area of the unstable region. Significant destabilization was found. VHVC was found to be more stable out of the two even with internal heat generation. Effect of wall and local pressure losses were not focused. Experimental validation was not present. We opine that destabilization due to internal heat generation case they studied, may be an apparent shift of VHHC to HHHC and VHVC to HHVC as proportion of IHG becomes 100%.

Pini *et al.* [28] included the phenomenon of variation of convective heat transfer at cooler with respect to flow in the model of Ruiz *et al.* [27] to investigate its effect on the stability behaviour of rectangular NCLs with internal heat generation. They used linear as well as non-linear stability analysis procedures. They introduced a parameter 'B' (Eq. 2.9) to incorporate the heat exchange effect.

$$B = \frac{d(Nu)}{d(Re)} \frac{Re_{ss}}{Nu_{ss}} \tag{2.9}$$

They constructed a composite correlation for evaluation of Nusselt number at different Reynolds numbers using Fermi-Dirac factors. The correlation is shown in Eq. 2.10 where subscripts S, H, G, D means Skupinski, Hausen, Gnielinski and Dittus-Boelter correlations [29]. It was noted that this Nusselt number correlation and 'B' were used in cooler section only as per the formulation.

$$\begin{aligned} Nu = & \left[Nu_H^{\psi_{Nu_1}} \left(Nu_S^{\psi_{Nu_3}} Nu_G^{1-\psi_{Nu_3}} \right)^{1-\psi_{Nu_1}} \right]^{\psi_{Nu_2}} \times \\ & \times \left(Nu_S^{\psi_{Nu_3}} Nu_D^{1-\psi_{Nu_3}} \right)^{1-\psi_{Nu_2}}, \end{aligned} \tag{2.10}$$

$$\begin{aligned} \psi_{Nu_1} &= \left[1 + \exp\left(\frac{Re - 2530}{20} \right) \right]^{-1}, \\ \psi_{Nu_2} &= \left[1 + \exp\left(\frac{Re - 10^5}{20} \right) \right]^{-1}, \\ \psi_{Nu_3} &= \left[1 + \exp\left(\frac{Pr - 0.6}{10^{-5}} \right) \right]^{-1}. \end{aligned} \tag{2.11}$$

Since constant surface temperature boundary condition was used at cooler, the overall heat transfer coefficient was same as internal heat transfer coefficient which can be found form Eq. 2.10. They studied HHHC and VHHC orientations and employed *Re*-St_m parameter space for stability maps. Since the St_m range required cannot be traced by changing Reynolds number alone, it was achieved by changing Prandtl number. They performed numerical

experiments with an Object-Oriented model (O-O), RELAP 5 and OpenFOAM to solely validate the stability maps generated by linear analysis.

They observed a significant stabilization of NCL due to heat exchange (HX) effect at cooler in the absence of internal heat generation. It is due to negative feedback of 'B' to the loop dynamics which diminishes the effectiveness of hot plug formation. However, with internal heat generation HX showed different effects in HHHC and VHHC orientations. In former orientation, stabilization was observed due to the reason mentioned above while in latter orientation, destabilization was observed due to increased symmetry of loop with internal heat generation. While studying the case of uniform internal heat generation with their formulation, both HHHC and VHHC orientations are essentially same. But, this fact has nowhere been recognized throughout the paper while it is apparent in their results.

Cammi *et al.* [30] introduced the wall thermal inertia into the linear analysis formulation of earlier works [26, 27] along with internal heat generation and theoretically studied the effect of wall thermo-physical and geometrical properties on the stability behaviour of NCL in HHHC orientation. They considered wall as two shells and imposed a constant temperature boundary condition for outer shell at cooler. They also used *Re*-St_m parameter space to represent stability maps and followed same procedure as [28]. They also used O-O model, RELAP 5 and OpenFOAM for numerical experiments to solely validate linear analysis results.

They observed that the wall density, specific heat and thermal conductivity individually have stabilization effect on NCLs. It is explained as follows. With the imposed temperature condition at cooler, the transients in fluid will reduce due to high wall thermal conductivity. With higher heat capacity of wall, the temperature fluctuations in wall will be out of phase with fluid which can stabilize the loop. At high Reynolds numbers, however, they observed

destabilization effect with increased thermal inertia. One more important observation was destabilization of NCL by IHG in laminar regime while stabilization of NCL by HX effect in turbulent regime. It was opined that in turbulent regime HX effect is so dominant that the destabilization induced by IHG could be overridden. On the other hand, HX effect is negligible in laminar regime due to negligible variation of internal heat transfer coefficient with flow rate.

Luzzi *et al.* [31] assessed the state of the art methodologies of stability analysis of NCLs for SHF/LH case with linear and non-linear models of [27, 28, 29] along with RELAP 5 and OpenFOAM against the experimental data at L2 facility of DIME-Tec labs (University of Genoa). They performed parametric studies for IHG case also. However, experimental validation of stability predictions for IHG case was not performed.

Their study was focused on HHHC orientation. They performed each experiment multiple times and observed that the oscillatory behaviour is not repeatable which led to the conclusion that exact prediction may not be possible with numerical codes. However, the Power Density Spectrum (PDS), which gives characteristics of instability, could be predicted accurately by numerical models.

They highlighted the importance of wall thermal inertia and heat exchange effects in improving the stability predictions. They also focused on the modelling of cooler as either surface temperature or co-axial heat exchanger using O-O model. After a detailed study and comparison with experiments, they found that modelling cooler as coaxial heat exchanger is required for accurate prediction of transient behaviour. However, this was not implemented in linear analysis. It is to be noted that the experiments were performed by controlling the coolant temperature at required value and mimicking the constant temperature condition by sufficiently high flow rate of coolant. O-O model was proven to be a handy tool for fast and

efficient simulation of system behaviour whereas CFD (3D) serves a supporting role in understanding the phenomena in detail. Regarding internal heat generation, no new conclusions were derived.

2.3. Concluding remarks

Having numerous advantages, natural circulation got a lot of focus in research community especially in nuclear industry. The concerns related to the instabilities have been under study. Various authors proposed different methodologies and models. Various phenomena pertaining to natural circulation have been incorporated in 1D models to simulate the NCL behaviour. The accuracy of predictions was reported to be increasing with state-of-the-art 1D linear and non-linear models as well as 3D CFD models. However, the experimental data useful for validating these stability predictions is still scarce in open literature even though numerous experimental studies were already done on this subject.

One of the important concerns with 1D models is the applicability of various closure relations for friction and heat transfer. While many researchers demonstrated the suitability of forced flow correlations for this purpose, universal acceptance to any specific set of correlations has not been arrived yet. Employing 3D CFD codes for overcoming this limitation has been attempted by some authors. But, the approximations involved in turbulence models and the flow regime switching during bidirectional oscillations still remains as an underlying uncertainty. This explains the complexities involved in simulation of natural circulation phenomena even in the simplest loops.

Though it is a quick tool for stability map generation, linear analysis formulation is still lacking in consideration of some important phenomena. With focus of high temperature reactors, where the secondary side coolant may not be maintained at constant temperature, modelling a cooler with constant temperature boundary is unphysical. It has been proven

[31], with non-linear models however, that the cooler should be modelled as coaxial heat exchanger for better prediction of loop behaviour. And one more important aspect which has not been implemented, even though it was quoted always, is heat losses from the system. For low temperature NCLs like [22] may not see significant heat losses, but, in high temperature systems like Molten Salt Natural Circulation Loop (MSNCL) heat losses are inevitable. Heat losses serve as distributed cooling in the loop. As orientation of heater and cooler were proven to have effect on NCL behaviour its modelling seems to be important. Without proper treatment of heat losses, the validation of stability predictions with the experimental data does not seem to be realistic.

CHAPTER 3

Experimental Studies

Experiments have been performed in Molten Salt Natural Circulation Loop (MSNCL) facility located in Hall-7, BARC to investigate the stability behaviour of the same and to utilize the observations in validation of theoretical analyses. Molten salt of $NaNO_3$ and KNO_3 at a composition of 60:40% (by weight) is used as working fluid.

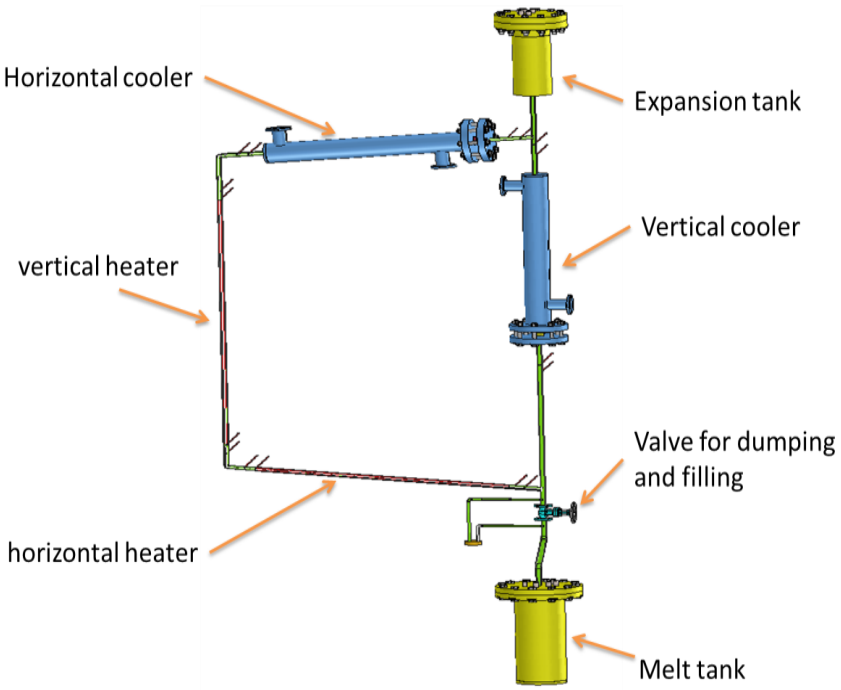

Fig. 3.1 Schematic of Molten Salt Natural Circulation Loop

3.1. MSNCL description

MSNCL is a quadrilateral loop with main heaters provided on bottom and left legs and coolers provided on top and right legs. Heaters and coolers can be independently operated, facilitating the experiments in all four orientations *viz.* Horizontal Heater Horizontal Cooler (HHHC), Vertical Heater and Horizontal Cooler (VHHC), Horizontal Heater and Vertical Cooler (HHVC) and Vertical Heater and Vertical Cooler (VHVC). 3D schematic of MSNCL is shown in Fig. 3.1.

Heaters are of 6 kW power rating each. Coolers are tube-in-tube type heat exchangers. A blower is used to pass air through the annulus region of coolers as secondary fluid. A needle valve at the outlet end of the cooler secondary side is used to control the flow rate of air. The top and bottom legs of the loop are provided with an angle of 5^0 from horizontal to facilitate proper filling and draining of molten salt during start-up and shutdown/trip stages respectively. MSNCL is also equipped with a melt tank and an expansion tank at bottom and top respectively. Band heaters are provided on melt tank and expansion tank. Expansion tank is kept partially filled with molten salt during the experiments. It accommodates the thermal expansion of the molten salt during operational transients. Surface heaters are provided throughout the piping of the loop, on connections of melt tank and expansion tank and on control valves. All the heaters in the loop can be operated either in temperature controlled mode or power controlled mode. The former setting facilitates the loop to be kept at a required temperature during start-up while the latter setting helps us to give specified power to the working fluid during experiments, if required. Argon gas is used as cover gas in the expansion tank and melt tank. A cover gas system having regulating valves controls the pressure of the Argon gas. Argon gas is also used to purge out the air present in the loop prior to filling.

Thermocouples are provided at the centre locations of piping at inlet and outlet of heaters, primary and secondary side of coolers. They are used to measure the temperature of molten salt and secondary air. Thermocouples are also placed on the surface of loop piping at several locations. These temperatures can be used for heat transfer analysis and they are used for real time control of the surface heaters in auto mode during start-up and for other safety related actions. Level of molten salt in melt tank and expansion tank is monitored through level sensors which work by gas purging method.

Several safety features are incorporated in the facility through automatic control by relay switches. Some of them are listed as follows –

1. If fluid temperature at critical locations like cooler outlet or expansion tank falls below 290^0C annunciation is given and if it falls below 270^0C, the control valve CV-2 will be opened to automatically dump the salt into melt tank. This feature is to avoid accidental solidification of salt in loop
2. If the wall temperature at critical locations like heater outlet goes beyond 600^0C annunciation will be given and if it goes beyond 620^0C main heater will be tripped.
3. Argon purging system is provided with two relief valves with set pressure of 1.5 bar

3.2. Experimental studies

Experiments with different orientations of heater and cooler have been performed at various power levels and cooling rates. Keeping the hysteresis phenomena in mind, some experiments have been performed as start-up and some have been performed by power step-back while most of the experiments have been performed as power raising transients. The experimental matrix has been designed based on the feasibility under the constraints of maximum and minimum possible operating temperatures of the loop. Methodologies for various experimental procedures are described below.

Filling the loop with molten salt

The nitrate salt which resides in melt tank during shut down conditions is in solid form. Before starting the experimental train, the melt tank is heated by band heaters up to 350^0C. While the salt is reaching 350^0C, the loop piping and expansion tank are heated to a temperature of 300^0C by surface heaters in temperature controlled mode. Once the whole system reaches the desired temperature, keeping CV-2 closed, the argon gas is purged

through level sensor line to the melt tank. Once the melt tank pressure reaches required head of molten salt (preferably to the height of expansion tank) which is 700 mbar in this case, CV-2 will be opened to allow the molten salt to fill the loop. Pressurization will be continued till the molten salt fills the expansion tank to half the level. Then CV-2 will be closed.

Start-up experiment

Once the molten salt is filled in the loop, temperature around the loop comes to equalization around at 300 – 320^{0}C from bottom leg to top leg. Since, local buoyant flows cannot be completely avoided at this temperatures, a temperature gradient of around 20^{0}C is accepted as initial condition for start-up. The flow start-up experiment is performed by switching off all the surface heaters, switching on main heater and blower within one minute.

Power raise, power step-back experiments

Once the steady state is achieved at a given operating power and cooling rate, the experiment for higher (or lower) power is performed by raising (or lowering) the main heater power while keeping the cooling flow rate constant.

Experiments at some power levels have been performed at multiple cooling rates also if the system temperatures fall in operable range.

3.3. Analysis of experimental data

Mass flow rate of molten salt at each power level has been calculated using heat balance (Eq. 3.1) at heater section. Reynolds number and modified Grashof number for each operating condition have been calculated using Eqs. 3.2 and 3.3 respectively.

$$w_{ss} = \frac{Q}{C_p \Delta T_h} \tag{3.1}$$

$$Re_{ss} = \frac{4w_{ss}}{\pi \mu D_i} \tag{3.2}$$

$$Gr_m = \frac{\rho^2 g \beta_f D^3 QH}{A\mu^3 C_p} \tag{3.3}$$

Modified Stanton number has been calculated from experimental data in following manner

$$\Delta T_{lm} = \frac{(T_{c,i} - T_{a,o}) - (T_{c,o} - T_{a,i})}{\ln\left(\frac{(T_{c,i} - T_{a,o})}{(T_{c,o} - T_{a,i})}\right)} \tag{3.4}$$

$$U_i = \frac{Q_{cooler}}{\pi D_i L_c \Delta T_{lm}} = \frac{w_{ss} C_{p,ms} \Delta T_c}{\pi D_o L_c \Delta T_{lm}} \tag{3.5}$$

$$Nu_i = \frac{U_i D_i}{k} \tag{3.6}$$

$$St_m = \frac{Nu_i}{Re_{ss} \mathrm{Pr}} . \frac{4L_t}{D_i} \tag{3.7}$$

All the calculations have been based on properties at loop average temperature for each operating condition.

3.4. Results

In all the operating conditions at which experiments have been performed, the loop behaviour has been observed to be stable. No global fluctuations of fluid flow have been observed. Required parameters for validation of stability analysis have been deduced from experimental data as discussed in previous section and they are summarized in Table 3.1. This data is used in subsequent chapters for validation of theoretical predictions of stability.

Table 3.1 Experimental data of MSNCL and calculated parameters

Orientation	Q (W)	Coolant flow (kg/h)	T_{mean} (^{0}C)	Gr_m	w_{ss} (kg/s)	Re_{ss}	Pr	St_m
HHHC	1098	60.12	331.0	1.67E+10	0.0276	860.29	5.95	0.44516
	1770	60.12	403.5	8.93E+10	0.0352	1657.82	5.08	0.42882
	2400	60.12	490.5	2.50E+11	0.0294	1787.70	3.81	0.59963
	1464	60.12	369.9	4.25E+10	0.0296	1301.92	6.10	0.44379
	2700	158.76	485.9	2.17E+11	0.0317	2809.74	4.19	0.55750
	2958	158.76	456.8	2.79E+11	0.0438	2823.45	3.94	0.53130
	2982	138.6	477.2	2.98E+11	0.0470	2144.97	3.85	0.74497
	2982	158.76	475.7	2.47E+11	0.0427	2769.67	4.14	0.55615
	3156	158.76	452.7	3.00E+11	0.0450	3119.31	3.93	0.53030
VHHC	1794	119.52	349.7	3.23E+10	0.0238	784.99	6.92	0.86753
	2400	119.52	432.7	1.49E+11	0.0280	1414.97	4.49	0.77825
	2682	84.89	463.0	2.32E+11	0.0322	2063.37	4.08	0.75330
	1488	84.89	333.5	2.24E+10	0.0213	745.61	7.71	0.86240
	2628	158.83	412.3	1.41E+11	0.0297	1609.89	4.88	0.86220
	3174	158.83	462.5	2.74E+11	0.0318	2038.06	4.08	0.81710
HHVC	1200	119.52	314.3	1.48E+10	0.0229	663.60	8.82	0.69672
	1776	119.52	347.3	4.12E+10	0.0299	1077.41	7.03	0.64838
	2400	119.52	399.3	1.23E+11	0.0336	1588.14	5.19	0.52911
	3000	119.52	447.4	2.48E+11	0.0372	2081.52	4.26	0.55635
VHVC	1794	119.52	338.0	1.17E+11	0.0157	502.00	7.47	1.52390
	2382	119.52	379.2	1.56E+11	0.0194	789.32	5.78	1.34920
	3000	119.52	405.0	1.96E+11	0.0218	1011.52	5.05	1.27529

3.5. Conclusions

In this chapter, the MSNCL experimental facility and the experimental procedures followed for stability analysis have been described. MSNCL has shown stable thermal hydraulic behaviour in all operating conditions and orientations experimented.

CHAPTER 4

Linear Stability Analysis of MSNCL for SHF/LH Case with Preliminary Model

The methodology of linear stability analysis (LSA) has been introduced in Chapter 1. Based on the assumptions taken, different authors reported different formulations following almost the same procedure. The formulation widely quoted in literature for single phase NCLs with localized surface heat flux input case is due to Vijayan *et al.* [22]. In current chapter, the formulation of Vijayan *et al.* is given briefly followed by some discussion on solution methodology. A computer code developed based on this formulation along with its validation studies are given next. Later the analysis performed to check the adequacy of this formulation in prediction of the stability behaviour of MSNCL is discussed.

4.1. Phenomena involved in natural circulation

In natural circulation loops, the basic components involved are working fluid, piping and pipe fittings, heater (can be an electric heater or a heat exchanger), cooler (generally a heat exchanger), expansion tank, insulation, coolant (secondary fluid in cooler). The phenomena involved are

1. Heat transfer from heater (or hot fluid of heat exchanger) to pipe outer surface at heating section
2. Convective heat transfer between working fluid and pipe inner wall
3. Radial and axial heat conduction in working fluid, piping and fittings
4. Heat transfer from pipe outer surface to coolant in cooler
5. Heat losses from the wall boundary through insulation
6. Acceleration or deceleration of working fluid due to heating or cooling in heater and cooler respectively

7. Momentum loss due to skin friction and local geometric features like elbows etc.
8. Expansion and contraction of working fluid which would be accommodated by expansion tank
9. Thermal expansion of piping
10. Secondary flows in heat exchange sections, generated by interplay between buoyancy and bulk flow

4.2. Formulation

The formulation of Vijayan *et al.*, modelling some of the phenomena mentioned in previous section, is given here in a very brief way. For further details, refer [22].

Considering the following assumptions to be valid –

1. Flow features are predominantly one-dimensional

2. Incompressible flow

3. Boussinesq approximation is valid

4. Local pressure losses are negligible compared to skin friction losses

5. Heat losses are negligible

6. Loop piping (wall) has negligible effect on stability behaviour

7. Axial heat conduction in fluid is negligible

The characteristic equation for stability is given by

$$n - \frac{Gr_m}{Re_{ss}^3}\frac{\bar{I}}{\bar{\omega}} + \frac{p}{Re_{ss}^b}\frac{L_t}{D}\frac{(2-b)}{2} = 0 \qquad (4.1)$$

here, $\bar{I} = \oint \bar{\theta} dZ$ and n is a complex number

To determine Ī, perturbed temperature distribution in the loop should be known which is given as

$$\overline{\theta(S)} = \left(\overline{\theta_{cl}} + \frac{L_t}{L_h}\frac{\bar{\omega}}{n}\right) e^{-\frac{nS}{\varphi}} - \frac{L_t}{L_h}\frac{\bar{\omega}}{n} \qquad \text{(heater)} \tag{4.2}$$

$$\overline{\theta(S)} = \overline{\theta_h} e^{\frac{n}{\varphi}(S_h - S)} \qquad \text{(hot leg)} \tag{4.3}$$

$$\overline{\theta(S)} = \frac{St_m \bar{\omega} \theta_{hl}}{n}\left(e^{-\frac{St_m}{\varphi}(S - S_{hl})} - e^{-\left(\frac{n+St_m}{\varphi}(S - S_{hl})\right)}\right) + \overline{\theta_{hl}} e^{\frac{n+St_m}{\varphi}(S_{hl} - S)} \quad \text{(cooler)} \tag{4.4}$$

$$\overline{\theta(S)} = \bar{\theta}_c e^{\frac{n}{\varphi}(S_c - S)} \qquad \text{(cold leg)} \tag{4.5}$$

where,

$$\overline{\theta_{cl}} = \frac{\bar{\omega}}{n}\left(\frac{\frac{L_t}{L_h}\left(1 - e^{\frac{nL_h}{L_t}}\right) + St_m \theta_{hl}\left(1 - e^{-\frac{nL_c}{L_t}}\right) e^{-n\left(\frac{L_{cl}}{L_t} - 1\right)}}{\left(e^{n + \frac{St_m L_c}{L_t}} - 1\right)}\right) \tag{4.6}$$

$$\overline{\theta_h} = \frac{\bar{\omega}}{n}\left(\frac{St_m \theta_{hl}\left(e^{\frac{nL_{hl}}{L_t}}\right)\left(e^{\frac{nL_c}{L_t}} - 1\right) + \frac{L_t}{L_h}\left(e^{-\frac{nL_h}{L_t}} - 1\right) e^{\frac{St_m L_c}{L_t} + n}}{\left(e^{n + \frac{St_m L_c}{L_t}} - 1\right)}\right) \tag{4.7}$$

$$\bar{\theta}_c = \frac{\bar{\omega}}{n}\left(\frac{St_m \theta_{hl} e^n \left(1 - e^{-\frac{nL_c}{L_t}}\right) + \frac{L_t}{L_h} e^{\frac{nL_{cl}}{L_t}}\left(1 - e^{\frac{nL_h}{L_t}}\right)}{e^{n + \frac{St_m L_c}{L_t}} - 1}\right) \tag{4.8}$$

$$\overline{\theta_{hl}} = \frac{\bar{\omega}}{n}\left(\frac{St_m \theta_{hl}\left(e^{\frac{nL_c}{L_t}} - 1\right) + \frac{L_t}{L_h} e^{\frac{St_m L_c + n(L_t - L_{hl})}{L_t}}\left(e^{-\frac{nL_h}{L_t}} - 1\right)}{e^{n + \frac{St_m L_c}{L_t}} - 1}\right) \tag{4.9}$$

Re_{ss} in Eq. (4.1) is given by

$$Re_{ss} = \left(\frac{2}{p}\, Gr_m \frac{D}{L_t} \oint \theta_{ss} dZ\right)^{\frac{1}{3-b}} \tag{4.10}$$

To determine $I_{ss} = \oint \theta_{ss} dZ$, steady state temperature distribution along the loop is required which is given as

$$\theta(S) = \theta_{cl} + \frac{H}{L_h} S \qquad \text{(heater)} \tag{4.11}$$

$$\theta(S) = \theta_{hl}\, exp\left(-\frac{St_m(S-S_{hl})}{\varphi}\right) \qquad \text{(cooler)} \tag{4.12}$$

$$\theta(S) = \theta_{hl} \qquad \text{(hot leg)} \tag{4.13}$$

$$\theta(S) = \theta_{cl} \qquad \text{(cold leg)} \tag{4.14}$$

where

$$\theta_{hl} = \frac{1}{1-e^{-\frac{St_m L_c}{L_t}}}; \quad \theta_{cl} = \frac{1}{e^{\frac{St_m L_c}{L_t}}-1} \text{ and } \theta_{\text{hl}} = \theta_{cl} + 1 \tag{4.15}$$

p and b in Eq. 4.10 are obtained from friction correlation of the form

$$f = \frac{p}{(Re)^b} \tag{4.16}$$

Vijayan *et al.* employed friction correlations obtained for fully developed forced flow in pipes i.e. p = 64 and 0.316, b = 1 and 0.25 for laminar and turbulent flows respectively. In all the above equations $\varphi = L_t/D$.

I_{ss} and $\bar{I}$ depends on orientation of heater and cooler and the flow direction. Since the top and bottom legs of MSNCL are slightly inclined from horizontal, the relations for I_{ss} and $\bar{I}$ for each orientation have been derived separately and used along with above formulation. With the same convention of coordinate system and length scales followed in Vijayan *et al.* [22], I_{ss} and $\bar{I}$ for all four orientations viz. HHHC, VHHC, HHVC and VHVC are summarized for clockwise flow as follows

***HHHC*:**

Using the temperature distribution given by Eq.4.11 to 4.14 and the length scales shown in Fig. 4.1 to perform integration gives

$$I_{ss} = \frac{\theta_{cl}}{H}\left(L_h\, sin(\alpha) + L_3\, sin(\beta) - (L_{cl} - L_3 - L_4) + L_4\, sin(\alpha)\right) + \frac{\theta_{hl}}{H}\Big(L_1\, sin(\alpha) +$$

$$(L_{hl} - L_1 - L_2) + L_2\, sin(\beta) - \frac{L_t}{St_m}\left(e^{-\frac{St_m L_c}{L_t}} - 1\right) sin(\beta)\Big) + \frac{L_h}{2H} sin(\alpha) \tag{4.17}$$

Using the perturbed temperature distribution given by Eq. 4.2 to 4.5 to perform integration gives

$$\begin{aligned}\oint \overline{\theta(S)}\, dZ = {} & \overline{\theta_h}\left(\frac{\varphi}{n}\right)\left[sin(\alpha)\left(1 - e^{-\frac{nL_1}{L_t}}\right) + e^{-\frac{nL_1}{L_t}} - e^{-\frac{n(L_{hl}-L_2)}{L_t}} + sin(\beta)\left(e^{-\frac{n(L_{hl}-L_2)}{L_t}} - e^{-\frac{nL_{hl}}{L_t}}\right)\right] \\ & + \overline{\theta_{hl}}\, sin(\beta)\left(\frac{\varphi}{n + St_m}\right)\left(1 - e^{-\frac{(n+St_m)L_c}{L_t}}\right) \\ & + \overline{\theta_c}\left(\frac{\varphi}{n}\right)\left[\left(1 - e^{-\frac{nL_3}{L_t}}\right) sin\beta - \left(e^{-\frac{nL_3}{L_t}} - e^{-\frac{n(L_{cl}-L_4)}{L_t}}\right)\right. \\ & \left. + \left(e^{-\frac{n(L_{cl}-L_4)}{L_t}} - e^{-\frac{nL_{cl}}{L_t}}\right) sin\alpha\right] + \overline{\theta_{cl}}\left(\frac{\varphi}{n}\right)\left(1 - e^{-\frac{nL_h}{L_t}}\right) sin(\alpha) \\ & + sin(\alpha)\left(\frac{L_t \bar{\omega} \varphi}{L_h n^2}\right)\left(1 - e^{-\frac{nL_h}{L_t}}\right) - sin(\alpha)\left(\frac{L_t \bar{\omega}}{Hn}\right) \\ & + \theta_{hl}\left(\frac{St_m \bar{\omega}}{n}\right) sin(\beta)\left[\frac{\varphi}{St_m}\left(1 - e^{-\frac{St_m L_c}{L_t}}\right) + \frac{\varphi}{n + St_m}\left(e^{-\frac{(n+St_m)L_c}{L_t}} - 1\right)\right]\end{aligned}$$

(4.18)

Similarly derivations for other orientations were also performed and results are summarized as follows

VHHC:

$$I_{ss} = \frac{\theta_{hl}}{H}\left(L_1 + L_2 \sin(\alpha) - \frac{L_t}{St_m}\left(e^{-\frac{St_m L_c}{L_t}} - 1\right)\sin(\alpha)\right) + \frac{\theta_{cl}}{H}(L_h + L_3 \sin(\alpha) - x + ysin(\beta) + L_4) + \frac{L_h}{2H} \tag{4.19}$$

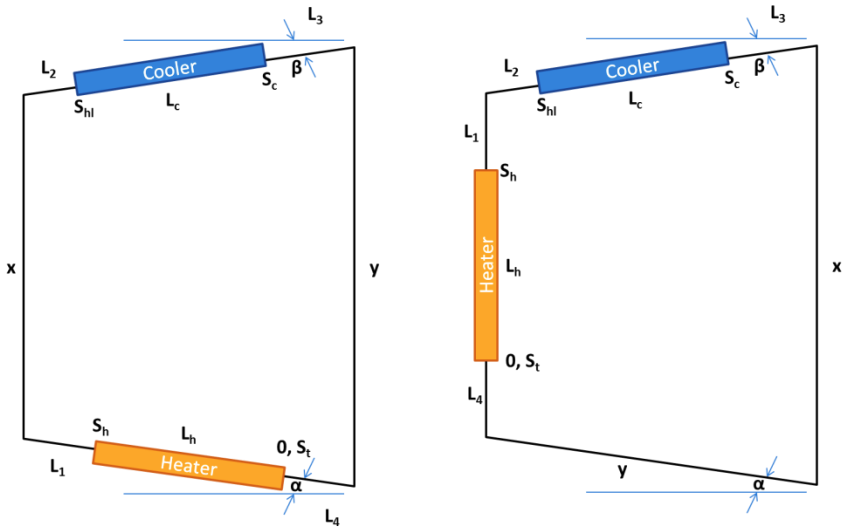

Fig. 4.1 Schematics of HHHC (left) and VHHC orientations showing length scales used in formulation

$$\frac{\bar{I}}{\bar{\omega}} = \frac{\overline{\theta_h}}{\bar{\omega}}\left(\frac{\varphi}{n}\left(1 - e^{-\frac{nL_1}{L_t}}\right) + \sin(\alpha)\frac{\varphi}{n}\left(e^{-\frac{nL_1}{L_t}} - e^{-\frac{nL_{hl}}{L_t}}\right)\right) + \frac{\overline{\theta_{hl}}}{\bar{\omega}}\left(\frac{\varphi}{n+St_m}\right)\left(1 - e^{-\frac{(n+St_m)L_c}{L_t}}\right)\sin(\alpha)$$

$$+ \frac{\bar{\theta}_c}{\bar{\omega}}\frac{\varphi}{n}\left(\left(1 - e^{-\frac{nL_3}{L_t}}\right)\sin(\alpha) + \left(e^{-\frac{n(x+L_3)}{L_t}} - e^{-\frac{nL_3}{L_t}}\right)\right.$$

$$\left. + \left(e^{-\frac{n(x+L_3)}{L_t}} - e^{-\frac{n(L_{cl}-L_4)}{L_t}}\right)\sin(\beta) + \left(e^{-\frac{n(L_{cl}-L_4)}{L_t}} - e^{-\frac{nL_{cl}}{L_t}}\right)\right)$$

$$+ \frac{\overline{\theta_{cl}}}{\bar{\omega}}\frac{\varphi}{n}\left(1 - e^{-\frac{nL_h}{L_t}}\right) + \frac{\varphi L_t}{n^2 L_h}\left(1 - e^{-\frac{nL_h}{L_t}}\right) - \frac{L_t}{nH}$$

$$+ \frac{St_m\theta_{hl}}{n}\left(\frac{\varphi}{St_m}\left(1 - e^{-\frac{St_m L_c}{L_t}}\right) - \left(\frac{\varphi}{n+St_m}\right)\left(1 - e^{-\frac{(n+St_m)L_c}{L_t}}\right)\right)\sin(\alpha)$$

(4.20)

Length scales for HHVC and VHVC orientations are given in Fig. 4.2.

HHVC:

$$I_{ss} = \frac{\theta_{hl}}{H}\left(L_1\sin(\alpha) + x + y\sin(\beta) - L_2 + \frac{L_t}{St_m}\left(e^{-\frac{St_m L_c}{L_t}} - 1\right)\right) + \frac{\theta_{cl}}{H}(L_h\sin(\alpha) - L_3 +$$

$$L_4\sin(\alpha)) + \frac{L_h}{2H}\sin(\alpha) \qquad (4.21)$$

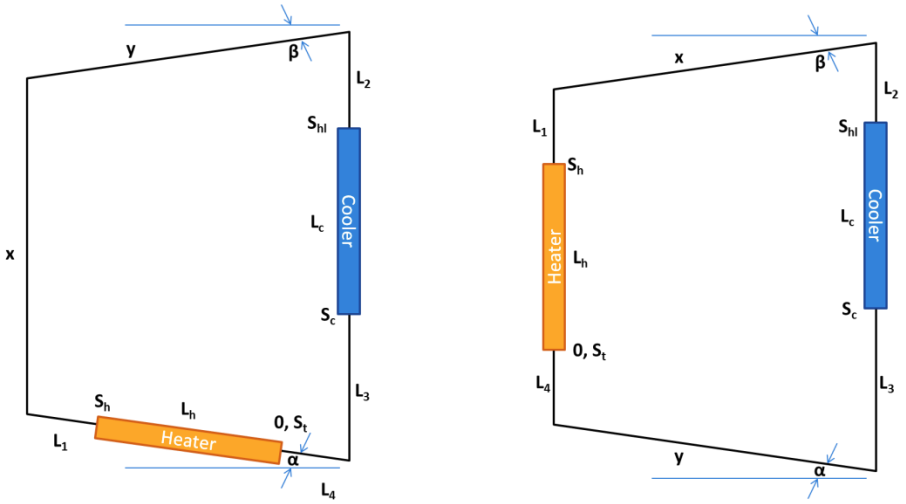

Fig. 4.2 Schematics of HHVC (left) and VHVC orientations showing length scales used in formulation

$$\frac{\bar{I}}{\bar{\omega}} = \frac{\overline{\theta_{cl}}}{\bar{\omega}}\frac{\varphi}{n}\left(1 - e^{-\frac{nL_h}{L_t}}\right)\sin(\alpha)$$

$$+ \frac{\overline{\theta_h}}{\bar{\omega}}\frac{\varphi}{n}\left(\left(1 - e^{-\frac{nL_1}{L_t}}\right)\sin(\alpha) + \left(e^{-\frac{nL_1}{L_t}} - e^{-\frac{n(L_1+x)}{L_t}}\right)\right.$$

$$\left. + \left(e^{-\frac{n(L_1+x)}{L_t}} - e^{-\frac{n(L_{hl}-L_2)}{L_t}}\right)\sin(\beta) + \left(e^{-\frac{nL_{hl}}{L_t}} - e^{-\frac{n(L_{hl}-L_2)}{L_t}}\right)\right)$$

$$+ \frac{\overline{\theta_{hl}}}{\bar{\omega}}\frac{\varphi}{n+St_m}\left(e^{-\frac{(n+St_m)L_c}{L_t}} - 1\right) + \frac{\bar{\theta}_c}{\bar{\omega}}\frac{\varphi}{n}\left(\left(e^{-\frac{nL_3}{L_t}} - 1\right) + \left(e^{-\frac{nL_3}{L_t}} - e^{\frac{nL_{cl}}{L_t}}\right)\sin(\alpha)\right)$$

$$+ \frac{L_t}{L_h}\frac{1}{n}\left(\frac{\varphi}{n}\left(1 - e^{-\frac{nL_h}{L_t}}\right) - \frac{L_h}{H}\right)\sin(\alpha)$$

$$- \frac{St_m\theta_{hl}}{n}\left(\frac{\varphi}{St_m}\left(1 - e^{-\frac{St_mL_c}{L_t}}\right) + \frac{\varphi}{n+St_m}\left(e^{-\frac{(n+St_m)L_c}{L_t}} - 1\right)\right) \quad (4.22)$$

VHVC:

$$I_{ss} = \frac{\theta_{hl}}{H}\left(L_1 + xsin(\beta) - L_2 + \frac{L_t}{St_m}\left(e^{-\frac{St_mL_c}{L_t}} - 1\right)\right) + \frac{\theta_{cl}}{H}(L_h - L_3 + L_4 + y\sin(\alpha)) + \frac{L_h}{2H} \quad (4.23)$$

$$\frac{\bar{I}}{\bar{\omega}} = \frac{\overline{\theta_{cl}}}{\bar{\omega}}\frac{\varphi}{n}\left(1 - e^{-\frac{nL_h}{L_t}}\right)$$
$$+ \frac{\overline{\theta_h}}{\bar{\omega}}\frac{\varphi}{n}\left(\left(1 - e^{-\frac{nL_1}{L_t}}\right) + \left(e^{-\frac{nL_1}{L_t}} - e^{-\frac{n(L_1+x)}{L_t}}\right)\sin(\beta) - \left(e^{-\frac{n(L_1+x)}{L_t}} - e^{-\frac{nL_{hl}}{L_t}}\right)\right)$$
$$+ \frac{\overline{\theta_{hl}}}{\bar{\omega}}\frac{\varphi}{n + St_m}\left(e^{-\frac{(n+St_m)L_c}{L_t}} - 1\right)$$
$$+ \frac{\overline{\theta_c}}{\bar{\omega}}\frac{\varphi}{n}\left(\left(e^{-\frac{nL_3}{L_t}} - 1\right) + \left(e^{-\frac{nL_3}{L_t}} - e^{-\frac{n(L_3+y)}{L_t}}\right)\sin(\alpha) + \left(e^{-\frac{n(L_3+y)}{L_t}} - e^{-\frac{nL_{cl}}{L_t}}\right)\right)$$
$$+ \frac{L_t}{L_h}\frac{1}{n}\left(\frac{\varphi}{n}\left(1 - e^{-\frac{nL_h}{L_t}}\right) - \frac{L_h}{H}\right)$$
$$- \frac{St_m\theta_{hl}}{n}\left(\frac{\varphi}{St_m}\left(1 - e^{-\frac{St_mL_c}{L_t}}\right) + \frac{\varphi}{n + St_m}\left(e^{-\frac{(n+St_m)L_c}{L_t}} - 1\right)\right)$$

(4.24)

4.3. Determination of stability behaviour from characteristic equation

The form of the perturbation functions (Eq. 4.25) chosen for arriving at the above formulation, facilitates the decision of stability based on the nature of roots.

$$\omega' = \bar{\omega}\varepsilon e^{n\tau};\ \theta' = \overline{\theta(S)}\varepsilon e^{n\tau} \tag{4.25}$$

The characteristic equation (Eq. 4.1) is in frequency domain with 'n' denoting the complex frequency. Being a transcendental equation, infinite number of roots can exist for this equation, for a given Grashof number (Gr_m) and Stanton number (St_m). Then the solution of the governing equation at a given operating condition will be of the form

$$\omega(\tau) = \omega_{ss} + \overline{\omega}\,(C_1e^{n_1\tau} + C_2e^{n_2\tau} + C_3e^{n_3\tau} + \cdots) \tag{4.26}$$

$$\theta(S,\tau) = \theta_{ss}(S) + \overline{\theta(S)}\,(D_1e^{n_1\tau} + D_2e^{n_2\tau} + D_3e^{n_3\tau} + \cdots) \tag{4.27}$$

where, C_1, C_2, C_3… and D_1, D_2, D_3… are integration constants to be determined from initial conditions

$$if\ n = a + ib\ then\ e^{n\tau} = e^{a\tau}\big(cos(b\tau) + isin(b\tau)\big) \tag{4.28}$$

where, a and b are arbitrary real numbers and $i = \sqrt{-1}$. From Eq. 4.28, it is clear that if any of these roots n_1, n_2, n_3 ... is having positive real part ($a > 0$), then the solution for flow rate as well as temperature increases with time continuously. And corresponding value of imaginary part b decides the frequency of oscillation in the flow rate and temperature. The overall frequency or wavelength of oscillations depends upon the collective response of all the roots of the characteristic equation. So, NCL is marked as stable if all the roots of the characteristic equation are having negative real parts, neutrally stable if all the roots of the characteristic equation are purely imaginary and unstable if at least one of the roots has positive real part.

The analysis mentioned above requires the determination of all roots of the characteristic equation to comment on stability at given operating conditions. From the complexity of characteristic equation, it is evident that this process is time consuming. One more method is available by use of mapping theorem of complex analysis which is stated as follows [32]

"Let F(s) be a ratio of two polynomials in 's'. Let P is the number of poles and Z is the number of zeros of F(s) that lie inside some closed contour in 's' plane with multiplicity of poles and zeros accounted for. Let the contour be such that it does not pass through any poles or zeros of F(s). This closed contour in the 's' plane is then mapped into F(s) plane as a closed curve. The total number (N) of clockwise encirclements of the origin of F(s) plane, as a representative point 's' traces the entire contour in the clockwise direction, is equal to Z-P."

In this theorem, pole of F(s) means the zero of the denominator of F(s) and zero of F(s) means the zero of numerator of F(s).

In stability analysis of control systems, Nyquist has proposed a criterion based on the mapping theorem to check the existence of zeros of a complex variable function in the right half of 's' plane graphically. According to this criterion if a complex variable function F(s) have 'k' number of poles in the right half of 's' plane and $\lim_{n\to\infty} F(s) = \text{constant}$, then for the absence of zeros of F(s) in the right half of 's' plane the $F(i\omega)$ locus, as ω varies from $-\infty$ to $+\infty$, must encircle the origin 'k' times in counter clockwise direction. This is called Nyquist criteria. Using this criteria stability of NCL at a given operating condition can be determined graphically with less computational cost.

To apply Nyquist criteria, the poles of the characteristic equation on the right half of 's' plane are to be determined. It can be easily observed that the denominator of characteristic equation is

$$n(e^{n+\frac{St_m L_c}{L_t}} - 1) \tag{4.29}$$

Writing $n\ as\ n_R + in_I$ and substituting in the above expression

$$(n_R + in_I)\left(e^{n_R + in_I + \frac{St_m L_c}{L_t}} - 1\right) = 0 \tag{4.30}$$

The roots of the above equation becomes either

$$n = n_R + in_I = 0 \rightarrow n_R = 0, n_I = 0 \tag{4.31}$$

or

$$e^{\frac{St_m L_c}{L_t} + n_R}\left(\cos(n_I) + isin(n_I)\right) = 1 \tag{4.32a}$$

$$e^{\frac{St_m L_c}{L_t} + n_R}.\cos(n_I) = 1 \quad \text{and} \quad \sin(n_I) = 0 \tag{4.32b}$$

To satisfy both equalities in Eq. 4.32b

$$n_I = r\pi \ \ (r = 0, 2, 4, 6, \dots) \text{ and } n_R = -\frac{St_m L_c}{L_t} < 0 \tag{4.33}$$

From the above result, it is evident that the characteristic equation does not have any poles in the right half of the 's' plane. So, for stability of NCL the locus of characteristic function $F(i\omega)$, as ω varies from $-\infty$ to $+\infty$, should not encircle the origin in clockwise direction.

Observing the complete formulation of LSA by Vijayan *et al.*, it can be pointed out that the stability behaviour a rectangular NCL depends on Gr_m, St_m, orientation of heater and cooler, flow direction and geometric parameters. Once the loop geometry and orientation is fixed for analysis then the operating conditions are represented solely by Gr_m and St_m. So, the stability maps are plotted on Gr_m-St_m space.

On the basis of above analysis, three different algorithms have been formulated for determining the stability behaviour. They are summarized below –

Algorithm 1:

1. Take Gr_m and St_m corresponding to the operating conditions.
2. Solve the characteristic equation numerically to determine the roots
3. Check whether any of these roots is having positive real part. If yes, then the NCL is unstable at given operating conditions.
4. If all roots are purely imaginary then the NCL is neutrally stable under the given conditions.
5. If all roots are having negative real parts then the NCL is stable under given conditions.

Algorithm 2:

1. Take Grashof number and Stanton number corresponding to the operating conditions.
2. Generate a table of values of the characteristic function *F* while varying *n* from –Ki to +Ki where K is sufficiently large real number.
3. Plot the imaginary part of the function values F_I against the real part of the function values F_R in the sequence of *n* value. (Nyquist plot)
4. Count the number of clockwise encirclements 'C', done by this plot around the origin.
5. If C>0, unstable, C=0 stable

Algorithm 3:

1. Take Grashof number corresponding to the operating conditions.
2. Substitute $n = iy$ and solve for Stanton number and y using any non-linear system solver (like trust-region dogleg algorithm) or graphical method. This Stanton number (let us say t_{mn}) corresponds to neutrally stable condition.
3. Determine the stability behaviour of NCL at $St_{m1} < St_{mn}$, $St_{m2} = St_{mn}$ $and\ St_{m3} > St_{mn}$ using Method 2. If stability behaviour reverses from $St_{m1}\ to\ St_{m3}$ then St_{mn} is confirmed as neutral Stanton number.
4. Plot all the confirmed neutral Stanton numbers in $Gr_m - St_m$ space.

A computer code has been developed based on the algorithm 1 described above. Provided the orientation, flow regime and the ranges of Grashof number and Stanton number, it is able to generate a stability map depicting the regions of stable and unstable behaviour.

In this code, roots of the characteristic equation are solved by a two-step procedure. In first step, locations of possible existence of root are determined by a linear search algorithm in the complex plane. And in the second step, all these locations are traced with Regula-Falsi

method to confirm the existence and to determine the value of the root with required accuracy.

For the purpose of confirming the stability behaviour predicted by the code, algorithm 2 has been used. Nyquist plots have been drawn at required operating conditions and the encirclement of origin has been observed to decide the stability behaviour at those operating conditions.

4.4. Validation of linear stability analysis code

Using the computer code described in previous section, stability maps have been generated for the water based natural circulation loop of Vijayan *et al.* [22] and compared with the stability behaviour predicted by them. Their experimental loop is a rectangular one with top and bottom legs horizontal. So, angles α and β are kept zero in analysis. Figs. 4.3 to 4.5 show the comparison of stability maps generated by code with published work for different orientations. For friction factor evaluation, the same correlations used by Vijayan *et al.* have been used for validation purpose. As shown, code is able to predict the stability behaviour

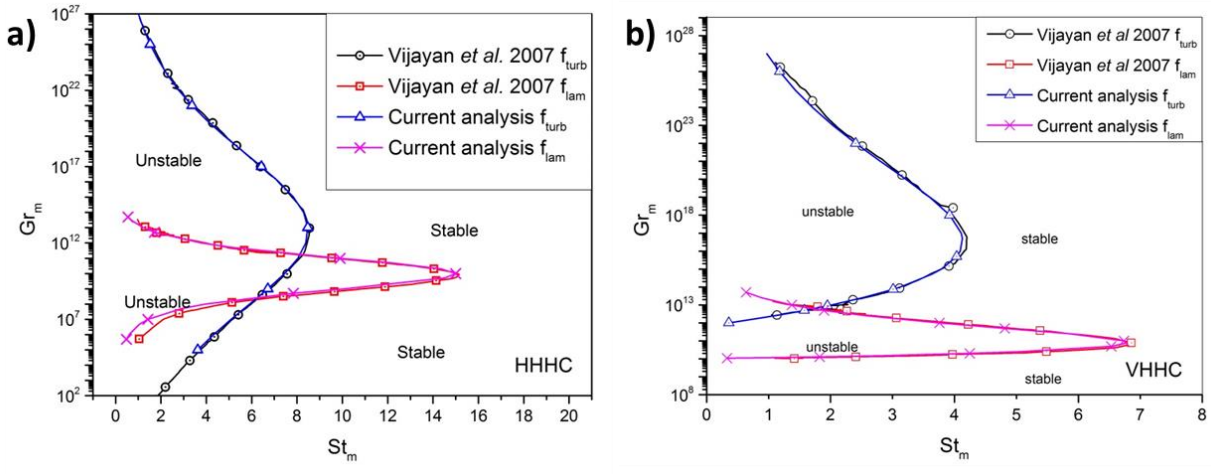

Fig. 4.3 Comparison of Stability maps for a) HHHC b) VHHC generated by code with published data of Vijayan *et al.* [22]

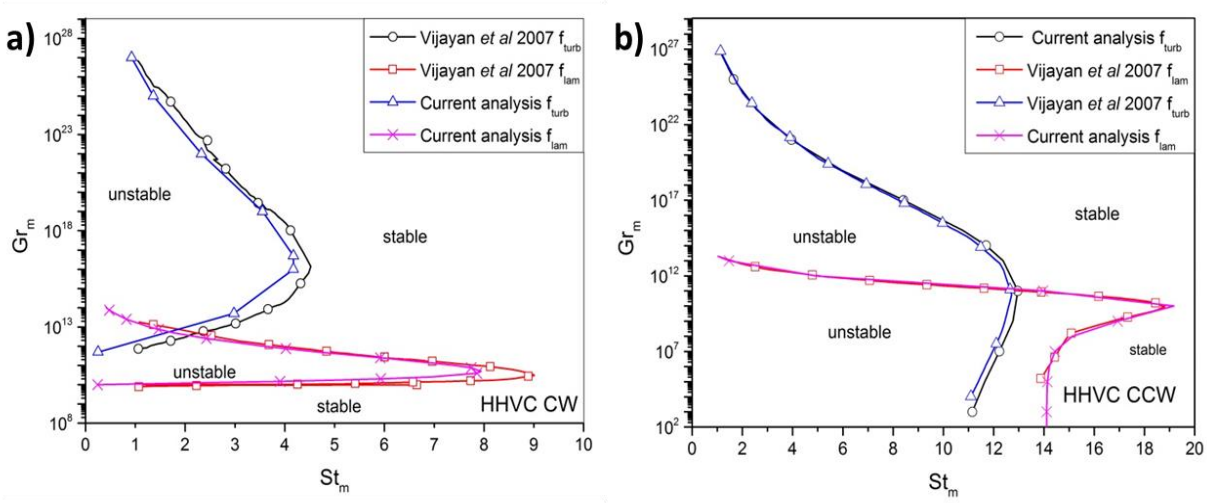

Fig. 4.4 Comparison of Stability maps for a) HHVC CW b) HHVC CCW generated by code with published data of Vijayan *et al.* [22]

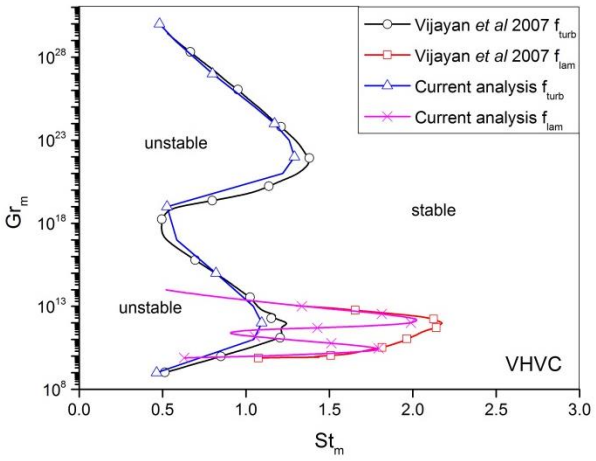

Fig. 4.5 Comparison of Stability maps for VHVC generated by code with published data of Vijayan *et al.* [22]

with good agreement with published work in HHHC, VHHC, HHVC clockwise (CW), HHVC Counter clockwise (CCW) orientations.

In VHVC orientation, shown in Fig. 4.5, predicted stability behaviour in turbulent zone is in agreement with published work. But, in laminar zone code prediction in slightly different in Gr_m range of 10^{10} to 10^{13}. Since the code is able to predict the behaviour in turbulent zone with good agreement, its predictions in laminar zone have not been suspected.

The performance of the computer code has been proven by above validation study. Since the validity of laminar and turbulent friction correlations is limited to certain range of Reynolds numbers, which was ignored in the theoretical analysis of Vijayan *et al.* [22], Churchill's [7] correlation in the modified form [27] has been used in subsequent analysis. This correlation has been reproduced from Ruiz *et al.* [27] in Chapter 2 Eq. 2.7. A stability map has been derived for the same loop which has been analysed in validation study with this friction correlation and given in Fig. 4.6. As expected, the stability boundary coincides with earlier published result in fully laminar (for $Gr_m<10^{11}$) and turbulent (for $Gr_m>10^{13}$) flow regimes and a smooth transition is obtained between them. Similar result is expected to be observed with other orientations also.

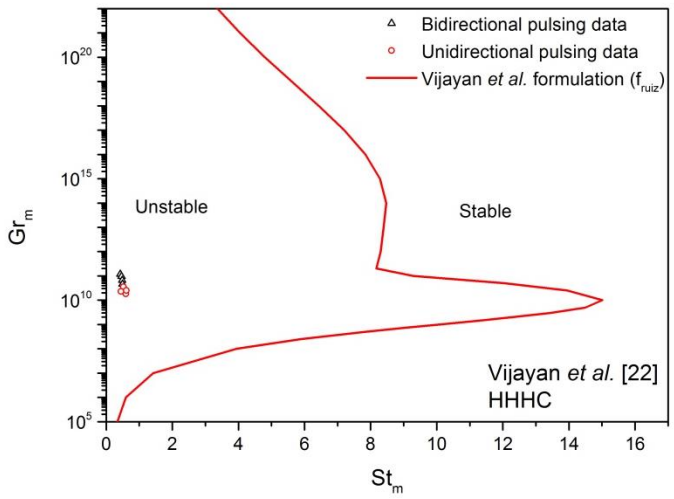

Fig. 4.6 Stability map derived by LSA of Vijayan *et al.* [22] 26.9 mm loop in HHHC orientation using Ruiz's form of Churchill's friction correlation

With the confidence given by above validation study, the computer code has been applied to MSNCL geometry in all four orientations. The stability maps for all orientations are shown in Figs. 4.7 and 4.8 along with experimental data.

It can be observed from these stability maps that, some or all of the stable data obtained from experiments have been determined to be unstable by this formulation, except in case of VHVC orientation. As discussed in Chapter 2, this was the situation in most of the attempts by various researchers using this formulation. Since, the unstable experimental data could be predicted unstable by the same formulation, it was concluded that these predictions are conservative. But, without extensive validation with sufficient experimental data, conclusions cannot be drawn.

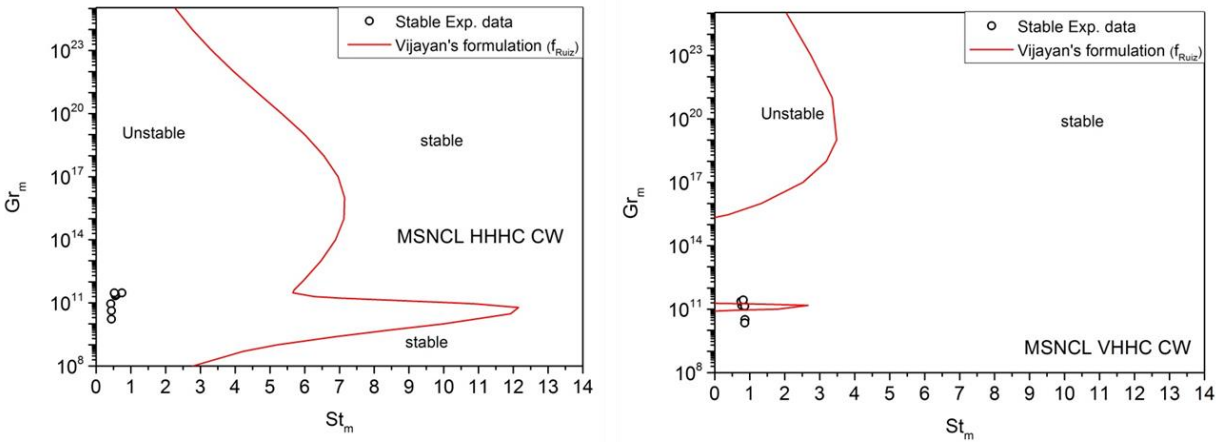

Fig. 4.7 The stability maps obtained for MSNCL in HHHC (left) and VHHC orientations along with respective experimental data

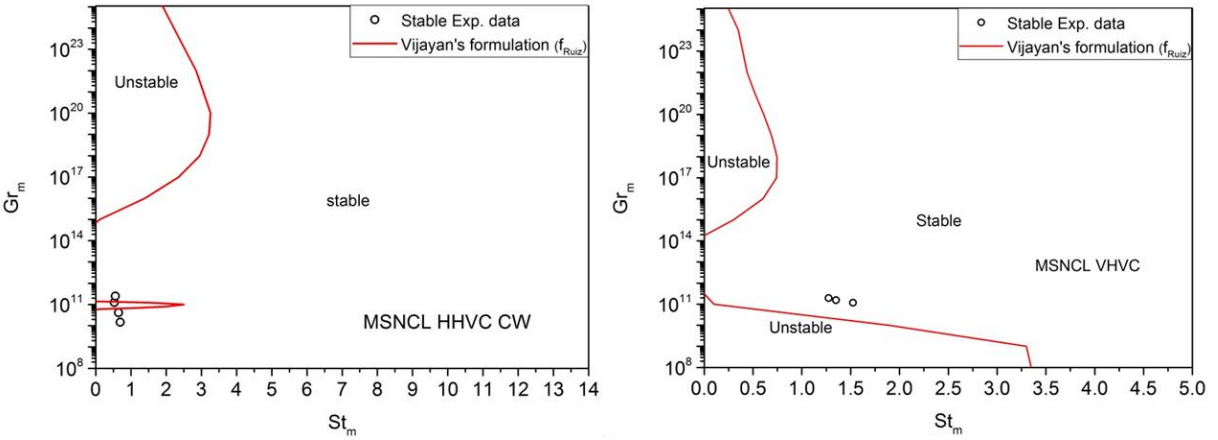

Fig. 4.8 The stability maps obtained for MSNCL in HHVC (left) and VHVC orientations along with respective experimental data

4.5. Inclusion of local pressure losses

Vijayan *et al.* [22] suggested that the local pressure losses can be taken in to account in terms of equivalent length. But, so far this facility provided virtually by this formulation has not been used by any researcher as per our observation. So, minding the evidence provided by Misale *et al.* [16, 18] that the local pressure drops can stabilize the NCLs, it has been decided to analyse the MSNCL stability including its local pressure losses.

Local pressure losses for MSNCL

MSNCL has four corners in the natural circulation flow path including two standard elbows and two Tees used as elbows. For standard elbows, a local pressure loss coefficient of 0.75 has been taken [8]. For Tees used as elbows, it is suggested [8] to use 1.0 for flow entering from either branch or run. Hence, the total pressure loss coefficient has been taken as 3.5.

Since, the local pressure losses are considered in terms of local loss coefficient 'K' instead of equivalent length, the characteristic equation becomes

$$n - \frac{1}{\hat{\omega}} . \frac{Gr_m}{Re_{ss}^3} \oint \hat{\theta}_f dZ + \frac{pL_t(2-b)}{2DRe_{ss}^b} + K = 0 \qquad (34)$$

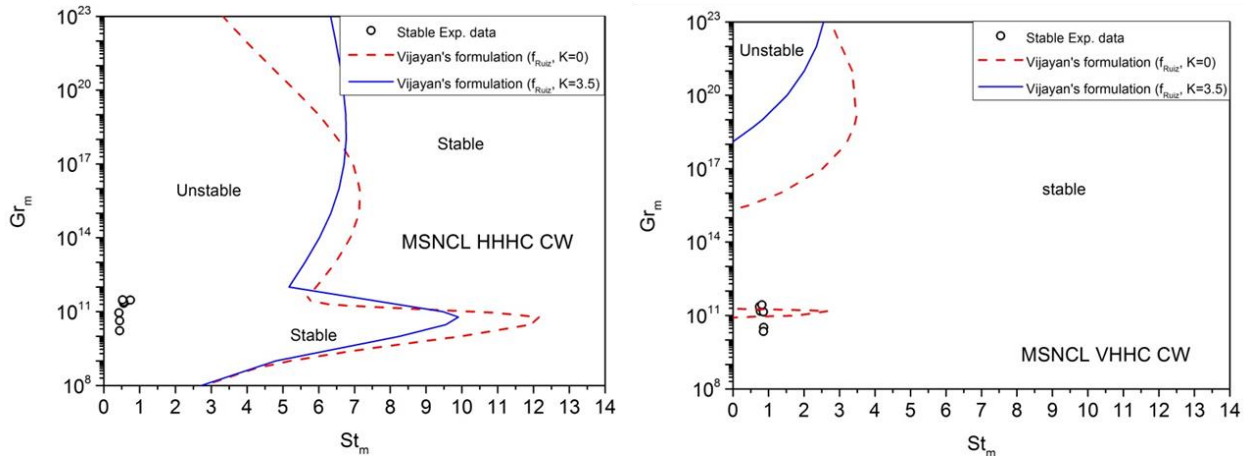

Fig. 4.9 Comparison of stability maps of MSNCL, generated by LSA, with and without local pressure losses along with experimental data in HHHC (left) and VHHC orientations

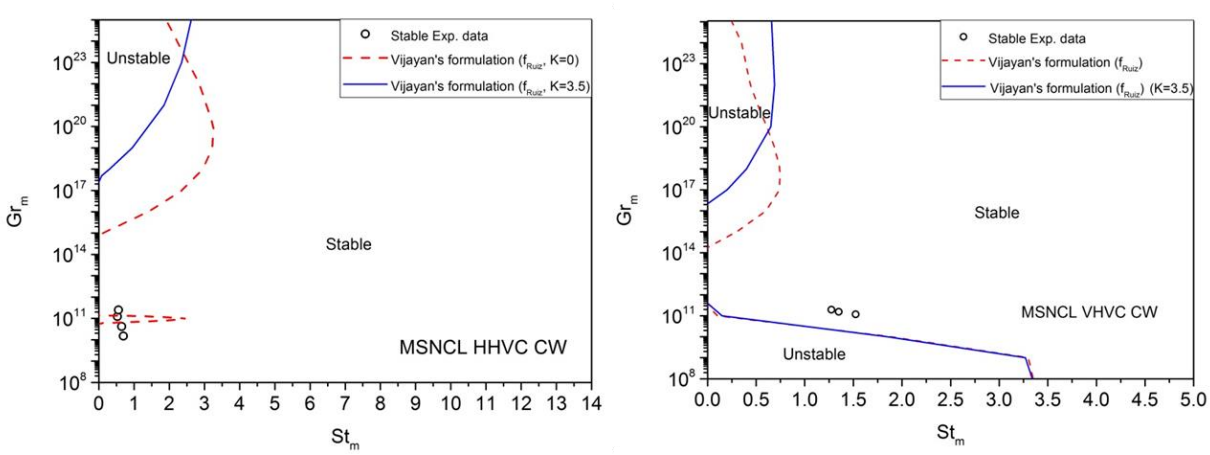

Fig. 4.10 Comparison of stability maps of MSNCL, generated by LSA, with and without local pressure losses along with experimental data in HHVC (left) and VHVC orientations

In the derivation of above equation, K has been assumed to be invariant of flow regime. Stability maps have been generated again with local pressure losses to quantify theoretically effect of local pressure losses on stability of NCLs for the first time and depicted in Figs. 4.9 and 4.10.

It can be observed that local pressure losses have significant effect on stability behaviour of NCLs. In laminar region, local pressure losses showed significant stabilization effect whereas in turbulent regime, they showed mixed effect. In near turbulent region, they showed stabilization effect while in fully turbulent region, destabilization was shown. The shift in the stability boundary towards lower St_m values has got apparently verified against the experimental conclusion of Misale *et al.* [18] which says that stabilization at any power requires a minimum local pressure drop.

It is apparent from figs. 4.9 and 4.10 that inclusion of local pressure losses improved the prediction of stability behaviour. However, the predictions in HHHC orientation are not improved to acceptable levels. Owing to the complex nature of natural circulation, there can be various reasons for this inaccuracy, main reason being the simplifying assumptions taken.

Other reasons include multidimensional nature of flow, existence of conditionally stable zones and hysteresis. These aspects have been under investigation by various authors as discussed in Chapter 2, but definitive conclusions have not been arrived at. This problem is addressed in next chapter by deriving an improved model for LSA.

4.6. Concluding remarks

In this chapter, the linear stability analysis model of Vijayan *et al.* [22] has been investigated for its accuracy in predicting the stability behaviour of MSNCL. The main conclusions are,

1. LSA model of Vijayan *et al.* is predicting stable operating conditions also as unstable, especially in case of HHHC orientation, despite the consideration of local pressure losses.

2. A detailed model considering important phenomena like wall thermal inertia, variable internal heat transfer coefficient and heat losses etc. should be formulated.

CHAPTER 5

An Improved Formulation for Linear Stability Analysis of MSNCL for SHF/LH Case

5.1. Improvements undertaken over the preliminary model

As evident from the literature and analysis performed by self in previous chapter, the accuracy of theoretical predictions of stability should be improved. It has been done by relaxing the highly impacting assumptions so as to model the physical system as closer to actual case as possible. The choice of assumptions which have to be relaxed has been based on the evidences found on the effect of them on stability behaviour, from experiments of various researchers. The following phenomena have been included in the improvements undertaken in current project envisaging betterment in accuracy of predictions

1. Wall has been modelled to consider the effect of its thermal capacity and conductivity

2. Local pressure losses have been incorporated by 'K' factor

3. Variation of convective heat transfer coefficient between wall inner surface and fluid during flow fluctuations has been modelled

4. Heat transfer from wall outer surface to secondary fluid in cooler has been modelled with finite convective heat transfer coefficient

5. Heat losses from various sections of the loop have been modelled

6. In presence of heat losses, the cooling water temperature (which can be different than ambient temperature) may affect stability. So, it has been incorporated.

5.2. Integral approach in derivation of improved model

It is attractive from research point of view to develop improved model by adding one of the above phenomena at a time to understand the effect of each phenomena on stability behaviour of NCLs. But, from the stand point of application of full pledged model to MSNCL to validate the same, the derivation has been carried out including all the phenomena. Arriving at the final formulation, some sub models have been deducted from the improved model by mathematical manipulation of relevant parameters. This will be discussed in detail in section 5.4.

5.3. Detailed derivation of improved model

5.3.1 Governing equations

Continuity equation:

Let us consider an infinitesimal element of working fluid of length 'ds' where, 's' be the coordinate along the axis of the pipe and γ be the inclination of the element. According to the conservation of mass, the rate of increase of mass of a control volume is due to convection of mass into the CV and production. It can be represented mathematically in differential form for the element in Fig. 5.1 as

$$\frac{\partial(\rho A ds)}{\partial t} = (\rho A u) - \left(\rho A u + \frac{\partial(\rho A u)}{\partial s} ds\right) \tag{5.1}$$

where ρ is the density of the fluid element, A is cross sectional area and u is velocity.

For uniform diameter loops Eq. 5.1 reduces to

$$A ds \frac{\partial \rho}{\partial t} = -A ds \frac{\partial(\rho u)}{\partial s} \tag{5.2}$$

As per Boussinesq approximation, all fluid properties are assumed to be constant except the density in buoyancy term of momentum conservation equation. It results the time derivative of density to vanish in Eq. 5.2 leading to

$$\frac{\partial(\rho u)}{\partial s} = \frac{1}{A}\frac{\partial(w)}{\partial s} = 0 \tag{5.3}$$

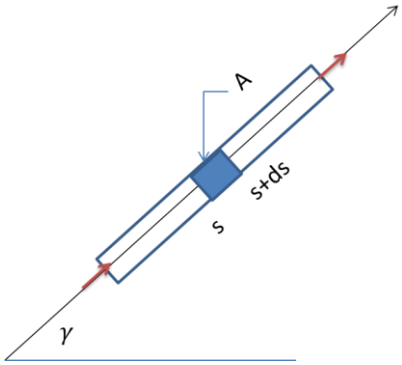

Fig. 5.1 Infinitesimal control volume taken for derivation of governing equations

Momentum equation:

Considering viscous shear stress at wall τ_w, pressure force *p*, gravitational acceleration *g* and local pressure losses per unit length K_i, the momentum conservation in the differential control volume shown in fig.5.1 is

$$\frac{\partial}{\partial t}(\rho A.ds.u) = \rho A|u|.u - \left(\rho A|u|.u + \frac{\partial}{\partial s}(\rho A|u|.u)ds\right) + pA - \left(p + \frac{\partial p}{\partial s}.ds\right)A -$$

$$\tau_w \pi D.ds - (\rho A.ds)g.\sin(\gamma) - K_i.\frac{\rho u^2}{2}.A.ds \tag{5.4}$$

where, D is internal diameter of pipe and γ is angle of inclination of the element as shown in fig. 5.1. Bringing A.ds outside of the integrals which will then be cancelled out in all terms results in

$$\frac{\partial}{\partial t}(\rho u) = -\frac{\partial}{\partial s}(\rho|u|.u) - \frac{\partial p}{\partial s} - \frac{\tau_w \pi D}{A} - \rho g.\sin(\gamma) - K_i.\frac{\rho u^2}{2} \tag{5.5}$$

Introducing mass flow rate $w = \rho A u$ and $\tau_w = \frac{1}{2}\, C_D \rho u^2$ into above equation gives

$$\frac{1}{A}\frac{\partial w}{\partial t} = -\frac{\partial p}{\partial s} - \frac{1}{A^2}\,\frac{\partial}{\partial s}\left(\frac{|w|w}{\rho}\right) - \rho g sin(\gamma) - \frac{2C_D w^2}{D\rho A^2} - K_i.\frac{w^2}{2\rho A^2} \tag{5.6}$$

The drag coefficient in the above equation can be replaced (as done conventionally) by Darcy's friction factor using the relation $f = 4C_D$ resulting in

$$\frac{1}{A}\frac{\partial w}{\partial t} = -\frac{\partial p}{\partial s} - \frac{1}{A^2}\,\frac{\partial}{\partial s}\left(\frac{|w|w}{\rho}\right) - \rho g sin(\gamma) - \frac{f w^2}{2D\rho A^2} - K_i.\frac{w^2}{2\rho A^2} \tag{5.7}$$

It is conventional in literature to perform a closed loop integration of the above equation, to eliminate pressure variable which can significantly reduce the complexity of solution procedure. Additionally, the convective momentum transfer term (second term on right hand side of Eq. 5.7) vanishes.

$$\frac{L_t}{A}\frac{\partial w}{\partial t} = -\oint \rho g sin(\gamma) ds - \left(\frac{f L_t}{D} + K\right)\frac{w^2}{2\rho A^2} \tag{5.8}$$

In the above equation *K* denotes total local pressure losses in the loop. It is assumed that the density is linear function of temperature in buoyancy term (first term on right hand side of Eq. 5.8) as given in Eq. 5.9.

$$\rho = \rho_0\big(1 - \beta(T - T_0)\big) \tag{5.9}$$

Where, ρ_0 and T_0 are reference density and temperature respectively whereas, β is volumetric expansion coefficient of working fluid. Substituting Eq. 5.9 in Eq. 5.8 and simplifying, results in

$$\frac{L_t}{A}\frac{\partial w}{\partial t} = \rho_0 g \beta \oint T.sin(\gamma).ds - \left(\frac{f L_t}{D} + K\right)\frac{w^2}{2\rho_0 A^2} \tag{5.10}$$

It should be noted that in further derivation, the subscript of density is dropped.

Energy conservation equation for working fluid:

Assuming pressure work, change in kinetic energy and viscous dissipation to be negligible the one-dimensional energy equation can be written as

$$\frac{\partial(\rho A ds.C_p T)}{\partial t} = \rho A|u|.C_p T - \left(\rho A|u|.C_p T + \frac{\partial}{\partial s}\left(\rho A|u|.C_p T\right)ds\right) + q_c A - \left(q_c + \frac{\partial q_c}{\partial s}ds\right)A + h_i \pi D(T_{wi} - T).ds \quad (5.11)$$

where, C_p and T are specific heat capacity and temperature of working fluid, q_c is conductive heat transfer in axial direction in working fluid and h_i is convective heat transfer coefficient between piping inner surface and working fluid and T_{wi} is piping inner surface temperature.

After quick simplification by dividing with $A.ds$ term on both sides of the above equation and using the Fourier's law of heat conduction for q_c, we obtain energy equation in terms of mass flow rate as

$$\frac{\partial(T)}{\partial t} = -\frac{w}{\rho A}\frac{\partial T}{\partial s} + \frac{1}{\rho C_p}\frac{\partial}{\partial s}\left(k\frac{\partial T}{\partial s}\right) + \frac{h_i P(T_{wi} - T)}{\rho A C_p} \quad (5.12)$$

Energy conservation in piping:

In order to consider the radial conduction of heat in the piping and to determine inner and outer surface temperature separately, energy equation is written separately for inner volume and outer volume considering the split, half way along thickness as depicted in Fig. 5.2.

For inner shell energy balance is written as

$$\frac{\partial(\rho_w A_1 ds.C_{pw} T_{wi})}{\partial t} = q_{cw}A_1 - \left(q_{cw} + \frac{\partial q_{cw}}{\partial s}ds\right)A_1 - h_i \pi D(T_{wi} - T).ds + \frac{T_{wo} - T_{wi}}{R_w}.ds \quad (5.13)$$

Where, C_{pw} is specific heat capacity of piping material, A_1 is cross sectional area of inner shell and R_w is thermal conduction resistance in radial direction given per unit length. They are given by following expressions.

$$A_1 = \frac{\pi}{4}(D_1^2 - D^2);\ \ D_1 = D + t_w \tag{5.14}$$

$$R_w = \frac{\ln\left(\frac{D_2}{D}\right)}{2\pi k_w}; D_2 = D + 2t_w \tag{5.15}$$

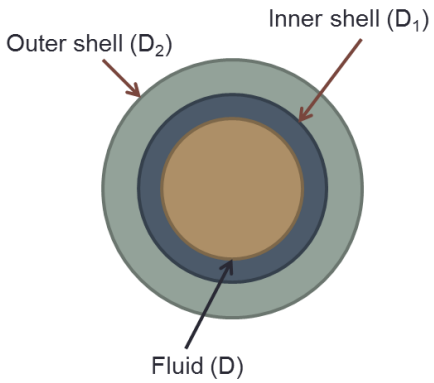

Fig. 5.2 Schematic showing geometry of piping wall considered with inner and outer shells

A quick simplification of Eq. 5.13 using Fourier's law of conduction and dividing all the terms with volume of the element gives

$$\frac{\partial(T_{wi})}{\partial t} = \frac{1}{\rho_w C_{pw}} \frac{\partial}{\partial s}\left(k_w \frac{\partial T_{wi}}{\partial s}\right) - \frac{h_i P(T_{wi} - T)}{A_1 \rho_w C_{pw}} + \frac{T_{wo} - T_{wi}}{R_w \rho_w C_{pw} A_1} \tag{5.16}$$

The energy conservation equation for outer shell is slightly different than inner shell due to the different boundary phenomena at different sections in loop. It is represented as

$$\frac{\partial(\rho_w A_2 ds. C_{pw} T_{wo})}{\partial t} = q_{cw} A_2 - \left(q_{cw} + \frac{\partial q_{cw}}{\partial s} ds\right) A_2 - \frac{T_{wo} - T_{wi}}{R_w}. ds + Q_b. ds \tag{5.17}$$

where, $A_2 = \frac{\pi}{4}(D_2^2 - D_1^2)$ and Q_b is boundary heat transfer which is given as

$$Q_b = \begin{cases} h_o(T_{amb} - T_{wo})P_2 + qP_2 & Heater \\ h_o(T_{amb} - T_{wo})P_2 & piping \\ h_o(T_s - T_{wo})P_2 & cooler \end{cases} \quad (5.18)$$

Where, h_o and q are heat transfer coefficient from outer surface of piping to secondary fluid in cooler and heat flux at heater respectively, whereas T_s is secondary side fluid temperature in cooler. In case of piping and heater, T_{amb} and h_o are ambient temperature and equivalent heat loss coefficient respectively.

Substituting the above relation in Eq. 5.17 and simplifying, in the same way as done for Eq. 5.13, results in

$$\frac{\partial(T_{wo})}{\partial t} = \frac{1}{\rho_w C_{pw}} \frac{\partial}{\partial s}\left(k_w \frac{\partial T_{wo}}{\partial s}\right) - \frac{T_{wo} - T_{wi}}{R_w \rho_w C_{pw} A_2} + \frac{Q_b}{A_2 \rho_w C_{pw}} \quad (5.19)$$

5.3.2 Non-dimensionalization of governing equations:

The Governing equations derived in last section are summarized as follows neglecting the axial heat conduction in working fluid and in piping.

$$\frac{\partial(w)}{\partial s} = 0 \quad (5.20)$$

$$\frac{L_t}{A}\frac{\partial w}{\partial t} = \rho_0 g \beta \oint T.sin(\gamma).ds - \left(\frac{f L_t}{D} + K\right)\frac{w^2}{2\rho_0 A^2} \quad (5.21)$$

$$\frac{\partial(T)}{\partial t} = -\frac{w}{\rho A}\frac{\partial T}{\partial s} + \frac{h_i P(T_{wi} - T)}{\rho A C_p} \quad (5.22)$$

$$\frac{\partial(T_{wi})}{\partial t} = -\frac{h_i P(T_{wi} - T)}{A_1 \rho_w C_{pw}} + \frac{T_{wo} - T_{wi}}{R_w \rho_w C_{pw} A_1} \quad (5.23)$$

$$\frac{\partial(T_{wo})}{\partial t} = -\frac{T_{wo} - T_{wi}}{R_w \rho_w C_{pw} A_2} + \frac{Q_b}{A_2 \rho_w C_{pw}} \quad (5.24)$$

$$Q_b = \begin{cases} h_o(T_{amb} - T_{wo})P_2 + qP_2 & Heater \\ h_o(T_{amb} - T_{wo})P_2 & piping \\ h_o(T_s - T_{wo})P_2 & cooler \end{cases} \quad (5.25)$$

It can be observed that there are numerous parameters which can affect the thermal hydraulic behaviour of natural circulation loop. To reduce the total number of independent parameters to be studied, non-dimensionalization is conventionally sought in literature which will be adopted here also. The following scales are utilized for the purpose.

$$\omega = \frac{w}{w_{ss}}; S = \frac{s}{H}; \tau = \frac{tw_{ss}}{\rho A L_t}; \theta_i = \frac{T_i - T_{amb}}{\Delta T_{h,ss}} \ (i = f, wi, wo, s); \tag{5.26}$$

Where, w_{ss} and $\Delta T_{h,ss}$ are steady state mass flow rate and temperature rise across heater. Physical time is non-dimensionalized by the time period of circulation of working fluid in the loop in steady state conditions. Height of the loop is taken as length scale.

By direct substitution of the above non-dimensional variables in Eq. 5.20 to 5.24 and rearranging the terms results in

$$\frac{\partial \omega}{\partial S} = 0 \tag{5.27}$$

$$\frac{d\omega}{d\tau} = -\left(\frac{fL_t}{D} + K\right)\frac{\omega^2}{2} + \frac{\rho^2 g \beta H \Delta T_{h,ss} A^2}{w_{ss}^2} \oint \theta_f . \sin(\gamma)\, dS \tag{5.28}$$

$$\frac{\partial \theta_f}{\partial \tau} = -\frac{\omega L_t}{H}\frac{\partial \theta_f}{\partial S} + \frac{h_i P L_t}{w_{ss} C_p}\left(\theta_{wi} - \theta_f\right) \tag{5.29}$$

$$\frac{\partial \theta_{wi}}{\partial \tau} = -\frac{h_i P \rho A L_t}{\rho_w C_{pw} w_{ss} A_1}\left(\theta_{wi} - \theta_f\right) + \frac{\rho A L_t}{w_{ss} R_w \rho_w C_{pw} A_1}\left(\theta_{wo} - \theta_{wi}\right) \tag{5.30}$$

$$\frac{\partial \theta_{wo}}{\partial \tau} = \frac{(\theta_{wi} - \theta_{wo})\rho A L_t}{\rho_w C_{pw} A_2 R_w w_{ss}} - \frac{h_o P_2 \rho A L_t}{\rho_w C_{pw} A_2 w_{ss}}\theta_{wo} \qquad piping \tag{5.31a}$$

$$\frac{\partial \theta_{wo}}{\partial \tau} = \frac{(\theta_{wi} - \theta_{wo})\rho A L_t}{\rho_w C_{pw} A_2 R_w w_{ss}} - \frac{h_o P_2 \rho A L_t}{\rho_w C_{pw} A_2 w_{ss}}\theta_{wo} + \frac{q P_2 \rho A L_t}{\rho_w C_{pw} A_2 w_{ss} \Delta T_{h,ss}} \qquad heater \tag{5.31b}$$

$$\frac{\partial \theta_{wo}}{\partial \tau} = \frac{(\theta_{wi} - \theta_{wo})\rho A L_t}{\rho_w C_{pw} A_2 R_w w_{ss}} - \frac{h_o P_2 \rho A L_t}{\rho_w C_{pw} A_2 w_{ss}}\left(\theta_{wo} - \theta_s\right) \qquad cooler \tag{5.31c}$$

To represent the non-dimensional groups appearing as coefficients in above equations in simple form, following parameters are defined

$$Gr_m = \frac{\rho^2 g \beta D^3 q P_2 L_h H}{A \mu^3 C_p} \tag{5.32}$$

$$Re_{ss} = \frac{4 w_{ss}}{\pi D \mu} \tag{5.33}$$

$$St_{mi} = \frac{4L_t}{D} \frac{\left(\frac{h_i D}{k}\right)}{Re_{ss} Pr} \tag{5.34}$$

$$St_{mo} = \frac{4L_t}{D} \frac{\left(\frac{h_o D_2}{k}\right)}{Re_{ss} Pr} \tag{5.35}$$

$$\xi = \frac{4L_t}{D} \frac{1}{Re_{ss} Pr} \frac{\overline{k}}{\overline{R}_w} \tag{5.36}$$

$$\overline{\rho} = \frac{\rho_w}{\rho}; \overline{k} = \frac{k_w}{k}; \overline{C}_p = \frac{C_{pw}}{C_p}; \overline{R}_w = R_w k_w \pi = \frac{1}{2} \ln\left(1 + \frac{2t_w}{D}\right); \varphi = \frac{L_t}{H}; \tag{5.37}$$

The Eqs. 5.27 to 5.31 can be rewritten in terms of above non-dimensional parameters as

$$\frac{\partial \omega}{\partial S} = 0 \tag{5.38}$$

$$\frac{d\omega}{d\tau} = -\left(\frac{f L_t}{D} + K\right) \frac{\omega^2}{2} + \frac{Gr_m}{Re_{ss}^3} \oint \theta_f . \sin(\gamma)\, dS \tag{5.39}$$

$$\frac{\partial \theta_f}{\partial \tau} = -\omega \varphi \frac{\partial \theta_f}{\partial S} + St_{mi} \left(\theta_{wi} - \theta_f\right) \tag{5.40}$$

$$\frac{\partial \theta_{wi}}{\partial \tau} = -St_{mi} \frac{A}{A_1} \frac{1}{\overline{\rho} \overline{C}_p} \left(\theta_{wi} - \theta_f\right) + \xi \frac{1}{\overline{\rho} \overline{C}_p} \frac{A}{A_1} \left(\theta_{wo} - \theta_{wi}\right) \tag{5.41}$$

$$\frac{\partial \theta_{wo}}{\partial \tau} = \xi \frac{1}{\overline{\rho} \overline{C}_p} \frac{A}{A_2} (\theta_{wi} - \theta_{wo}) - St_{mo} \frac{A}{A_2} \frac{1}{\overline{\rho} \overline{C}_p} \theta_{wo} \qquad piping \tag{5.42a}$$

$$\frac{\partial \theta_{wo}}{\partial \tau} = \xi \frac{1}{\overline{\rho} \overline{C}_p} \frac{A}{A_2} (\theta_{wi} - \theta_{wo}) - St_{mo} \frac{A}{A_2} \frac{1}{\overline{\rho} \overline{C}_p} \theta_{wo} + \frac{L_t}{L_h} \frac{A}{A_2} \frac{1}{\overline{\rho} \overline{C}_p} \qquad heater \tag{5.42b}$$

$$\frac{\partial \theta_{wo}}{\partial \tau} = \xi \frac{1}{\overline{\rho}\overline{C}_p} \frac{A}{A_2} (\theta_{wi} - \theta_{wo}) - St_{mo} \frac{A}{A_2} \frac{1}{\overline{\rho}\overline{C}_p} (\theta_{wo} - \theta_s) \qquad cooler \qquad (5.42c)$$

It should be noted that St_{mo} definition involves thermal conductivity, Reynolds number and Prandtl number of working fluid.

5.3.3 Steady state solution

For stability analysis in frequency domain, the transient governing equations derived above are perturbed from theoretical steady state at a given set of operating conditions. To obtain steady state solution the above governing equations are solved without time derivatives as described below

Keeping the transient terms in Eqs. 5.42a to 5.42c zero, the wall outer temperature can be expressed in terms of wall inner temperature as follows

$$\theta_{wo} = \frac{\xi \theta_{wi} + \frac{L_t}{L_h}}{\xi + St_{mo}} \qquad heater \qquad (5.43a)$$

$$\theta_{wo} = \frac{\xi \theta_{wi}}{\xi + St_{mo}} \qquad piping \qquad (5.43b)$$

$$\theta_{wo} = \frac{\xi \theta_{wi} + St_{mo} \theta_s}{\xi + St_{mo}} \qquad cooler \qquad (5.43c)$$

The above relations are substituted in the steady state form of Eq. 5.41 to obtain relation between inner temperature of wall and fluid temperature

$$\theta_{wi} = \left(St_{mi} \theta_f + \xi \left(\frac{\frac{L_t}{L_h}}{\xi + St_{mo}} \right) \right) \div \left(St_{mi} + \xi \left(\frac{St_{mo}}{\xi + St_{mo}} \right) \right) \qquad heater \qquad (5.44a)$$

$$\theta_{wi} = \left(St_{mi} \theta_f \right) \div \left(St_{mi} + \xi \left(\frac{St_{mo}}{\xi + St_{mo}} \right) \right) \qquad piping \qquad (5.44b)$$

$$\theta_{wi} = \left(St_{mi}\theta_f + \xi\left(\frac{St_{mo}\,\theta_s}{\xi + St_{mo}}\right)\right) \div \left(St_{mi} + \xi\left(\frac{St_{mo}}{\xi + St_{mo}}\right)\right) \qquad cooler \tag{5.44c}$$

Finally these relations are substituted in steady state energy equation of fluid

$$\frac{\partial\theta_f}{\partial S} = \frac{1}{\omega\varphi}\left(\theta_{wi} - \theta_f\right)St_{mi} \tag{5.45}$$

$$\frac{\partial\theta_f}{\partial S} + \frac{St_{mi}}{\omega\varphi}\left(\frac{\xi\left(\frac{St_{mo}}{\xi + St_{mo}}\right)}{St_{mi} + \xi\left(\frac{St_{mo}}{\xi + St_{mo}}\right)}\right)\theta_f = \frac{1}{\omega\varphi}\left(\frac{\xi\left(\frac{L_t/L_h}{\xi + St_{mo}}\right)St_{mi}}{St_{mi} + \xi\left(\frac{St_{mo}}{\xi + St_{mo}}\right)}\right) \quad heater \tag{5.46a}$$

$$\frac{\partial\theta_f}{\partial S} + \frac{St_{mi}}{\omega\varphi}\left(\frac{\xi\left(\frac{St_{mo}}{\xi + St_{mo}}\right)}{St_{mi} + \xi\left(\frac{St_{mo}}{\xi + St_{mo}}\right)}\right)\theta_f = \frac{1}{\omega\varphi}\left(\frac{\xi\left(\frac{St_{mo}\theta_s}{\xi + St_{mo}}\right)St_{mi}}{St_{mi} + \xi\left(\frac{St_{mo}}{\xi + St_{mo}}\right)}\right) \quad cooler \tag{5.46b}$$

$$\frac{\partial\theta_f}{\partial S} + \frac{St_{mi}}{\omega\varphi}\left(\frac{\xi\left(\frac{St_{mo}}{\xi + St_{mo}}\right)}{St_{mi} + \xi\left(\frac{St_{mo}}{\xi + St_{mo}}\right)}\right)\theta_f = 0 \quad piping \tag{5.46c}$$

It should be noted here that ω is equal to one in steady state. Eqs. 5.46 a and 5.46 b are in the form of linear first order differential equation as shown in Eq. 5.47 with solution defined as Eq. 5.48

$$\frac{dy}{dx} + P(x)y = Q(x) \tag{5.47}$$

$$y = e^{-\int P(x).dx}.\left(\int e^{\int P(x).dx}Q(x).dx + c\right); c = integration\ constant \tag{5.48}$$

Equations 5.46a and 5.46b are solved and following boundary conditions are substituted

$$\text{At } S = 0, \theta_f = \theta_{clf}; \text{ At } S = S_{hl}, \theta_f = \theta_{hlf} \tag{5.49}$$

With above boundary conditions, the temperature distribution in heater and cooler is obtained as

$$\theta_f = \frac{L_t}{L_h}\frac{1}{St_{ml,h}} + \left(\theta_{clf} - \frac{L_t}{L_h}\frac{1}{St_{mo,h}}\right)e^{-\frac{\chi_h S}{\varphi}} \qquad 0 \le S \le S_h \tag{5.50}$$

$$\theta_f = \theta_s + \left(\theta_{hlf} - \theta_s\right)e^{-\frac{\chi_c (S - S_{hl})}{\varphi}} \qquad S_{hl} \le S \le S_c \tag{5.51}$$

Equation 5.46c is directly integrated to obtain temperature distribution in piping. With the boundary conditions below, temperature distributions in hot leg and cold leg are obtained.

$$\text{At } S = S_h, \theta_f = \theta_h; \text{ At } S = S_c, \theta_f = \theta_c \tag{5.52}$$

$$\theta_f = \theta_{hf} e^{-\frac{\chi_{hl}(S - S_h)}{\varphi}} \qquad S_h \le S \le S_{hl} \tag{5.53}$$

$$\theta_f = \theta_{cf} e^{-\frac{\chi_{cl}(S - S_c)}{\varphi}} \qquad S_c \le S \le S_t \tag{5.54}$$

In the above equations

$$\chi_j = \left(\frac{1}{St_{mi,j}} + \frac{1}{\xi} + \frac{1}{St_{mo,j}}\right)^{-1}; j = h, hl, c, cl \tag{5.55}$$

From this expression, it is evident that χ signifies the overall heat transfer coefficient from fluid to the secondary side fluid in cooler or ambient otherwise. Using the temperature continuity as boundary condition between each section, the expressions for $\theta_j (j = h, hl, c, cl)$ can be obtained as follows

$$\theta_{clf} = \frac{\theta_s e^{-\frac{\chi_{cl} L_{cl}}{L_t}}\left(1 - e^{-\frac{\chi_c L_c}{L_t}}\right) + \frac{L_t}{L_h St_{mo,h}}\left(1 - e^{-\frac{\chi_h L_h}{L_t}}\right)e^{-\frac{\chi_{hl} L_{hl} + \chi_c L_c + \chi_{cl} L_{cl}}{L_t}}}{1 - e^{-\frac{\chi_h L_h + \chi_{hl} L_{hl} + \chi_c L_c + \chi_{cl} L_{cl}}{L_t}}} \tag{5.56}$$

$$\theta_{hf} = \frac{L_t}{L_h}\frac{1}{St_{mo,h}}\left(1 - e^{-\frac{\chi_h L_h}{L_t}}\right) + \theta_{clf}e^{-\frac{\chi_h L_h}{L_t}} \tag{5.57}$$

$$\theta_{hlf} = \theta_{hf}e^{-\frac{\chi_{hl} L_{hl}}{L_t}} \tag{5.58}$$

$$\theta_{cf} = \theta_s\left(1 - e^{-\frac{\chi_c L_c}{L_t}}\right) + \theta_{hlf}e^{-\frac{\chi_c L_c}{L_t}} \tag{5.59}$$

Finally to obtain steady state Reynolds number the momentum equation is solved. Assuming the functional relationship between friction factor and Reynolds number as

$$f = \frac{p}{Re^b} \tag{5.60}$$

and that the local pressure loss factor 'K' independent of flow regime, momentum equation in steady state can be written as

$$\frac{p}{(Re_{ss})^b}\frac{L_t}{2D} + \frac{K}{2} = \frac{Gr_m}{(Re_{ss})^3}\oint \theta_{f,ss}dZ \tag{5.61}$$

where, $Z = S.\sin(\gamma)$

the above equation can be rearranged as

$$K.Re_{ss}^3 + \left(\frac{pL_t}{D}\right)Re_{ss}^{3-b} = 2Gr_m \oint \theta_{f,ss}dZ \tag{5.62}$$

The integral in Eq. 5.62 can be evaluate for different orientations of heater and cooler using the steady state temperature distribution given by Eq.5.50, 5.51, 5.53 and 5.54. For HHHC orientation, it is given in Eq. 5.63

$$\oint \theta_{fss} dZ = \theta_{clf}\left(\frac{\phi}{\chi_h}\left(1 - e^{-\frac{\chi_h L_h}{L_t}}\right)\sin(\alpha)\right)$$
$$+ \frac{\theta_{hf}\phi}{\chi_{hl}}\left(\left(1 - e^{-\frac{\chi_{hl} L_1}{L_t}}\right)\sin(\alpha) + \left(e^{-\frac{\chi_{hl} L_1}{L_t}} - e^{-\frac{\chi_{hl}(L_{hl}-L_2)}{L_t}}\right)\right.$$
$$\left. + \left(e^{-\frac{\chi_{hl}(L_{hl}-L_2)}{L_t}} - e^{-\frac{\chi_{hl} L_{hl}}{L_t}}\right)\sin(\beta)\right) + \frac{\theta_{hlf}\phi}{\chi_c}\left(1 - e^{-\frac{\chi_c L_c}{L_t}}\right)\sin(\beta)$$
$$+ \frac{\theta_{cf}\phi}{\chi_{cl}}\left[\left(1 - e^{-\frac{\chi_{cl} L_3}{L_t}}\right)\sin(\beta) + \left(e^{-\frac{\chi_{cl}(L_{cl}-L_4)}{L_t}} - e^{-\frac{\chi_{cl} L_3}{L_t}}\right)\right.$$
$$\left. + \left(e^{-\frac{\chi_{cl}(L_{cl}-L_4)}{L_t}} - e^{-\frac{\chi_{cl} L_{cl}}{L_t}}\right)\sin(\alpha)\right] + \frac{L_t}{L_h St_{mo,h}}\left[\frac{L_h}{H} + \frac{\phi}{\chi_h}\left(e^{-\frac{\chi_h L_h}{L_t}} - 1\right)\right]\sin(\alpha)$$
$$+ \theta_s \sin(\beta)\left[\frac{L_c}{H} + \frac{\phi}{\chi_c}\left(e^{-\frac{\chi_c L_c}{L_t}} - 1\right)\right]$$

(5.63)

Unlike the basic model, the momentum equation cannot be solved analytically to represent Reynolds number as an explicit function of Grashof number and other geometric parameters. It should be noted here that the temperature integral itself is a function of Reynolds number for the reason that heat transfer coefficients are dependent of it. So, the above equation is numerically solved by an iterative procedure to obtain the solution.

5.3.4 Perturbation of governing equations – characteristic equation

The variables ω, θ_j $(j = f, wi, wo)$ in the transient form of governing Eqs. 5.39 to 5.42 are substituted with their perturbed forms given as

$$\omega = \omega_{ss} + \hat{\omega} e^{n\tau} \tag{5.64a}$$

$$\theta_j = \theta_{j,ss} + \hat{\theta_j} e^{n\tau} \; (j = f, wi, wo) \tag{5.64b}$$

Perturbation of continuity equation gives raise to conclusion that the perturbation in the mass flow rate instantaneously appears throughout the loop. In mathematical form it is given as

$$\frac{\partial \hat{\omega}}{\partial S} = 0 \tag{5.65}$$

Characteristic equation is obtained by perturbation of momentum equation and subtracting steady state momentum equation from it.

$$n - \frac{1}{\hat{\omega}} . \frac{Gr_m}{Re_{ss}^3} \oint \hat{\theta}_f dZ + \frac{pL_t(2-b)}{2DRe_{ss}^b} + K = 0 \tag{5.66}$$

To obtain the integral of perturbed temperature, the energy equations for fluid and piping are perturbed and then resulting equations are solved.

Perturbation of the fluid energy equation (Eq. 5.4) results in

$$\frac{\partial}{\partial \tau}\left(\theta_{f,ss} + \hat{\theta}_f e^{n\tau}\right) + (1 + \hat{\omega} e^{n\tau})\varphi \frac{\partial}{\partial S}\left(\theta_{f,ss} + \hat{\theta}_f e^{n\tau}\right) = \left(\theta_{wi,ss} + \hat{\theta}_{wi} e^{n\tau} - \theta_{f,ss} - \hat{\theta}_f e^{n\tau}\right)\left(St_{mi,ss} + B\hat{\omega} e^{n\tau} St_{mi,ss}\right) \tag{5.67}$$

where, $B = \frac{d(Nu_i)}{d(Re)} \frac{Re_{ss}}{Nu_{i,ss}}$ is a parameter to consider the perturbation in internal heat transfer coefficient with the perturbation in flow.

Steady state form of Eq. 5.40 is given as

$$\frac{\varphi}{St_{mi}} \frac{\partial \theta_{f,ss}}{\partial S} = \left(\theta_{wi,ss} - \theta_{f,ss}\right) \tag{5.68}$$

Subtracting Eq. 5.68 from Eq. 5.67 and using Eq. 5.68 for further simplification results in

$$n\hat{\theta}_f + \hat{\omega}\varphi(1 - B)\frac{\partial \theta_{f,ss}}{\partial S} + \frac{\varphi \partial \hat{\theta}_f}{\partial S} = \left(\hat{\theta}_{wi} - \hat{\theta}_f\right) St_{mi,ss} \tag{5.69}$$

Substitution of perturbed variables in the energy equation of inner shell of piping (Eq. 5.19) results in

$$\frac{\partial}{\partial\tau}\left(\theta_{wi,ss}+\hat{\theta}_{wi}e^{n\tau}\right)$$
$$=\left(St_{mi,ss}+B\hat{\omega}e^{n\tau}St_{mi,ss}\right)\frac{A}{A_1}\frac{1}{\overline{\rho}\overline{C}_p}\left(\theta_{f,ss}-\theta_{wi,ss}+\hat{\theta}_f e^{n\tau}-\hat{\theta}_{wi}e^{n\tau}\right)$$
$$+\xi\frac{1}{\overline{\rho}\overline{C}_p}\frac{A}{A_1}\ \left(\theta_{wo,ss}+\hat{\theta}_{wo}e^{n\tau}-\theta_{wi,ss}-\hat{\theta}_{wi}e^{n\tau}\right) \tag{5.70}$$

Subtracting the steady state form of Eq. 5.40 from Eq. 5.70 and rearranging the terms results in

$$n\hat{\theta}_{wi}=-St_{mi,ss}\frac{A}{A_1}\frac{1}{\overline{\rho}\overline{C}_p}\left(\hat{\theta}_{wi}-\hat{\theta}_f\right)-B\hat{\omega}St_{mi,ss}\frac{A}{A_1}\frac{1}{\overline{\rho}\overline{C}_p}\left(\theta_{wi,ss}-\theta_{f,ss}\right)$$
$$+\xi\frac{1}{\overline{\rho}\overline{C}_p}\frac{A}{A_1}\ \left(\hat{\theta}_{wo}-\hat{\theta}_{wi}\right) \tag{5.71}$$

In the similar lines, perturbed energy equations for outer shell of piping can also be derived

$$n\hat{\theta}_{wo}=\xi\frac{1}{\overline{\rho}\overline{C}_p}\frac{A}{A_2}\left(\hat{\theta}_{wi}-\hat{\theta}_{wo}\right)-St_{mo}\frac{A}{A_2}\frac{1}{\overline{\rho}\overline{C}_p}\hat{\theta}_{wo} \tag{5.72}$$

Since the secondary fluid is not modelled, the perturbations in the secondary flow rate or inlet temperature are not perturbed in current analysis.

To evaluate the integral of perturbed temperature in Eq. 5.66, perturbed temperature distribution is determined by solving the Eqs. 5.69, 5.71 and 5.72 in the similar way as solved for steady state temperature distribution. The steps of this derivation are given briefly.

Starting from Eq. 5.72,

$$\hat{\theta}_{wo}=\left(\xi\frac{1}{\overline{\rho}\overline{C}_p}\frac{A}{A_2}\hat{\theta}_{wi}\right)\Big/\left(n+\frac{1}{\overline{\rho}\overline{C}_p}\frac{A}{A_2}\left(\xi+St_{mo,j}\right)\right);\ \ j=h,hl,c,cl \tag{5.73}$$

Since the form of perturbed energy equations is same for all sections, they are simultaneously solved using a subscript *'j'* which avail choice for different heat transfer coefficients (both

inside and outside of piping) in different sections. From Eq. 5.71, with the substitution of Eq. 5.73,

$$n\hat{\theta}_{wi} = -St_{mi,ss}\frac{A}{A_1}\frac{1}{\overline{\rho}\overline{C}_p}\left(\hat{\theta}_{wi} - \hat{\theta}_f\right) - B_j\hat{\omega}St_{mi,ss}\frac{A}{A_1}\frac{1}{\overline{\rho}\overline{C}_p}\left(\theta_{wi,ss} - \theta_{f,ss}\right) + \xi\frac{1}{\overline{\rho}\overline{C}_p}\frac{A}{A_1}\left(\frac{-n - St_{mo,j}\frac{A}{A_2}\frac{1}{\overline{\rho}\overline{C}_p}}{n + \frac{A}{A_2}\frac{1}{\overline{\rho}\overline{C}_p}\left(\xi + St_{mo,j}\right)}\right) \tag{5.74}$$

Rearranging this expression for $\hat{\theta}_{wi}$ gives

$$\hat{\theta}_{wi} = \frac{St_{mi,ss}\frac{A}{A_1}\frac{1}{\overline{\rho}\overline{C}_p}\,\hat{\theta}_f + B_j\hat{\omega}St_{mi,ss}\frac{A}{A_1}\frac{1}{\overline{\rho}\overline{C}_p}\left(\theta_{f,ss} - \theta_{wi,ss}\right)}{n + St_{mi,ss}\frac{A}{A_1}\frac{1}{\overline{\rho}\overline{C}_p} + \xi\frac{1}{\overline{\rho}\overline{C}_p}\frac{A}{A_1}\left(\frac{n + St_{mo,j}\frac{A}{A_2}\frac{1}{\overline{\rho}\overline{C}_p}}{n + \frac{A}{A_2}\frac{1}{\overline{\rho}\overline{C}_p}\left(\xi + St_{mo,j}\right)}\right)} \tag{5.75}$$

Let us introduce the following parameters to represent the above equations in more compact manner

$$\Sigma_1 = \frac{A}{A_1}\frac{1}{\overline{\rho}\overline{C}_p};\ \Sigma_2 = \frac{A}{A_2}\frac{1}{\overline{\rho}\overline{C}_p} \tag{5.76}$$

Eq. 5.75 is written in compact form as

$$\hat{\theta}_{wi} = \frac{\Sigma_1 St_{mi,ss}\,\hat{\theta}_f + B_j\hat{\omega}St_{mi,ss}\Sigma_1\left(\theta_{f,ss} - \theta_{wi,ss}\right)}{n + St_{mi,ss}\Sigma_1 + \xi\Sigma_1\left(\frac{n + St_{mo,j}\Sigma_2}{n + \Sigma_2\left(\xi + St_{mo,j}\right)}\right)} \tag{5.77}$$

This expression is substituted in Eq. 5.69 and following parameter is introduced for compact representation

$$M_{l,j} = n + \xi\Sigma_1\left(\frac{n+St_{mo,j}\Sigma_2}{n+\Sigma_2(\xi+St_{mo,j})}\right) \tag{5.78}$$

Resulting equation is

$$\varphi\ \frac{\partial\widehat{\theta_f}}{\partial S} + \hat{\theta}_f\left(n + \frac{M_{l,j}St_{mi,ss}}{M_{l,j}+St_{mi,ss}\Sigma_1}\right) = -\hat{\omega}\varphi\frac{\partial\theta_{f,ss}}{\partial S}\left(1 - B_j + \frac{B_j\Sigma_1 St_{mi,ss}}{M_{l,j}+St_{mi,ss}\Sigma_1}\right) \tag{5.79}$$

The steady state term $\frac{\partial\theta_{f,ss}}{\partial S}$ is substituted with corresponding expressions for each section by determining from steady state temperature distribution

For heater: $\varphi\frac{\partial\theta_{f,ss}}{\partial S} = \chi_h\left(\frac{L_t}{L_hSt_{mo,h}} - \theta_{f,ss}\right) = -\chi_h\left(\theta_{clf,ss} - \frac{L_t}{L_hSt_{mo,h}}\right)e^{\frac{-\chi_hS}{\varphi}}$ (5.80a)

For cooler: $\varphi\frac{\partial\theta_{f,ss}}{\partial S} = \chi_c(\theta_s - \theta_{f,ss}) = \chi_c(\theta_s - \theta_{hlf,ss})e^{-\frac{\chi_c(S-S_{hl})}{\varphi}}$ (5.80b)

For hot leg: $\varphi\frac{\partial\theta_{f,ss}}{\partial S} = -\chi_{hl}\theta_{f,ss} = -\chi_{hl}\theta_{hf,ss}e^{-\frac{\chi_{hl}(S-S_h)}{\varphi}}$ (5.80c)

For cold leg: $\varphi\frac{\partial\theta_{f,ss}}{\partial S} = -\chi_{cl}\theta_{f,ss} = -\chi_{cl}\theta_{cf,ss}e^{-\frac{\chi_{cl}(S-S_c)}{\varphi}}$ (5.80d)

From now onwards, the subscript 'ss' is dropped from steady state parameters for simple representation. Substituting Eq. 5.80a to 5.80d in Eq. 5.79 separately for each section and rearranging into standard form of linear ODE

$$\frac{\partial\widehat{\theta_f}}{\partial S} + \hat{\theta}_f\frac{1}{\varphi}\left(n + \frac{M_{lh}St_{mi,h}}{M_{lh}+St_{mi,h}\Sigma_1}\right) = \frac{1}{\varphi}\hat{\omega}\chi_h\left(\theta_{clf} - \frac{L_t}{L_hSt_{mo,h}}\right)\left(1 - B_h + \frac{B_h\Sigma_1 St_{mi,h}}{M_{lh}+St_{mi,h}\Sigma_1}\right)e^{\frac{-\chi_hS}{\varphi}}$$

(heater) (5.81)

$$\frac{\partial\widehat{\theta_f}}{\partial S}+\hat{\theta}_f\frac{1}{\varphi}\left(n+\frac{M_{lhl}St_{mi,hl}}{M_{lhl}+St_{mi,hl}\Sigma_1}\right)=\frac{1}{\varphi}\hat{\omega}\chi_{hl}\theta_{hf}\left(1-B_{hl}+\frac{B_{hl}\Sigma_1St_{mi,hl}}{M_{lhl}+St_{mi,hl}\Sigma_1}\right)e^{-\frac{\chi_{hl}(S-S_h)}{\varphi}}$$

(hot leg) (5.82)

$$\frac{\partial\widehat{\theta_f}}{\partial S}+\hat{\theta}_f\frac{1}{\varphi}\left(n+\frac{M_{lc}St_{mi,c}}{M_{lc}+St_{mi,c}\Sigma_1}\right)$$
$$=\frac{1}{\varphi}\hat{\omega}\chi_c(\theta_{hlf}-\theta_s)\left(1-B_c+\frac{B_c\Sigma_1St_{mi,c}}{M_{lc}+St_{mi,c}\Sigma_1}\right)e^{-\frac{\chi_c(S-S_{hl})}{\varphi}}$$

(cooler) (5.83)

$$\frac{\partial\widehat{\theta_f}}{\partial S}+\hat{\theta}_f\frac{1}{\varphi}\left(n+\frac{M_{lcl}St_{mi,cl}}{M_{lcl}+St_{mi,cl}\Sigma_1}\right)=\frac{1}{\varphi}\hat{\omega}\chi_{cl}\theta_{cf}\left(1-B_{cl}+\frac{B_{cl}\Sigma_1St_{mi,cl}}{M_{lcl}+St_{mi,cl}\Sigma_1}\right)e^{-\frac{\chi_{cl}(S-S_c)}{\varphi}}$$

(cold leg) (5.84)

The following parameters are introduced to represent above equations in compact form

$$\lambda_{1j}=n+\frac{M_{lj}St_{mi,j}}{M_{lj}+St_{mi,j}\Sigma_1};j=h,hl,c,cl \quad (5.85)$$

$$\lambda_{2h}=\chi_h\left(\theta_{clf}-\frac{L_t}{L_hSt_{moh}}\right)\left(1-B_h+\frac{B_hSt_{mi,h}\Sigma_1}{M_{lh}+St_{mi,h}\Sigma_1}\right) \quad (5.86)$$

$$\lambda_{2c}=\chi_c(\theta_{hlf}-\theta_s)\left(1-B_c+\frac{B_cSt_{mi,c}\Sigma_1}{M_{lc}+St_{mi,c}\Sigma_1}\right) \quad (5.87)$$

$$\lambda_{2hl}=\chi_{hl}(\theta_{hf})\left(1-B_{hl}+\frac{B_{hl}St_{mi,hl}\Sigma_1}{M_{lhl}+St_{mi,hl}\Sigma_1}\right) \quad (5.88)$$

$$\lambda_{2cl}=\chi_{cl}(\theta_{cf})\left(1-B_{cl}+\frac{B_{cl}St_{mi,cl}\Sigma_1}{M_{lcl}+St_{mi,cl}\Sigma_1}\right) \quad (5.89)$$

The equations 5.81 to 5.84 are written in compact form as

$$\frac{\partial \widehat{\theta_f}}{\partial S} + \hat{\theta}_f \frac{\lambda_{1h}}{\varphi} = \frac{\lambda_{2h}}{\varphi} \hat{\omega} e^{\frac{-\chi_h S}{\varphi}} \tag{5.90}$$

$$\frac{\partial \widehat{\theta_f}}{\partial S} + \hat{\theta}_f \frac{\lambda_{1c}}{\varphi} = \frac{\lambda_{2c}}{\varphi} \hat{\omega} e^{-\frac{\chi_c (S - S_{hl})}{\varphi}} \tag{5.91}$$

$$\frac{\partial \widehat{\theta_f}}{\partial S} + \hat{\theta}_f \frac{\lambda_{1hl}}{\varphi} = \frac{\lambda_{2hl}}{\varphi} \hat{\omega} e^{-\frac{\chi_{hl} (S - S_h)}{\varphi}} \tag{5.92}$$

$$\frac{\partial \widehat{\theta_f}}{\partial S} + \hat{\theta}_f \frac{\lambda_{1cl}}{\varphi} = \frac{\lambda_{2cl}}{\varphi} \hat{\omega} e^{-\frac{\chi_{cl} (S - S_c)}{\varphi}} \tag{5.93}$$

These equations are first order ODE which can be solved by same procedure as discussed in sec. 5.3.3 with following boundary conditions applied.

$$\text{At } S = 0, \hat{\theta}_f = \hat{\theta}_{clf} \text{ (heater)} \tag{5.94a}$$

$$\text{At } S = S_h, \hat{\theta}_f = \hat{\theta}_{hf} \text{ (hot leg)} \tag{5.94b}$$

$$\text{At } S = S_{hl}, \hat{\theta}_f = \hat{\theta}_{hlf} \text{ (cooler)} \tag{5.94c}$$

$$\text{At } S = S_c, \hat{\theta}_f = \hat{\theta}_{cf} \text{ (cold leg)} \tag{5.94d}$$

The resulting solutions are

$$\hat{\theta}_f = \hat{\theta}_{clf} e^{-\frac{\lambda_{1h} S}{\varphi}} + \frac{\hat{\omega} \lambda_{2h}}{\lambda_{1h} - \chi_h} \left(e^{-\frac{\chi_h S}{\varphi}} - e^{-\frac{\lambda_{1h} S}{\varphi}} \right) \qquad 0 \le S \le S_h \tag{5.95}$$

$$\hat{\theta}_f = \hat{\theta}_{hf} e^{-\frac{\lambda_{1hl} (S - S_h)}{\varphi}} + \frac{\hat{\omega} \lambda_{2hl}}{\lambda_{1hl} - \chi_{hl}} \left(e^{-\frac{\chi_{hl} (S - S_h)}{\varphi}} - e^{-\frac{\lambda_{1hl} (S - S_h)}{\varphi}} \right) \qquad S_h \le S \le S_{hl} \tag{5.96}$$

$$\hat{\theta}_f = \hat{\theta}_{hlf} e^{-\frac{\lambda_{1c} (S - S_{hl})}{\varphi}} + \frac{\hat{\omega} \lambda_{2c}}{\lambda_{1c} - \chi_c} \left(e^{-\frac{\chi_c (S - S_{hl})}{\varphi}} - e^{-\frac{\lambda_{1c} (S - S_{hl})}{\varphi}} \right) \qquad S_{hl} \le S \le S_c \tag{5.97}$$

$$\hat{\theta}_f = \hat{\theta}_{cf} e^{-\frac{\lambda_{1cl}(S-S_c)}{\varphi}} + \frac{\hat{\omega}\lambda_{2cl}}{\lambda_{1cl} - \chi_{cl}} \left(e^{-\frac{\chi_{cl}(S-S_c)}{\varphi}} - e^{-\frac{\lambda_{1cl}(S-S_c)}{\varphi}} \right) \qquad S_c \leq S \leq S_t$$

(5.98)

Equations 5.95 to 5.98 define the perturbed temperature distribution along the loop. Using the temperature continuity boundary condition at the exit of each section, as done earlier in steady state derivation, the expressions for perturbed temperatures at inlet and outlet of heater and cooler are obtained

$$\begin{aligned} \frac{\hat{\theta}_{clf}}{\hat{\omega}} = \Bigg[& a_{cl} \left(e^{-\frac{\chi_{cl}L_{cl}}{L_t}} - e^{-\frac{\lambda_{1cl}L_{cl}}{L_t}} \right) + a_c e^{-\frac{\lambda_{1cl}L_{cl}}{L_t}} \left(e^{-\frac{\chi_c L_c}{L_t}} - e^{-\frac{\lambda_{1c}L_c}{L_t}} \right) \\ & + a_{hl} e^{-\frac{\lambda_{1cl}L_{cl}+\lambda_{1c}L_c}{L_t}} \left(e^{-\frac{\chi_{hl}L_{hl}}{L_t}} - e^{-\frac{\lambda_{1hl}L_{hl}}{L_t}} \right) \\ & + a_h e^{-\frac{\lambda_{1cl}L_{cl}+\lambda_{1c}L_c+\lambda_{1hl}L_{hl}}{L_t}} \left(e^{-\frac{\chi_h L_h}{L_t}} - e^{-\frac{\lambda_{1h}L_h}{L_t}} \right) \Bigg] \\ & \div \left[1 - e^{-\frac{\lambda_{1cl}L_{cl}+\lambda_{1c}L_c+\lambda_{1h}L_h+\lambda_{1hl}L_{hl}}{L_t}} \right] \end{aligned}$$

(5.99)

$$\frac{\hat{\theta}_{hf}}{\hat{\omega}} = \frac{\hat{\theta}_{clf}}{\hat{\omega}} e^{-\frac{\lambda_{1h}L_h}{L_t}} + a_h \left(e^{-\frac{\chi_h L_h}{L_t}} - e^{-\frac{\lambda_{1h}L_h}{L_t}} \right) \tag{5.100}$$

$$\frac{\hat{\theta}_{hlf}}{\hat{\omega}} = \frac{\hat{\theta}_{hf}}{\hat{\omega}} e^{-\frac{\lambda_{1hl}L_{hl}}{L_t}} + a_{hl} \left(e^{-\frac{\chi_{hl}L_{hl}}{L_t}} - e^{-\frac{\lambda_{1hl}L_{hl}}{L_t}} \right) \tag{5.101}$$

$$\frac{\hat{\theta}_{cf}}{\hat{\omega}} = \frac{\hat{\theta}_{hlf}}{\hat{\omega}} e^{-\frac{\lambda_{1c}L_c}{L_t}} + a_c \left(e^{-\frac{\chi_c L_c}{L_t}} - e^{-\frac{\lambda_{1c}L_c}{L_t}} \right) \tag{5.102}$$

Where,

$$a_j = \frac{\lambda_{2j}}{\lambda_{1j} - \chi_j}; j = h, hl, c, cl \tag{5.103}$$

Using the perturbed temperature distribution, the integral in characteristic equation (Eq. 5.66) can be obtained for different orientations as done earlier. Using the same length scale and coordinate system as mentioned in Chapter 4 following expression for HHHC orientation is derived.

$$\oint \frac{\widehat{\theta_f}}{\widehat{\omega}} dZ = \frac{\widehat{\theta_{clf}}}{\widehat{\omega}}\left(\frac{\phi}{\lambda_{1h}}\right)\left(1 - e^{-\frac{\lambda_{1h}L_h}{L_t}}\right)\sin(\alpha)$$
$$+ a_h \sin(\alpha)\left(\frac{\phi}{\chi_h}\left(1 - e^{-\frac{\chi_h L_h}{L_t}}\right) + \frac{\phi}{\lambda_{1h}}\left(e^{-\frac{\lambda_{1h}L_h}{L_t}} - 1\right)\right)$$
$$+ \frac{\widehat{\theta_{hf}}}{\widehat{\omega}}\left(\frac{\phi}{\lambda_{1hl}}\right)\left(1 - e^{-\frac{\lambda_{1hl}L_1}{L_t}}\right)\sin(\alpha)$$
$$+ a_{hl} \sin(\alpha)\left(\frac{\phi}{\chi_{hl}}\left(1 - e^{-\frac{\chi_{hl}L_1}{L_t}}\right) + \frac{\phi}{\lambda_{1hl}}\left(e^{-\frac{\lambda_{1hl}L_1}{L_t}} - 1\right)\right)$$
$$+ \frac{\widehat{\theta_{hf}}}{\widehat{\omega}}\left(\frac{\phi}{\lambda_{1hl}}\right)\left(e^{-\frac{\lambda_{1hl}L_1}{L_t}} - e^{-\frac{\lambda_{1hl}(L_{hl}-L_2)}{L_t}}\right)$$
$$+ a_{hl}\left(\frac{\phi}{\chi_{hl}}\left(e^{-\frac{\chi_{hl}L_1}{L_t}} - e^{-\frac{\chi_{hl}(L_{hl}-L_2)}{L_t}}\right) + \frac{\phi}{\lambda_{1hl}}\left(e^{-\frac{\lambda_{1hl}(L_{hl}-L_2)}{L_t}} - e^{-\frac{\lambda_{1hl}L_1}{L_t}}\right)\right)$$
$$+ \frac{\widehat{\theta_{hf}}}{\widehat{\omega}}\left(\frac{\phi}{\lambda_{1hl}}\right)\left(e^{-\frac{\lambda_{1hl}(L_{hl}-L_2)}{L_t}} - e^{-\frac{\lambda_{1hl}L_{hl}}{L_t}}\right)\sin(\beta)$$
$$+ a_{hl} \sin(\beta)\left(\frac{\phi}{\chi_{hl}}\left(e^{-\frac{\chi_{hl}(L_{hl}-L_2)}{L_t}} - e^{-\frac{\chi_{hl}L_{hl}}{L_t}}\right)\right.$$
$$\left. + \frac{\phi}{\lambda_{1hl}}\left(e^{-\frac{\lambda_{1hl}L_{hl}}{L_t}} - e^{-\frac{\lambda_{1hl}(L_{hl}-L_2)}{L_t}}\right)\right) + \frac{\widehat{\theta_{hlf}}}{\widehat{\omega}}\left(\frac{\phi}{\lambda_{1c}}\right)\left(1 - e^{-\frac{\lambda_{1c}L_c}{L_t}}\right)\sin(\beta)$$
$$+ a_c \sin(\beta)\left(\frac{\phi}{\chi_c}\left(1 - e^{-\frac{\chi_c L_c}{L_t}}\right) + \frac{\phi}{\lambda_{1c}}\left(e^{-\frac{\lambda_{1c}L_c}{L_t}} - 1\right)\right)$$
$$+ \frac{\widehat{\theta_{cf}}}{\widehat{\omega}}\left(\frac{\phi}{\lambda_{1cl}}\right)\left(1 - e^{-\frac{\lambda_{1cl}L_3}{L_t}}\right)\sin(\beta)$$
$$+ a_{cl} \sin(\beta)\left(\frac{\phi}{\chi_{cl}}\left(1 - e^{-\frac{\chi_{cl}L_3}{L_t}}\right) + \frac{\phi}{\lambda_{1cl}}\left(e^{-\frac{\lambda_{1cl}L_3}{L_t}} - 1\right)\right)$$
$$- \frac{\widehat{\theta_{cf}}}{\widehat{\omega}}\left(\frac{\phi}{\lambda_{1cl}}\right)\left(e^{-\frac{\lambda_{1cl}L_3}{L_t}} - e^{-\frac{\lambda_{1cl}(L_{cl}-L_4)}{L_t}}\right)$$
$$- a_{cl}\left(\frac{\phi}{\chi_{cl}}\left(e^{-\frac{\chi_{cl}L_3}{L_t}} - e^{-\frac{\chi_{cl}(L_{cl}-L_4)}{L_t}}\right) + \frac{\phi}{\lambda_{1cl}}\left(e^{-\frac{\lambda_{1cl}(L_{cl}-L_4)}{L_t}} - e^{-\frac{\lambda_{1cl}L_3}{L_t}}\right)\right)$$
$$+ \frac{\widehat{\theta_{cf}}}{\widehat{\omega}}\left(\frac{\phi}{\lambda_{1cl}}\right)\left(e^{-\frac{\lambda_{1cl}(L_{cl}-L_4)}{L_t}} - e^{-\frac{\lambda_{1cl}L_{cl}}{L_t}}\right)\sin(\alpha)$$
$$+ a_{cl}\left(\frac{\phi}{\chi_{cl}}\left(e^{-\frac{\chi_{cl}(L_{cl}-L_4)}{L_t}} - e^{-\frac{\chi_{cl}L_{cl}}{L_t}}\right) + \frac{\phi}{\lambda_{1cl}}\left(e^{-\frac{\lambda_{1cl}L_{cl}}{L_t}} - e^{-\frac{\lambda_{1cl}(L_{cl}-L_4)}{L_t}}\right)\right)$$

(5.104)

5.4. Deduction of sub models

To study sequentially the effect of each phenomenon mentioned above, the progressive simplification has been performed to the full model as depicted in Table 5.1. The major phenomena included in full model are given identifiers as: wall thermal inertia – WTI, variable internal heat transfer coefficient – HX, heat losses – HL. The simplest model which resembles the preliminary model studied in last chapter is designated as BM (Basic Model). So, full model is designated as BM+WTI+HX+HL. The names of other sub models have been formed by removing the identifiers of the phenomena which are neglected from full model. For example, a sub model with heat loss (HL) effect removed from full model is named as BM+WTI+HX. A sub model BM* has been introduced as an alias to sub model BM to generate stability map in a different parameter space (this is discussed in detail in next section). The effect caused by variable internal heat transfer coefficient is denoted by HX (heat exchange) effect hereafter.

Table 5.1 Summary of sub models deduced from full model derived in section 5.3

Model	**Model short name**	**Deduction procedure**	**Parameters affecting stability**
Full model	BM+WTI+HX+HL	-	$St_{mo,j}, Pr, \overline{\rho}\overline{C}_p, \overline{k}, \frac{t}{D}, K, Gr_m,$ Other geometric parameters (j=h,hl,c,cl)
No heat loss	BM+WTI+HX	Apply limits $St_{mo,j} \rightarrow 0$ $(j = h, hl, cl)$ by L'Hôpital rule to BM+WTI+HX+HL	$St_{mo,c}, Pr, \overline{\rho}\overline{C}_p, \overline{k}, \frac{t}{D}, K, Gr_m,$ Other geometric parameters
No heat loss, No HX effect	BM+WTI	Apply limits $B \rightarrow 0$ by L'Hôpital rule to BM+WTI+HX model	$St_{mo,c}, Pr, \overline{\rho}\overline{C}_p, \overline{k}, \frac{t}{D}, K, Gr_m,$ Other geometric parameters

No heat loss No HX, WTI effects (alias to BM)	BM*	Apply limits $\overline{\rho}\overline{C}_p \to 0, \overline{k} \to \infty$ by L'Hôpital rule to BM+WTI model	$St_{mo,c}, Pr, K, Gr_m,$ Other geometric parameters
Basic model	BM	Direct specification of St_m at cooler in BM* model	St_m, K, Gr_m And other geometric parameters

5.5. Need for development of new computer code

The computer code developed for model of Vijayan *et al.*, as discussed in Chapter 4, has been improved to incorporate the improved model. Due to tremendous increase in the computational time requirements, as observed during preliminary analysis, a new computer code has been developed based on algorithm 3 mentioned in Section 4.3. For solution of characteristic equation, graphical method has been employed which has been observed to be quickest in preliminary studies. This code has been validated in the same way as performed in Chapter 4, before deploying it to current model.

5.6. Selection of parameter space for stability maps

From table 5.1, it can be observed that for all the models except for BM, the parameters affecting stability are more than two. The common parameters encountered here are $Pr, \overline{\rho}, \overline{C}_p, \overline{k}$ and $\frac{t}{D}$. The last of them i.e. ratio of wall thickness to inner diameter of the loop is fixed for a given uniform diameter NCL. Remaining four parameters signify relative properties of the wall and working fluid. They are temperature dependent. So, a survey of possible values taken by these parameters has been done in the operating temperature range considering the materials of concerned NCL and conclusions on minimum number of parameters to be studied are arrived. Table 5.2 shows these parameter values for MSNCL in

which molten nitrate salt (MS) is the working fluid with operating range of 300^0C to 600^0C and Inconel 625 is wall material.

Table 5.2 Summary of property dependent parameter values at different temperatures for MSNCL

Temperature (^{0}C)	Density (kg/m^3)			Specific heat capacity (J/kgK)			Thermal conductivity (W/mK)			Pr
	MS	Inconel 625	$\overline{\rho}$	MS	Inconel 625	$\overline{C}_p$	MS	Inconel 625	$\overline{k}$	MS
300	1898.1	8440	4.45	1500.7	480	0.32	0.49997	15.5	31.00	9.78
450	1802.0		4.68	1523.3	504.5	0.33	0.52925	18.6	35.14	4.23
600	1706		4.95	1550.1	560	0.36	0.55853	21.3	38.14	2.74

Though the variation of properties with temperature is significant, the ratio of properties does not vary significantly in the operating temperature range. It is evident from Table 5.2. Hence, in the validation studies with MSNCL, average values of these parameters i.e. 4.65, 0.33 and 35 are considered for $\overline{\rho}, \overline{C}_p$ and $\overline{k}$ respectively. However, the Prandtl number of molten nitrate salt is varying significantly in the operating range which does not lend us to use an average value without confirming its effect on stability behaviour. So, Prandtl number is considered as one of the parameter.

With the above analysis, it is evident that the parameter group that remains for the analysis of any specified NCL geometry is either (Gr_m, $St_{mo,c}$ and Pr) or (Gr_m, St_m and Pr).

$$\chi_c = \left(\frac{1}{St_{mi,c}} + \frac{1}{\xi} + \frac{1}{St_{ml,c}}\right)^{-1} = St_{m,c} \tag{5.105}$$

From the practical point of view, high overall heat transfer coefficients (signified by high St_m) may not be feasible due to the limitation of convective heat transfer at the inner surface of the piping. This limits the applicability of stability maps generated in Gr_m-St_m space to

some extent. (This aspect is explained with example in Section 5.7.1 with help of Fig.5.5) And numerically this will give negative values for $St_{mo,c}$ which are physically unrealistic. From stand point of practical usage of stability maps, it seems to be more convenient to use former parameter group since both the parameters Gr_m and $St_{ml,c}$ signify the operating conditions directly. This is in a way similar to the stability maps generated using dimensional parameter spaces like Power – secondary side heat transfer coefficient.

With the above discussion, it is concluded to use Gr_m – $St_{mo,c}$ space with Pr as additional parameter, except for model BM for which conventional Gr_m - St_m space will be used.

5.7. Closure relations

For stability analysis with the formulation derived above, closure relations for friction and internal heat transfer coefficient are required.

For friction factor, the correlation of Churchill [7] modified to the functional form of Eq. 5.60 by Ruiz *et al.* [27] has been used in the current analysis.

For internal heat transfer coefficient, different correlations are available in literature for different flow regimes and Prandtl numbers. Switching between different correlations is required based on the Reynolds number and Prandtl number. And it is also to be noted that the formulation involves a derivative of internal Nusselt number with respect to Reynolds number (Eq. 5.69). So, the correlation should be continuous and differentiable.

In the sections of the loop where boundary heat transfer takes place, thermal boundary layer would not be developed due to high Prandtl number of molten salts and water and smaller dimensions of experimental facilities. And the boundary condition at cooler is neither constant temperature nor constant surface heat flux. And usage of finite secondary side heat transfer coefficient defies the applicability of constant temperature boundary condition at

cooler. So, Shah and London correlation for constant surface heat flux case has been used. For turbulent flows, the boundary conditions do not affect the heat transfer and thermal boundary layer develops very fast. So, Gnielinski and Dittus-Boelter correlations [29] have been selected. The selected correlations are summarized in Table 5.3. The correlations are differentiated by employing subscripts to *Nu* with respective names (ref. second column of table 5.3)

Table 5.3 Nusselt number correlations selected for application in current model

Name	**Correlation**	**Applicability**
Shah and London	$Nu_{sl} = \begin{cases} 1.953\ (x^*)^{-\frac{1}{3}} & x^* \leq 0.03 \\ 4.364 + \dfrac{0.0722}{x^*} & x^* > 0.03 \end{cases}$ where $x^* = \frac{L}{D.Re.\mathrm{Pr}}$	Hydrodynamically developed, thermally developing laminar flow in circular pipe under constant surface heat flux
-	$Nu_l = 4.364$	Fully developed laminar flow in circular pipe with constant surface heat flux boundary
Gnielinski	$Nu_g = \dfrac{(f/8)(Re - 1000)\mathrm{Pr}}{1 + 12.7\sqrt{\mathrm{f/8}}\ (\mathrm{Pr}^{0.67} - 1)}$ where $f = (0.79\log(Re) - 1.64)^{-2}$	Re>3000 Pr>0.6
Dittus-Boelter	$Nu_d = 0.023Re^{0.8}Pr^n$ n=0.3 for cooling, 0.4 for heating	Re>10000 Pr>0.7
Cheng and Tak	$Nu_c = \begin{cases} 4.5 + 0.018\ Pe^{0.8} & Pe < 1000 \\ 5.4 - 0.0009Pe + 0.018Pe^{0.8} & 1000 \leq Pe < 2000 \\ 3.6 + 0.018Pe^{0.8} & Pe \geq 2000 \end{cases}$	Liquid metals

The composite correlation is constructed by the methodology suggested by Pini *et al.* [28] using Fermi-Dirac distribution factors ψ. These factors provide a smooth transition from one correlation to another without any discontinuities. The requirement of differentiability is also ensured. Two Fermi-Dirac factors $\psi_1 and\ \psi_2$ are required for transition from $Nu_{sl}\ to\ Nu_g$

and $Nu_g to\, Nu_d$ while transition from low Prandtl numbers to high Prandtl numbers is achieved by the factor ψ_3.Expressions for these factors and final composite correlation are given as

$$\psi_1 = \frac{1}{1+\exp\left(\frac{Re-2500}{500}\right)}; \psi_2 = \frac{1}{1+\exp\left(\frac{Re-10000}{100}\right)}\ ;\ \psi_3 = \frac{1}{1+\exp\left(\frac{Pr-0.6}{0.00001}\right)} \tag{5.106}$$

$$Nu_i = \begin{cases} \left(\left(Nu_{sl}^{\psi_1} Nu_g^{1-\psi_1}\right)^{\psi_2} Nu_d^{1-\psi_2}\right)^{1-\psi_3} Nu_c^{\psi_3} & (heater, cooler) \\ \left(\left(Nu_l^{\psi_1} Nu_g^{1-\psi_1}\right)^{\psi_2} Nu_d^{1-\psi_2}\right)^{1-\psi_3} Nu_c^{\psi_3} & (piping) \end{cases} \tag{5.107}$$

In the above expression, subscripts of *Nu*, sl, g, d, c and l denote Shah & London, Gnielinski, Dittus-Boelter, Cheng & Tak and laminar respectively.

5.8 Validation studies

To perform detailed validation studies of the above formulation diverse methodologies have been employed. First of all, to validate the formulation, solution methodology and accuracy, the model has been applied to the loop analysed by Cammi *et al.* [30] and compared with their theoretical predictions. As a second step, it has been applied sequentially to two water based loops and then MSNCL. The predictions have been validated with experimental stability data available for respective loops in literature. Focus has been on HHHC orientation only.

5.8.1 Validation with published theoretical results

Cammi *et al.* [30] published theoretical predictions by linear stability analysis in their work. They took wall thermal inertia, variable heat exchange between wall and working fluid into account. This allowed us to verify our model BM+WTI+HX. However, they modelled cooler as constant surface temperature boundary whereas in our case it is modelled with finite

secondary side heat transfer coefficient. So, to validate against predictions of Cammi *et al.*, a limiting condition of $St_{moc} \rightarrow \infty$ has been used on BM+WTI+HX model to convert current cooler model to that they employed (new model is referred as BM+WTI+HX (CSTC), where CSTC stands for constant surface temperature cooler). It is to be noted that validation against Cammi *et al.* has been performed against their predictions for surface heating case ($\alpha = 1$, as per their nomenclature) only. Analysis has been performed for both the thickness values they analysed and the results are presented in fig. 5.3.

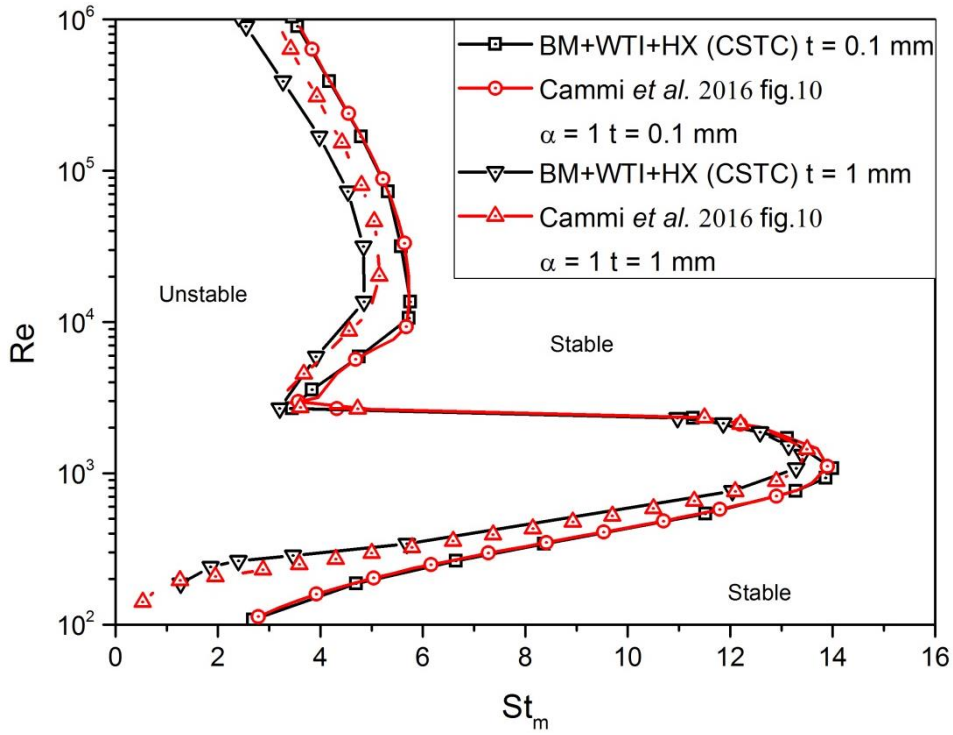

Fig. 5.3 Validation of model BM+WTI+HX (CSTC) against theoretical predictions of Cammi *et al.* [30] for HHHC orientation

As for the closure relation for friction, Cammi *et al.* considered Ruiz *et al.* [27] model and for internal heat transfer coefficient, they employed Pini *et al.* [28] model. Same relations have been used in generation of stability maps for current validation exercise with their predictions. It has been observed that at 0.1 mm thickness, the predictions are in full agreement with those published. Whereas, in case of 1 mm thickness, model BM+WTI+HX

(CSTC) has predicted slightly smaller unstable region in fully turbulent region. This sufficiently validates the current model in the context of formulation and solution strategy.

Table 5.4 Geometrical and operating details of Vijayan's, Swapnalee's and MSNCL loops

Loop details		Vijayan [22] /Loop#1	Swapnalee [24] /Loop#2	MSNCL
parameter	units			
L_1	(m)	0.41	0.86	0.13
L_2	(m)	0.31	0.97	0.17
L_3	(m)	0.305	0.84	0.36
L_4	(m)	0.385	0.85	0.17
L_{hl}	(m)	2.92	5.93	2.056
L_{cl}	(m)	2.89	5.79	2.53
L_h	(m)	0.62	1.3	1.1
L_c	(m)	0.8	1.2	0.87
H	(m)	2.2	4.1	1.878
D	(mm)	26.9	13.88	14
t_w	(mm)	1	3.73	3.7
L_t	(m)	7.23	14.22	6.556
α	(deg)	0	0	5
β	(deg)	0	0	5
Piping material		Glass	SS 347	Inconel 625
Working fluid		water	water	Molten nitrate salt
Operating pressure		1 bar	30 bar	1 bar

5.8.2 Validation with experimental data

Water based rectangular NCL of Vijayan *et al.* [22] and Swapnalee and Vijayan [24] have been selected for this purpose. The rationale of selecting these two loops is that both are having same working fluid but different wall materials. Later the model has been applied on molten salt based loop MSNCL and validated against its experimental data. Various aspects of all three loops are summarized in Table 5.4

Water based NCLs:

The first step in applying the current model is to determine the values of various parameters affecting the stability behaviour. This procedure has already been described in Section 5.5. For loop#1, all the experimental data were in the temperature range of 30^0C – 40^0C [22]. So, the property dependent parameters $\bar{\rho}, \overline{C_p}, \bar{k}\ and\ Pr$ have been evaluated at average temperature 35^0C. They are given as

$$\bar{\rho} = 2.24, \qquad \overline{C_p} = 0.191, \qquad \bar{k} = 1.925, \qquad Pr = 4.82$$

Table 5.5 Property dependent parameter values at different temperatures for loop #2

Temperature (^{0}C)	Density (kg/m^3)			Specific heat capacity (J/kgK)			Thermal conductivity (W/mK)			Pr
	Water	SS 347	$\overline{\rho}$	water	SS 347	$\overline{C_p}$	Water	SS 347	$\overline{k}$	Water
29.6	997.06	7960	7.98	4172.3	500	0.12	0.616	16.3	26.46	5.44
96.1	962.55		8.27	4205.3		0.12	0.679		24.00	1.82

For loop#2 [24], the temperature range of experimental data was from 30^0C to 100^0C at the operating pressure of 30 bar. Table 5.5 summarizes the property dependent parameter values at different temperatures in operating range.

Since, the variation of dimensionless density, specific heat and thermal conductivity is small, they have been considered as constants during analysis with the values 8.124, 0.119 and 25.25 respectively. Prandtl number variation is observed to be large. So, Prandtl number has been taken as a parameter for analysis.

Deduction of experimental data from source

Experimental data available in the source papers have been used to calculate the required parameters of current analysis (Gr_m, St_m, St_{moc} and Pr), so that the theoretical predictions can be validated.

Vijayan *et al.* presented their experimental data related to unidirectional and bidirectional oscillations in the stability map in terms of Gr_m and St_m. Swapnalee and Vijayan presented their stable experimental data in terms of input power, Gr_m and overall heat transfer coefficient U. St_m has been calculated from U using following relation

$$St_m = 4\frac{L_t}{D}\frac{\left(\frac{UD}{k}\right)}{Re_{ss}\mathrm{Pr}} \tag{5.108}$$

Table 5.6 Experimental data of [22] published and deducted

Gr_m	St_m	Stability	St_{moc}
3.59E+10	5.24E-01	UDO	0.98
2.29E+10	4.46E-01	UDO	0.68
1.82E+10	5.91E-01	UDO	1.025
2.51E+10	6.09E-01	UDO	1.18
1.18E+11	4.23E-01	BDO	0.72
9.50E+10	4.65E-01	BDO	0.85
4.59E+10	4.90E-01	BDO	0.9

For models superior to BM, St_{moc} is required to plot the experimental data on stability map. For this purpose, the Eq. 5.105 was utilized. The calculations were based on experimental steady state Reynolds number for stable data and theoretical Reynolds number for unstable data. The experimental data of Vijayan *et al.* and Swapnalee and Vijayan are summarized in Table 5.6 and 5.7 respectively. In table 5.6 UDO denotes unidirectional oscillations and BDO denotes bidirectional oscillations.

Table 5.7 Experimental data of [24] published and deducted

Power (W)	T_{mean} (^{0}C)	Gr_m	Re_{ss}	U (W/m^{2}K)	Pr	St_m	St_{moc}
225.4	29.6	2.11E+10	482	262.103	5.44	8.774257	113.7031
1251	59	1.05E+12	2610	432.433	3.024	4.809288	45.16148
1716.6	68.3	2.1E+12	3860	497.348	2.611	4.331621	11.23837
2233.6	77.7	4.72E+12	6380	569.97	2.2849	3.432009	6.423372
2540.8	82.1	6.66E+12	6520	602.419	2.1555	3.762594	7.413855
2734.2	85.9	8.2E+12	7200	622.51	2.05498	3.693095	7.125454
3096.5	89.6	1.06E+13	8540	659.584	1.9644	3.451172	6.401087
3253.4	93.1	1.22E+13	9120	681.205	1.8861	3.476182	6.451109
3507.1	96.1	1.55E+13	10200	707.465	1.82	3.345166	6.298871

Prediction of stability boundary with model BM(K=0)

The predictions of stability boundary for both loops #1 and #2 are depicted along with experimental data in Fig. 5.4. The preliminary model itself could predict the unstable behaviour of loop #1 as was the case published, whereas most of the stable experimental data of loop #2 have been predicted as unstable by the same model.

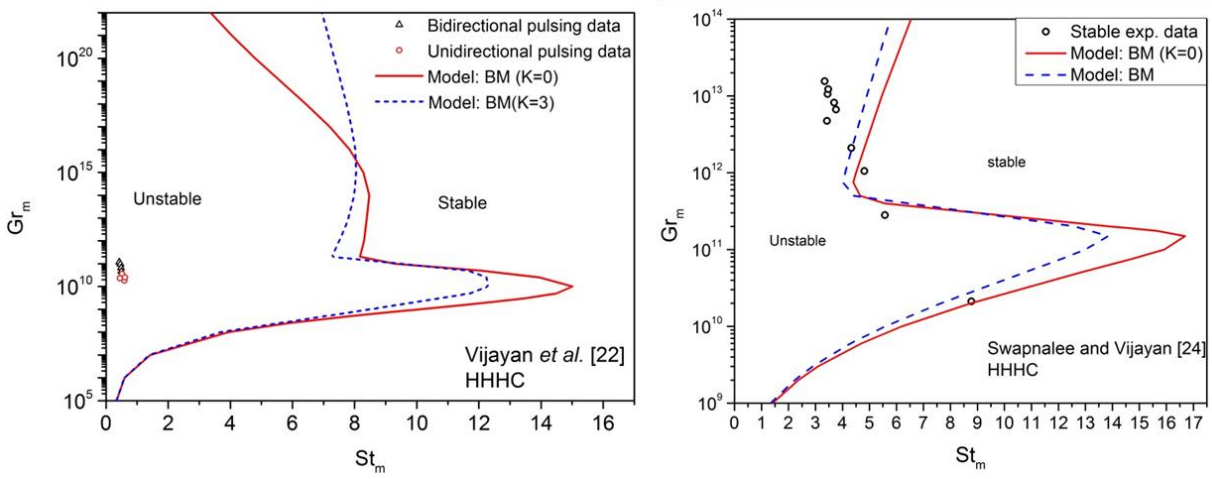

Fig. 5.4 Stability boundary obtained by LSA with model BM (K=0) and BM for loop #1 (left) and loop#2 along with corresponding experimental data

Predictions of stability boundary with model BM

With consideration of local pressure loss of K=3.0 for loop #1 and loop #2 (0.75 for each elbow X 4), the improvement in the accuracy of predictions is marginal as can be observed from Fig. 5.4.

*Prediction of Stability behaviour with model BM**

Performing stability analysis with BM* model is a way of converting the coordinates of stability map obtained by BM model. This model serves as a bridge between BM and BM+WTI models. The predicted stability boundaries are plotted in Fig. 5.5. The fact raised during the discussion of parameter space for stability analysis in Section 5.5 has been apparently proved by the shape of these stability boundaries. For detailed explanation of this aspect, St_m contours are given in stability map of loop #1. It can be easily observed that St_m gradually becomes independent of St_{moc} at higher Gr_m, especially as higher Reynolds number. It is due to the dominance of the internal heat transfer coefficient which is low in value. Evidence for that shape of stability boundary is also apparent from these contours. For

example, St_m>0.13 is not practically possible at $Gr_m=10^{26}$ in loop #1. But, as per model BM, loop #1 is stable at St_m>1.2 which is not achievable. So, stability map by model BM* shows complete unstable zone for this Gr_m. This explains the need of selection of parameter space (Gr_m, St_{mlc}) instead of (Gr_m, St_m).

For loop #2, Prandtl number is also a parameter as discussed earlier in this section. So, stability boundaries have been derived for the two extreme Prandtl numbers for the temperature range of the experimental data. It can be observed that stable region is smaller for low Prandtl number case (Pr = 1.82). Assuming density, specific heat capacity and thermal conductivity to remain constant, as was the case assumed, increase in the Prandtl number is equivalent to increase in dynamic viscosity of working fluid. Stability is linked with balance of buoyancy and friction forces in NCL and it can be observed from fig. 5.4 that a certain cooling rate (St_m) is required to make this balance stable. For the case of high viscosity, frictional forces will be high which gives more stabilization to the loop. So, less contribution from the cooler effectiveness (represented by St_m) is required for ultimate stabilization of NCL. This could be the reason for shift of stability boundary to lower St_m values for high Prandtl numbers.

Prediction of stability behaviour with model BM+WTI

The effect of wall thermal inertia on stability of loop #1 has been observed to be negligible whereas that on loop #2 is remarkably stabilizing. No unstable zone is predicted in the parameter range under analysis for loop #2. Predictions along with experimental data are shown in Fig. 5.6

The formulation could capture the observations done by various researchers [17, 21, 30, 31] regarding the stabilizing effect of wall thermal inertia on dynamic behaviour of NCLs in excellent way.

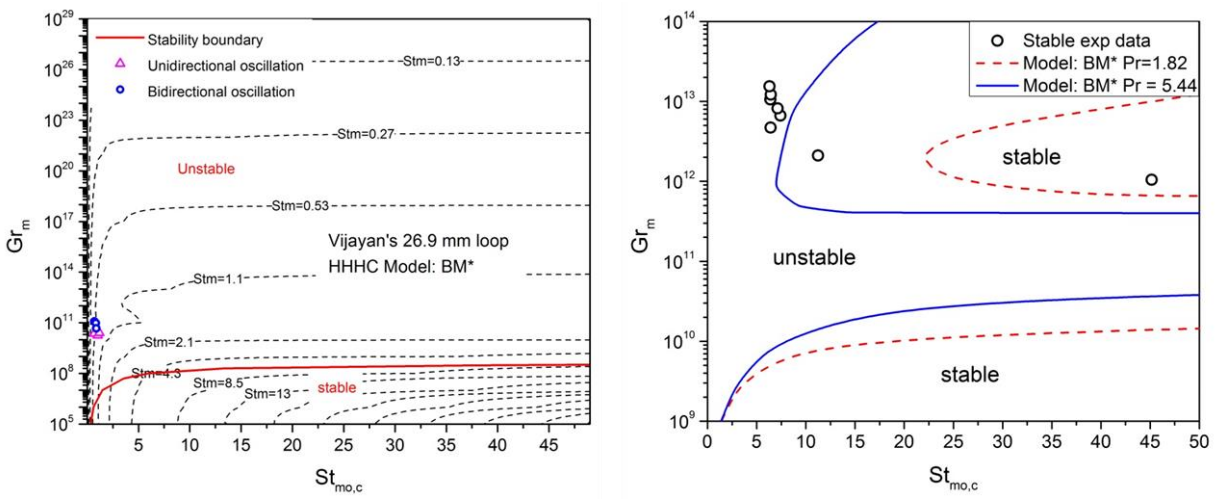

Fig. 5.5 Stability boundary obtained by LSA with model BM* for loop #1 (left) and loop #2 along with corresponding experimental data

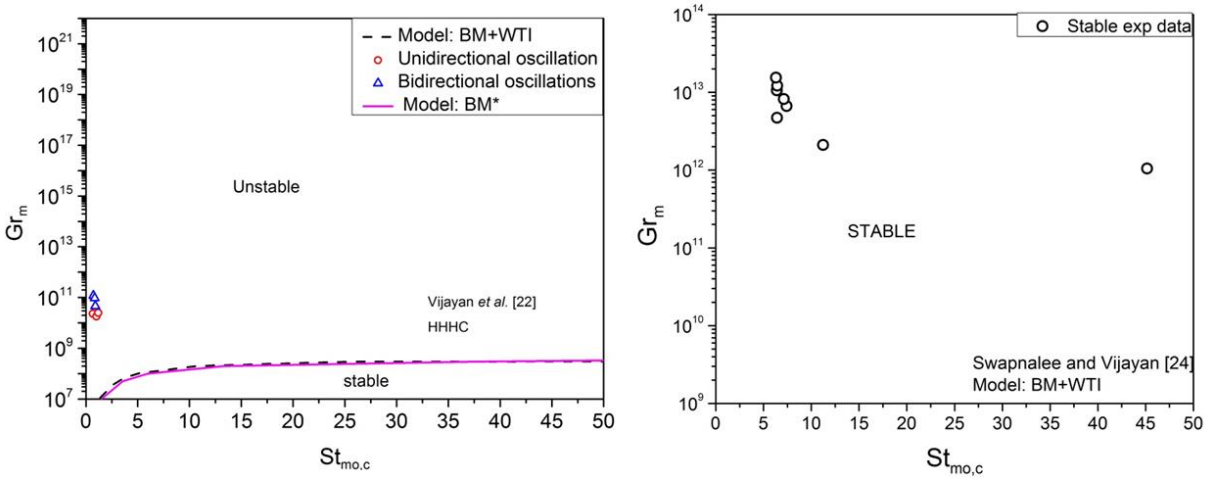

Fig. 5.6 Stability boundary obtained by LSA with model BM+WTI for loop #1 (left) and loop #2 along with corresponding experimental data

The predictions of the model BM+WTI+HX have not been given here since it has been observed to be same as the result of BM+WTI for both the loops. The reason for this lies in the way heat exchange effect stabilizes NCL dynamics. In laminar regime the internal heat transfer coefficient is almost constant whereas in turbulent regime, it increases with Reynolds number. So, stabilization is expected in case of turbulent flow regime [28, 31] i.e. for high

Gr_m values. Since loop#2 is already stable in this flow regime, further change in stability map is not expected by HX effect. But, in case of loop#1 stabilization can be expected in turbulent flow regime while HX effect could not stabilize the loop in the St_{moc} range studied.

Molten salt based loop MSNCL:

The improved model has been applied to MSNCL from the stage of model BM* directly since the predictions through earlier models were already discussed in Chapter 4. The St_{moc} values corresponding to each operating condition are given in Table 5.8 for the purpose of validation of BM* and higher models.

Table 5.8 Summary of experimental data of MSNCL used for validation of LSA predictions

Gr_m	Pr	St_m	St_{moc}
1.67E+10	5.95	0.44516	0.52622
8.93E+10	5.08	0.428818	0.544525
2.50E+11	3.81	0.59963	0.802596
4.25E+10	6.097	0.44379	0.566098
2.17E+11	4.191	0.5575	0.750905
2.79E+11	3.943	0.5313	0.694382
2.98E+11	3.849	0.74497	1.121639
2.47E+11	4.14	0.55615	0.74769
3.00E+11	3.929	0.5303	0.683205

*Predictions with model BM**

Fig. 5.7 shows the iso-St_m contours at two Prandtl numbers. It can be observed that at low Prandtl numbers the St_{moc} can have effect on St_m up to higher Reynolds numbers (corresponds to high Grashof numbers in the Fig. 5.7) compared to the situation at high

Prandtl numbers. It is implying that the St_{mic} is decreasing with increasing Prandtl number. The reason lies in the fact that the proportionality of heat transfer coefficient to Prandtl number is always less than one. Observing the following equation, it is evident that at high Prandtl numbers St_{mic} will be limiting the St_m, even at lower Reynolds numbers.

$$St_m \propto \frac{Nu}{Pr} \propto \frac{Pr^n}{Pr} \approx Pr^{n-1} \text{ ; ususally } n < 1 \tag{5.109}$$

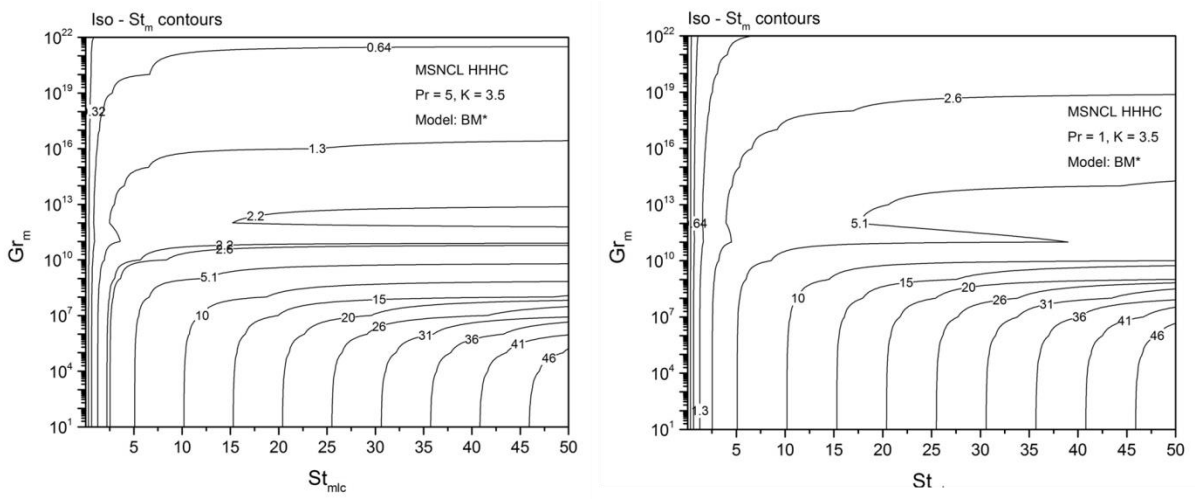

Fig. 5.7 Iso-St_m contours in the parameter space of Gr_m-St_{mlc} for Pr = 5 (left) and Pr = 1 for MSNCL in HHHC orientation

The above discussion is useful in understanding the prediction of larger unstable zone at high Prandtl numbers as shown for MSNCL with BM* model in Fig. 5.8. Prandtl number values of 1, 5 and 10 were selected for analysis to cover the whole range of values attained by MS during experiments. The existence of stability island for Pr = 1 is also due to the reasons discussed above.

Predictions with model BM+WTI

With the property dependent parameter values mentioned in Section 5.6, the BM+WTI model has been applied to MSNCL in HHHC orientation. Similar to that observed with loop #2, a

remarkable stabilization has been observed after including wall thermal inertia in formulation (Fig. 5.9). All the operating conditions which were observed to be stable experimentally have now been predicted as stable by the improved model.

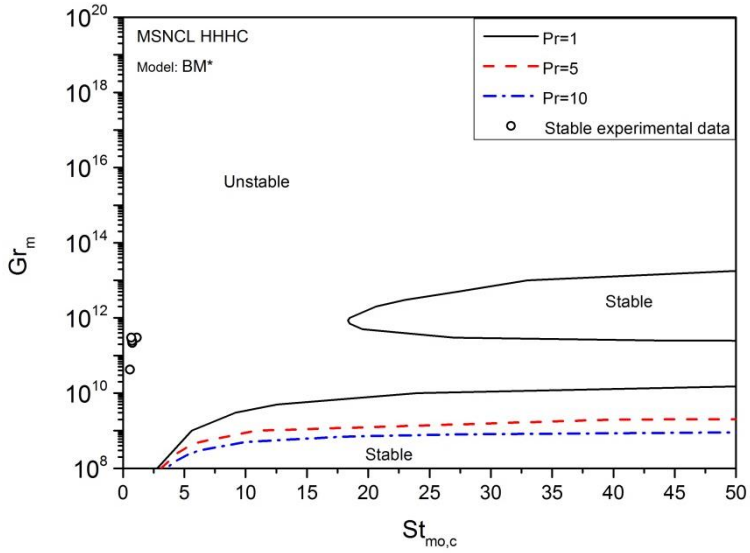

Fig. 5.8 Stability boundaries predicted by LSA with BM* model at different Prandtl numbers for MSNCL in HHHC orientation

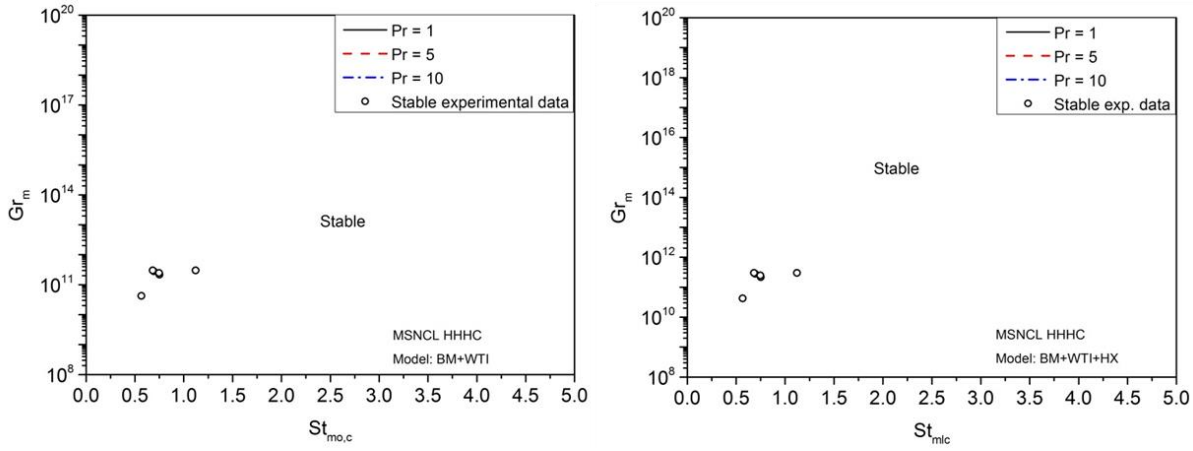

Fig. 5.9 Stability boundaries predicted by LSA with BM+WTI (left) and BM+WTI+HX models for MSNCL in HHHC orientation

Predictions with model BM+WTI+HX

As discussed earlier, heat exchange effect is generally insignificant in laminar regime due to negligible change in internal heat transfer coefficient. In turbulent regime, it induces stabilization on the NCL dynamics [27, 30]. In case of MSNCL, loop is completely stable in the turbulent regime. So, further difference is not expected in stability map with respect to BM+WTI model. The same can be observed from fig. 5.9.

Heat losses

The formulation accounts for heat losses in all four sections of the loop viz. heater, cooler, hot leg and cold leg. In the computer code, they are incorporated in such a way that the user need to give input of equivalent heat loss coefficient (including the resistance of insulation) on wall outer surface. The code calculates the corresponding $St_{mo,j}$ (j=h,hl,cl) using constant thermal conductivity of working fluid (acceptable as per the observation summarized in Tables 5.2 and 5.5). The stability map can be generated mathematically using this procedure, but the very sense of 'orientation' would be missing due to the fact that near zero St_{moc} cases do not satisfy the condition of horizontal cooler i.e. cooling at other section may dominate compared to main cooler. So, it was thought appropriate not to generate a complete stability map for this case, instead, formulation can be validated against individual experimental data points.

5.9. Effect of wall thickness on stability behaviour

Observing the significant stabilization of NCL dynamics due to wall thermal inertia in case of MSNCL and the NCL of Swapnalee and Vijayan [24], it has been sought to study the effect of wall thickness on stability. The same has been carried out considering MSNCL geometry, material of construction and working fluid at two different thicknesses *viz.* t = 1 mm and t =

3.7 mm (actual). The results are plotted in fig. 5.10. When the wall thickness is 1 mm, MSNCL is found to be unstable in some operating conditions, one of which is denoted by point *A* in the fig. 5.9. To investigate the thickness effect further non-linear analysis has been employed in chapter 7.

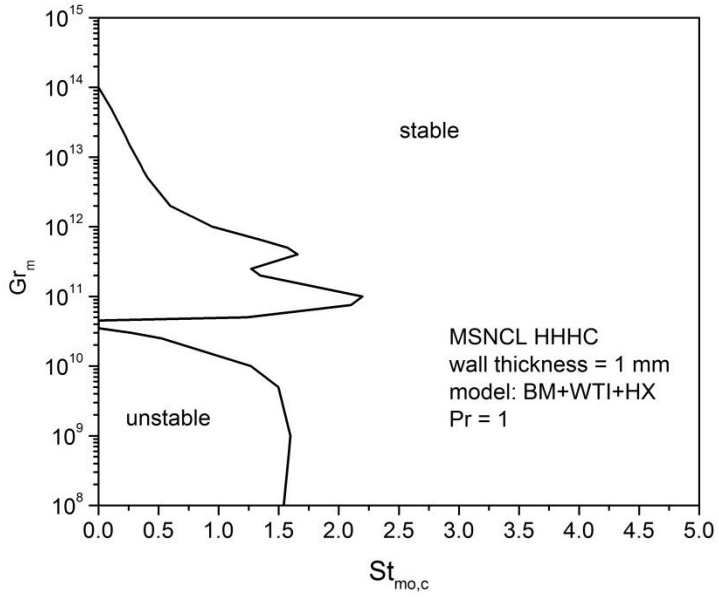

Fig. 5.10 Stability map of MSNCL for a wall thickness of 1 mm.

5.10. Concluding remarks

In this chapter, a new LSA model has been derived by incorporation of wall thermal inertia, variable heat transfer coefficient, finite secondary side heat transfer coefficient, local pressure losses and heat losses in the preliminary model of Vijayan *et al.* [22]. This model has been successfully validated with theoretical predictions as well as experimental data from literature for HHHC orientation. The main conclusions are,

1. The predictive power of newly developed LSA model is very good.

2. For NCLs with metallic loops, stability is considerably high due to wall thermal inertia.

3. Increase in the thickness of wall can stabilize the NCL dynamic behaviour.

CHAPTER 6

A Model for Linear Stability Analysis of NCLs for IHG/DH Case

6.1. Description of thermal hydraulic phenomena in MSR PHT system

For a typical MSR operating in thermal spectrum, the fuel salt is made to circulate through the channels provided in the moderator blocks, typically graphite [33]. The fissile atoms employed in the fuel salt are either ^{235}U or ^{233}U. The major part of the fission energy which is in the form of kinetic energy of fission products gets deposited within the flowing salt. Remaining energy gets deposited in moderator blocks and/or reflector blocks. The radioactive fission products decay into daughter nuclides followed by a chain of alpha/beta decays leading to stable nuclide formation. Short lived nuclides decay very fast within the span of core to heat exchanger whereas long lived nuclides may not decay at all in the loop. They have to be removed by an auxiliary reprocessing system, either batch or online. The energy associated with alpha/beta/gamma emanated from decay of radioactive nuclides gets deposited to some extent within the working fluid. This energy can be estimated from a mathematical relation of the form

$$q'''_{decay}(s) = \sum_i \left(C_i \lambda_i \left(\sum_j E_{i,j}.\left(1 - \varepsilon_{i,j}\right).p(i,j) \right) \right) \tag{6.1}$$

where, C_i, λ_i are concentration and decay constant of nuclide i respectively; $p(i,j)$ is the probability of j type of decay of nuclide i and $E_{i,j}$ is the corresponding energy of emanated particle/radiation. $\varepsilon_{i,j}$ takes into account the fraction of energy lost by escape of particle/radiation from working fluid. Here, s is spatial coordinate along the length of the PHT loop.

The concentration of nuclides, C_i, in PHT loop can be obtained by solving conservation of mass equation for individual nuclides which is given as

$$\frac{\partial}{\partial t}(C_i) + u.\frac{\partial}{\partial s}(C_i) = D_i \frac{\partial^2}{\partial s^2}(C_i) + S_i \tag{6.2}$$

where, u is fuel salt flow velocity, D_i is effective diffusion coefficient of species i in salt mixture and S_i is the source term for nuclide i which comprises generation/destruction from fission, decay and neutron capture. For estimation of S_i related to fission in the core region, neutron kinetics equations are to be solved. Besides these neutronic phenomena, reprocessing also affects the concentration of nuclides in the loop. So, from eq. 6.1 and 6.2 it can be observed that spatial distribution of internal heat generation in the working fluid outside the core depends on activity of respective nuclides which in turn depends on reactor power and salt flow rate. If forced circulation is employed in main heat transport system, the salt flow rate becomes independent parameter from the reactor power. The activity along the length of loop can be estimated for different flow rates based on the decay data of nuclides involved. In case of natural circulation, the flow rate itself depends on the way the working fluid is heated and cooled. This in turn affects the radioactive nuclide concentration and corresponding decay heat generation outside the core. Natural circulation is inherently a coupled thermal hydraulic phenomenon and neutronics also comes into picture in solid fuelled nuclear reactors. But in the context of MSRs, it is further coupled with orientation effect in a complex manner. This makes the thermal hydraulic design of natural circulation cooled MSR, a really challenging task.

6.1.1. Scope of present work

Current study aimed at analysing the case of distributed nature of internal heat generation for its effect on stability of natural circulation. In this preliminary study, the neutronics has been

assumed not to affect the stability behaviour substantially and the decay heat has been assumed to be constant throughout the loop. Similar to the case of SHF/LH, the stability analysis of IHG/DH case has been performed by both frequency domain (linear) and time domain (non-linear) analyses. In this chapter, the formulation for frequency domain analysis for stability of NCLs in IHG/DH case is given. Application of a computer code developed based on this formulation to MSNCL follows. Time domain analysis of this case is discussed in next chapter.

6.2. Formulation

With the assumptions mentioned in earlier section regarding internal heat generation, following assumptions are also taken similar to the case of SHF/LH,

1. Flow features are predominantly one-dimensional

2. Incompressible flow

3. Boussinesq approximation is valid

The resulting equations from conservation of mass, momentum and energy are

$$\frac{\partial(w)}{\partial s} = 0 \tag{6.3}$$

$$\frac{L_t}{A}\frac{\partial w}{\partial t} = \rho g \beta \oint T.sin(\gamma).ds - \left(\frac{fL_t}{D} + K\right)\frac{w^2}{2\rho A^2} \tag{6.4}$$

$$\frac{\partial(T)}{\partial t} = -\frac{w}{\rho A}\frac{\partial T}{\partial s} + \frac{1}{\rho C_p}\frac{\partial}{\partial s}\left(k\frac{\partial T}{\partial s}\right) + \frac{h_i P(T_{wi}-T)}{\rho A C_p} + \frac{q'''(s)}{\rho C_p} \tag{6.5}$$

$$\frac{\partial(T_{wi})}{\partial t} = \frac{1}{\rho_w C_{pw}}\frac{\partial}{\partial s}\left(k_w\frac{\partial T_{wi}}{\partial s}\right) - \frac{h_i P(T_{wi}-T)}{A_1 \rho_w C_{pw}} + \frac{T_{wo}-T_{wi}}{R_w \rho_w C_{pw} A_1} \tag{6.6}$$

$$\frac{\partial(T_{wo})}{\partial t} = \frac{1}{\rho_w C_{pw}}\frac{\partial}{\partial s}\left(k_w\frac{\partial T_{wo}}{\partial s}\right) - \frac{T_{wo}-T_{wi}}{R_w \rho_w C_{pw} A_2} + \frac{Q_b}{A_2 \rho_w C_{pw}} \tag{6.7}$$

$$Q_b = \begin{cases} h_o(T_{amb} - T_{wo})P_2 & heater, piping \\ h_o(T_s - T_{wo})P_2 & cooler \end{cases} \quad (6.8)$$

All the terminology has been maintained the same as earlier. The coordinate system *s* and the length scales are also same as earlier. $q'''(s)$ is the volumetric heat generation (in W/m^3) at position *s*. Due to similarity with the derivation of stability analysis formulation given in Chapter 5, only major steps of the derivation process are given here for brevity.

The axial heat conduction in the fluid and piping wall is assumed to be negligible in the further derivation. The resulting governing equations are non-dimensionalized using the parameters defined by equations 5.32 to 5.36 along with the following

$$Gr_m = \frac{\rho^2 g \beta D^3 q_h''' L_h H}{\mu^3 C_p} \quad (6.9)$$

$$\Lambda_j = \frac{q_j'''}{q_h'''}; \text{(j=hl,c,cl)} \quad (6.10)$$

Here, Gr_m is modified Grashof number whereas Λ_j signifies the fraction of IHG that gets generated uniformly in section *j* relative to that generated in heater. The governing equations in dimensionless form can be written as

$$\frac{\partial \omega}{\partial S} = 0 \quad (6.11)$$

$$\frac{d\omega}{d\tau} = -\left(\frac{fL_t}{D} + K\right)\frac{\omega^2}{2} + \frac{Gr_m}{Re_{ss}^3}\oint \theta_f . \sin(\gamma)\, dS \quad (6.12)$$

$$\frac{\partial \theta_f}{\partial \tau} = -\omega\varphi \frac{\partial \theta_f}{\partial S} + St_{mi}\left(\theta_{wi} - \theta_f\right) + \frac{\Lambda_j L_t}{L_h}; (j = h, hl, c, cl) \quad (6.13)$$

$$\frac{\partial \theta_{wi}}{\partial \tau} = -St_{mi}\frac{A}{A_1}\frac{1}{\overline{\rho C}_p}\left(\theta_{wi} - \theta_f\right) + \xi \frac{1}{\overline{\rho C}_p}\frac{A}{A_1}\left(\theta_{wo} - \theta_{wi}\right) \quad (6.14)$$

$$\frac{\partial \theta_{wo}}{\partial \tau} = \xi \frac{1}{\overline{\rho C}_p}\frac{A}{A_2}(\theta_{wi} - \theta_{wo}) - St_{mo}\frac{A}{A_2}\frac{1}{\overline{\rho C}_p}\theta_{wo} \qquad heater, piping \quad (6.15a)$$

$$\frac{\partial \theta_{wo}}{\partial \tau} = \xi \frac{1}{\overline{\rho C}_p} \frac{A}{A_2} (\theta_{wi} - \theta_{wo}) - St_{mo} \frac{A}{A_2} \frac{1}{\overline{\rho C}_p} (\theta_{wo} - \theta_s) \qquad cooler \qquad (6.15b)$$

6.2.1. Steady state solution

As prerequisite to obtain characteristic equation for stability analysis, steady state solution of the above governing equations is derived in the similar lines as given in Section 5.3.3. The final expressions are summarized below.

Momentum equation: $$K\, Re_{ss}^3 + \left(\frac{pL_t}{D}\right) Re_{ss}^{3-b} = 2Gr_m \oint \theta_{fss} dZ \qquad (6.16)$$

Fluid temperature distribution:

$$\theta_f = \frac{L_t}{L_h} \frac{1}{\chi_h} + \left(\theta_{clf} - \frac{L_t}{L_h} \frac{1}{\chi_h}\right) e^{-\frac{\chi_h S}{\varphi}} \qquad 0 \le S \le S_h \qquad (6.17)$$

$$\theta_f = \frac{L_t}{L_h} \frac{\Lambda_{hl}}{\chi_{hl}} + \left(\theta_{hf} - \frac{L_t}{L_h} \frac{\Lambda_{hl}}{\chi_{hl}}\right) e^{-\frac{\chi_{hl}(S - S_h)}{\varphi}} \qquad S_h \le S \le S_{hl} \qquad (6.18)$$

$$\theta_f = \frac{L_t}{L_h} \frac{\Lambda_c}{\chi_c} + \theta_s + \left(\theta_{hlf} - \theta_s - \frac{L_t}{L_h} \frac{\Lambda_c}{\chi_c}\right) e^{-\frac{\chi_c(S - S_{hl})}{\varphi}} \qquad S_{hl} \le S \le S_c \qquad (6.19)$$

$$\theta_f = \frac{L_t}{L_h} \frac{\Lambda_{cl}}{\chi_{cl}} + \left(\theta_{cf} - \frac{L_t}{L_h} \frac{\Lambda_{cl}}{\chi_{cl}}\right) e^{-\frac{\chi_{cl}(S - S_c)}{\varphi}} \qquad S_c \le S \le S_t \qquad (6.20)$$

where,

$$\theta_{clf} = \left(\frac{\Lambda_{cl} L_t}{\chi_{cl} L_h}\left(1 - e^{-\frac{\chi_{cl} L_{cl}}{L_t}}\right) + \left(\theta_s + \frac{\Lambda_c L_t}{\chi_c L_h}\right)\left(1 - e^{-\frac{\chi_c L_c}{L_t}}\right) e^{-\frac{\chi_{cl} L_{cl}}{L_t}} + \frac{L_t}{\chi_h L_h}\left(1 - e^{-\frac{\chi_h L_h}{L_t}}\right) e^{-\frac{\chi_{hl} L_{hl} + \chi_c L_c + \chi_{cl} L_{cl}}{L_t}} + \frac{\Lambda_{hl} L_t}{\chi_{hl} L_h}\left(1 - e^{-\frac{\chi_{hl} L_{hl}}{L_t}}\right) e^{-\frac{\chi_c L_c + \chi_{cl} L_{cl}}{L_t}}\right) \div \left(1 - e^{-\frac{\chi_h L_h + \chi_{hl} L_{hl} + \chi_c L_c + \chi_{cl} L_{cl}}{L_t}}\right) \qquad (6.21)$$

$$\theta_{hf} = \frac{L_t}{\chi_h L_h} + \left(\theta_{clf} - \frac{L_t}{\chi_h L_h}\right) e^{-\frac{\chi_h L_h}{L_t}} \tag{6.22}$$

$$\theta_{hlf} = \frac{\Lambda_{\mathrm{hl}} L_t}{\chi_{hl} L_h} + \left(\theta_{hf} - \frac{\Lambda_{\mathrm{hl}} L_t}{\chi_{hl} L_h}\right) e^{-\frac{\chi_{hl} L_{hl}}{L_t}} \tag{6.23}$$

$$\theta_{cf} = \theta_s + \frac{\Lambda_c L_t}{\chi_c L_h} + \left(\theta_{hlf} - \theta_s - \frac{\Lambda_c L_t}{\chi_c L_h}\right) e^{-\frac{\chi_c L_c}{L_t}} \tag{6.24}$$

With the above temperature distribution, temperature integral in momentum equation can be determined based on orientation. For HHHC orientation, it is given by Eq. 6.25.

$$\begin{aligned}
\oint \theta_{fss} dZ = \sin(\alpha) \frac{\varphi}{\chi_h} &\left[1 + \left(\theta_{clf} - \frac{L_t}{\chi_h L_h}\right)\left(1 - e^{-\frac{\chi_h L_h}{L_t}}\right)\right] \\
&+ \frac{\Lambda_{\mathrm{hl}} \varphi}{\chi_{hl} L_h} [L_1 \sin(\alpha) + L_{hl} - L_1 - L_2 + L_2 \sin(\beta)] \\
&+ \frac{\varphi}{\chi_{hl}} \left(\theta_{hf} - \frac{\Lambda_{\mathrm{hl}} L_t}{\chi_{hl} L_h}\right) \left[\left(1 - e^{-\frac{\chi_{hl} L_1}{L_t}}\right) \sin(\alpha) + \left(e^{-\frac{\chi_{hl} L_1}{L_t}} - e^{-\frac{\chi_{hl}(L_{hl} - L_2)}{L_t}}\right)\right. \\
&\left. + \left(e^{-\frac{\chi_{hl}(L_{hl} - L_2)}{L_t}} - e^{-\frac{\chi_{hl} L_{hl}}{L_t}}\right) \sin(\beta)\right] \\
&+ \sin(\beta) \left[\left(\theta_s + \frac{\Lambda_c L_t}{\chi_c L_h}\right) \frac{L_c}{H} + \frac{\varphi}{\chi_c} \left(\theta_{hlf} - \theta_s - \frac{\Lambda_c L_t}{\chi_c L_h}\right)\left(1 - e^{-\frac{\chi_c L_c}{L_t}}\right)\right] \\
&+ \frac{\Lambda_{\mathrm{cl}} \varphi}{\chi_{cl} L_h} [L_3 \sin(\beta) - L_{cl} + L_3 + L_4 + L_4 \sin(\alpha)] \\
&+ \frac{\varphi}{\chi_{cl}} \left(\theta_{cf} - \frac{\Lambda_{\mathrm{cl}} L_t}{\chi_{cl} L_h}\right) \left[\left(1 - e^{-\frac{\chi_{cl} L_3}{L_t}}\right) \sin(\beta) + \left(e^{-\frac{\chi_{cl}(L_{cl} - L_4)}{L_t}} - e^{-\frac{\chi_{cl} L_3}{L_t}}\right)\right. \\
&\left. + \left(e^{-\frac{\chi_{cl}(L_{cl} - L_4)}{L_t}} - e^{-\frac{\chi_{cl} L_{cl}}{L_t}}\right) \sin(\alpha)\right]
\end{aligned} \tag{6.25}$$

6.2.2. Perturbation of governing equations – characteristic equation

Following the same procedure given in Section 5.3.4, governing equations 6.11 to 6.15 are perturbed and the following characteristic equation is obtained.

$$n - \frac{Gr_m}{Re_{ss}^3} \oint \frac{\widehat{\theta_f}}{\hat{\omega}} dZ + \frac{pL_t(2-b)}{2DRe_{ss}^b} + K = 0 \tag{6.26}$$

This equation is in the same form as eq. 5.65. The difference in the behaviour is shown by the temperature integral. For determining the temperature integral, following perturbed temperature distribution is used.

$$\frac{\hat{\theta}_f}{\hat{\omega}} = a_h e^{-\frac{\chi_h S}{\varphi}} + \frac{\lambda_{3h}}{\lambda_{1h}} + \left(\frac{\hat{\theta}_{clf}}{\hat{\omega}} - a_h - \frac{\lambda_{3h}}{\lambda_{1h}}\right) e^{-\frac{\lambda_{1h} S}{\varphi}} \qquad 0 \le S \le S_h \tag{6.27}$$

$$\frac{\hat{\theta}_f}{\hat{\omega}} = a_{hl} e^{-\frac{\chi_{hl}(S-S_h)}{\varphi}} + \frac{\lambda_{3hl}}{\lambda_{1hl}} + \left(\frac{\hat{\theta}_{hf}}{\hat{\omega}} - a_{hl} - \frac{\lambda_{3hl}}{\lambda_{1hl}}\right) e^{-\frac{\lambda_{1hl}(S-S_h)}{\varphi}} \qquad S_h \le S \le S_{hl} \tag{6.28}$$

$$\frac{\hat{\theta}_f}{\hat{\omega}} = a_c e^{-\frac{\chi_c(S-S_{hl})}{\varphi}} + \frac{\lambda_{3c}}{\lambda_{1c}} + \left(\frac{\hat{\theta}_{hlf}}{\hat{\omega}} - a_c - \frac{\lambda_{3c}}{\lambda_{1c}}\right) e^{-\frac{\lambda_{1c}(S-S_{hl})}{\varphi}} \qquad S_{hl} \le S \le S_c \tag{6.29}$$

$$\frac{\hat{\theta}_f}{\hat{\omega}} = a_{cl} e^{-\frac{\chi_{cl}(S-S_c)}{\varphi}} + \frac{\lambda_{3cl}}{\lambda_{1cl}} + \left(\frac{\hat{\theta}_{cf}}{\hat{\omega}} - a_{cl} - \frac{\lambda_{3cl}}{\lambda_{1cl}}\right) e^{-\frac{\lambda_{1cl}(S-S_c)}{\varphi}} \qquad S_c \le S \le S_t \tag{6.30}$$

where,

$$a_j = \frac{\lambda_{2j}}{\lambda_{1j} - \chi_j}; j = h, hl, c, cl \tag{6.31}$$

$$\lambda_{2h} = \chi_h \left(\theta_{clf} - \frac{L_t}{L_h \chi_h}\right)\left(1 - B_h + \frac{B_h St_{mih} \Sigma_1}{M_{lh} + St_{mih} \Sigma_1}\right) \tag{6.32a}$$

$$\lambda_{2c} = \chi_c \left(\theta_{hlf} - \theta_s - \frac{\Lambda_c L_t}{\chi_c L_h}\right)\left(1 - B_c + \frac{B_c St_{mic} \Sigma_1}{M_{lc} + St_{mic} \Sigma_1}\right) \tag{6.32b}$$

$$\lambda_{2hl} = \chi_{hl} \left(\theta_{hf} - \frac{\Lambda_{hl} L_t}{\chi_{hl} L_h}\right)\left(1 - B_{hl} + \frac{B_{hl} St_{mihl} \Sigma_1}{M_{lhl} + St_{mihl} \Sigma_1}\right) \tag{6.32c}$$

$$\lambda_{2cl} = \chi_{cl} \left(\theta_{cf} - \frac{\Lambda_{cl} L_t}{\chi_{cl} L_h}\right)\left(1 - B_{cl} + \frac{B_{cl} St_{micl} \Sigma_1}{M_{lcl} + St_{micl} \Sigma_1}\right) \tag{6.32d}$$

$$\lambda_{3j} = \frac{B_j \Lambda_j L_t}{L_h}\left(\frac{-M_{lj}}{St_{mij} \Sigma_1 + M_{lj}}\right); j = h, hl, c, cl \tag{6.33}$$

$\lambda_{1j}, M_{lj}, \Sigma_1$ and Σ_2 are same as defined in Section 5.3. The point temperatures in Eq. 6.27 to 6.30 are given by

$$\frac{\hat{\theta}_{clf}}{\hat{\omega}} = \left[\left\{a_{cl}\left(e^{-\frac{\chi_{cl}L_{cl}}{L_t}} - e^{-\frac{\lambda_{1cl}L_{cl}}{L_t}}\right) + \frac{\lambda_{3cl}}{\lambda_{1cl}}\left(1 - e^{-\frac{\lambda_{1cl}L_{cl}}{L_t}}\right)\right\}\right.$$
$$+ e^{-\frac{\lambda_{1cl}L_{cl}}{L_t}}\left\{a_c\left(e^{-\frac{\chi_c L_c}{L_t}} - e^{-\frac{\lambda_{1c}L_c}{L_t}}\right) + \frac{\lambda_{3c}}{\lambda_{1c}}\left(1 - e^{-\frac{\lambda_{1c}L_c}{L_t}}\right)\right\}$$
$$+ e^{-\frac{\lambda_{1cl}L_{cl}+\lambda_{1c}L_c}{L_t}}\left\{a_{hl}\left(e^{-\frac{\chi_{hl}L_{hl}}{L_t}} - e^{-\frac{\lambda_{1hl}L_{hl}}{L_t}}\right) + \frac{\lambda_{3hl}}{\lambda_{1hl}}\left(1 - e^{-\frac{\lambda_{1hl}L_{hl}}{L_t}}\right)\right\}$$
$$\left. + e^{-\frac{\lambda_{1cl}L_{cl}+\lambda_{1c}L_c+\lambda_{1hl}L_{hl}}{L_t}}\left\{a_h\left(e^{-\frac{\chi_h L_h}{L_t}} - e^{-\frac{\lambda_{1h}L_h}{L_t}}\right) + \frac{\lambda_{3h}}{\lambda_{1h}}\left(1 - e^{-\frac{\lambda_{1h}L_h}{L_t}}\right)\right\}\right]$$
$$\div \left[1 - e^{-\frac{\lambda_{1cl}L_{cl}+\lambda_{1c}L_c+\lambda_{1h}L_h+\lambda_{1hl}L_{hl}}{L_t}}\right] \quad (6.34)$$

$$\frac{\hat{\theta}_{hf}}{\hat{\omega}} = \frac{\hat{\theta}_{clf}}{\hat{\omega}} e^{-\frac{\lambda_{1h}L_h}{L_t}} + a_h\left(e^{-\frac{\chi_h L_h}{L_t}} - e^{-\frac{\lambda_{1h}L_h}{L_t}}\right) + \frac{\lambda_{3h}}{\lambda_{1h}}\left(1 - e^{-\frac{\lambda_{1h}L_h}{L_t}}\right) \quad (6.35)$$

$$\frac{\hat{\theta}_{hlf}}{\hat{\omega}} = \frac{\hat{\theta}_{hf}}{\hat{\omega}} e^{-\frac{\lambda_{1hl}L_{hl}}{L_t}} + a_{hl}\left(e^{-\frac{\chi_{hl}L_{hl}}{L_t}} - e^{-\frac{\lambda_{1hl}L_{hl}}{L_t}}\right) + \frac{\lambda_{3hl}}{\lambda_{1hl}}\left(1 - e^{-\frac{\lambda_{1hl}L_{hl}}{L_t}}\right) \quad (6.36)$$

$$\frac{\hat{\theta}_{cf}}{\hat{\omega}} = \frac{\hat{\theta}_{hlf}}{\hat{\omega}} e^{-\frac{\lambda_{1c}L_c}{L_t}} + a_c\left(e^{-\frac{\chi_c L_c}{L_t}} - e^{-\frac{\lambda_{1c}L_c}{L_t}}\right) + \frac{\lambda_{3c}}{\lambda_{1c}}\left(1 - e^{-\frac{\lambda_{1c}L_c}{L_t}}\right) \quad (6.37)$$

With the fluid temperature completely defined by Eq. 6.27 to 6.30 and eq. 6.34 to 6.37, the temperature integral in characteristic equation can be derived for given orientation. For HHHC, it is given by

$$\oint \frac{\widehat{\theta_f}}{\widehat{\omega}} dZ = \sin(\alpha)\left[a_h\left(\frac{\varphi}{\chi_h}\right)\left(1-e^{\frac{\chi_h L_h}{L_t}}\right)+\frac{\lambda_{3h}L_h}{\lambda_{1h}H}+\left(\frac{\hat{\theta}_{clf}}{\widehat{\omega}}-a_h-\frac{\lambda_{3h}}{\lambda_{1h}}\right)\left(\frac{\varphi}{\lambda_{1h}}\right)\left(1-e^{-\frac{\lambda_{1h}L_h}{L_t}}\right)\right]$$
$$+a_{hl}\left(\frac{\varphi}{\chi_{hl}}\right)\left[\sin(\alpha)\left(1-e^{-\frac{\chi_{hl}L_1}{L_t}}\right)+\left(e^{-\frac{\chi_{hl}L_1}{L_t}}-e^{-\frac{\chi_{hl}(L_{hl}-L_2)}{L_t}}\right)\right.$$
$$\left.+\sin(\beta)\left(e^{-\frac{\chi_{hl}(L_{hl}-L_2)}{L_t}}-e^{-\frac{\chi_{hl}L_{hl}}{L_t}}\right)\right]$$
$$+\frac{\lambda_{3hl}}{\lambda_{1hl}H}(L_1\sin(\alpha)+L_{hl}-L_1-L_2+L_2\sin(\beta))$$
$$+\left(\frac{\widehat{\theta_{hf}}}{\widehat{\omega}}-a_{hl}-\frac{\lambda_{3hl}}{\lambda_{1hl}}\right)\left(\frac{\phi}{\lambda_{1hl}}\right)\left[\left(1-e^{-\frac{\lambda_{1hl}L_1}{L_t}}\right)\sin(\alpha)\right.$$
$$\left.+\left(e^{-\frac{\lambda_{1hl}L_1}{L_t}}-e^{-\frac{\lambda_{1hl}(L_{hl}-L_2)}{L_t}}\right)+\left(e^{-\frac{\lambda_{1hl}(L_{hl}-L_2)}{L_t}}-e^{-\frac{\lambda_{1hl}L_{hl}}{L_t}}\right)\sin(\beta)\right]$$
$$+\sin(\beta)\left[a_c\left(\frac{\varphi}{\chi_c}\right)\left(1-e^{\frac{\chi_c L_c}{L_t}}\right)+\frac{\lambda_{3c}L_c}{\lambda_{1c}H}+\left(\frac{\hat{\theta}_{hlf}}{\widehat{\omega}}-a_c-\frac{\lambda_{3c}}{\lambda_{1c}}\right)\left(\frac{\varphi}{\lambda_{1c}}\right)\left(1-e^{-\frac{\lambda_{1c}L_c}{L_t}}\right)\right]$$
$$+a_{cl}\left(\frac{\varphi}{\chi_{cl}}\right)\left[\left(1-e^{-\frac{\chi_{cl}L_3}{L_t}}\right)\sin(\beta)+\left(e^{-\frac{\chi_{cl}(L_{cl}-L_4)}{L_t}}-e^{-\frac{\chi_{cl}L_3}{L_t}}\right)\right.$$
$$\left.+\left(e^{-\frac{\chi_{cl}(L_{cl}-L_4)}{L_t}}-e^{-\frac{\chi_{cl}L_{cl}}{L_t}}\right)\sin(\alpha)\right]$$
$$+\frac{\lambda_{3cl}}{\lambda_{1cl}H}(L_4\sin(\alpha)-L_{cl}+L_3+L_4+L_3\sin(\beta))$$
$$+\left(\frac{\widehat{\theta_{cf}}}{\widehat{\omega}}-a_{cl}-\frac{\lambda_{3cl}}{\lambda_{1cl}}\right)\left(\frac{\phi}{\lambda_{1cl}}\right)\left[\left(1-e^{-\frac{\lambda_{1cl}L_3}{L_t}}\right)\sin(\beta)\right.$$
$$\left.+\left(e^{-\frac{\lambda_{1cl}(L_{cl}-L_4)}{L_t}}-e^{-\frac{\lambda_{1cl}L_3}{L_t}}\right)+\left(e^{-\frac{\lambda_{1cl}(L_{cl}-L_4)}{L_t}}-e^{-\frac{\lambda_{1cl}L_{cl}}{L_t}}\right)\sin(\alpha)\right]$$

(6.38)

The closure relations for friction and internal heat transfer coefficient are considered same as SHF/LH case.

6.3. Results and discussion

With the experience attained during linear stability analysis for SHF/LH case, computer code for IHG/DH case has been developed based on graphical solution method (Algorithm 3) which has been explained in section 4.3. In this code all the sub-models i.e. BM+WTI+HX, BM+WTI, BM* and BM have been implemented for the purpose of analysis requirements

foreseen. In the current study, the analysis is focused on HHHC orientation which is of interest from stability perspective.

6.3.1. Validation of model and computer code

The solution methodology and formulation for IHG/DH case have been validated by comparing the code predictions with published theoretical results of Cammi *et al.* [30]. They employed a model which takes into account the surface heat flux at heater and constant internal heat generation throughout the loop. In their model, the amount of internal heat generation can be manipulated by a parameter 'α' which takes a value of one in case of zero internal heat generation and a value of zero for purely internal heat generation constant throughout the loop. For both cases they have analysed the loop of Vijayan *et al.* [22].

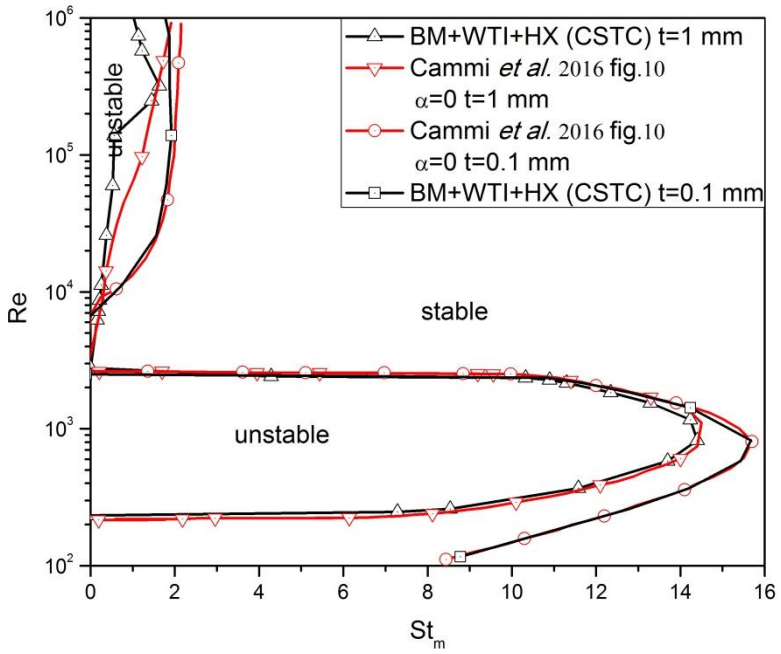

Fig. 6.1 Validation of LSA model BM+WTI+HX (CSTC) for IHG/DH case, with theoretical predictions of Cammi *et al.* [30]

They modelled cooler by taking constant temperature on outside surface of wall. By taking limiting condition $St_{m,oc} \rightarrow \infty$ to mimic the cooler model they used, developed computer

code has been used to generate stability maps for the same loop they analysed at two different thicknesses i.e. 1 mm and 0.1 mm. The dimensionless property parameters have been taken the same (it is to be noted that the definition of dimensionless property parameters in current study is inverse of the definition of Cammi *et al.*).The results are presented in fig. 6.1. In this validation trial, the closure relation for internal heat transfer coefficient and friction factor have been employed the same as used by them. It can be observed from fig. 6.1 that in the case of 0.1 mm thickness, the predictions agree very well whereas in case of 1 mm thickness, the developed code predicts smaller unstable zone in turbulent flow regime. Fig 6.1 also demonstrates the effect of wall thermal inertia (here, parameter is thickness) on stability behaviour. It can be observed that SS wall of higher thickness could induce some stabilization in the loop in both laminar and turbulent region.

Unfortunately, other than the theoretical predictions with which the validation has been performed, no experimental data for the case of internal heat generation is available in literature.

6.3.2 Studies on MSNCL

A detailed analysis has been performed for IHG/DH case, considering MSNCL geometry, material of construction and working fluid. Model BM+WTI+HX has been applied with different percentages of IHG distributed uniformly in the loop. For the study purpose, cases with $\Lambda_j = 0, 0.05, 0.10$ ($j = hl, c, cl$) have been analysed. It has been observed that MSNCL is stable in its actual configuration for all these three cases of IHG at all operating conditions studied (Gr_m: 10^8 to 10^{25}, St_{moc}: 0 to 50). For the sake of investigating the effect of distributed IHG on stability, a special case of "no wall" has been analysed using model BM. Initially, the case of internal heat generation in core ($\Lambda_j = 0; j = hl, cl, c$) has been compared with

SHF/LH case to investigate the effect of heating mode on stability. The result is plotted in fig. 6.2.

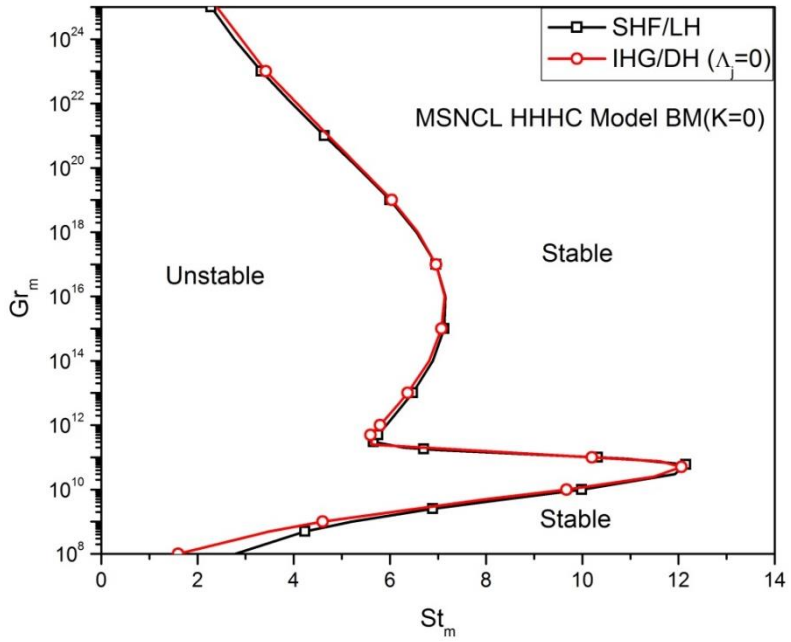

Fig 6.2 Comparison of stability maps of MSNCL predicted by model BM (K=0) for different heating modes

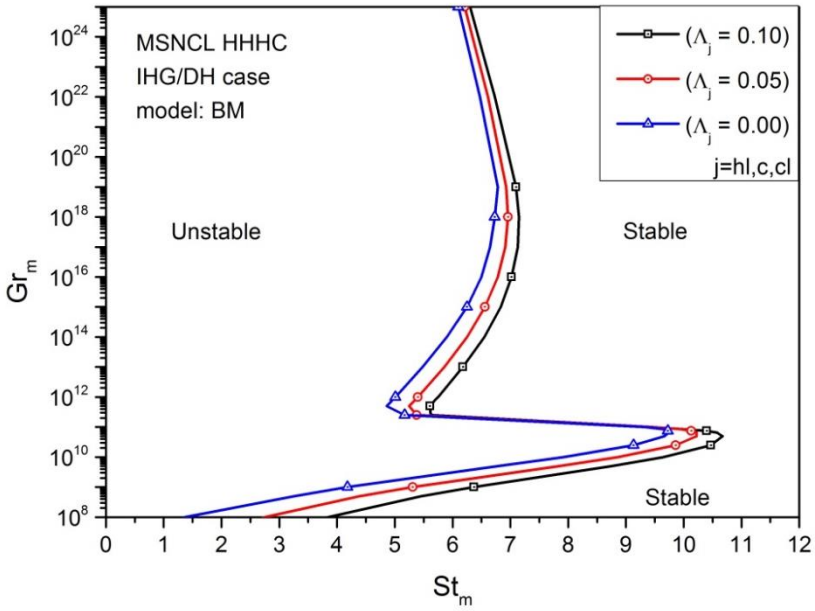

Fig 6.3 Effect of IHG outside the heater on the stability behaviour of MSNCL (generated by model BM)

It can be observed that stability of the loop is not much affected by the mode of heating as far as the assumptions taken in the formulation are satisfied. Next, the cases with IHG of 5% ($\Lambda_j = 0.05; j = hl, cl, c$) and 10% ($\Lambda_j = 0.10; j = hl, cl, c$) are analysed and the results are plotted along with IHG of 0% in fig. 6.3. It has been observed that the unstable zone increases for the loop as the IHG outside the heater increases. The possible reason for this result can be net reduction in effectiveness of cooler due to internal heat generation. So, a higher cooling rate would be required to achieve stabilization at a given core power.

For the same case of MSNCL, presence and absence of the wall has been observed to make significant difference. This is similar to that observed in SHF/LH case. Validation of predictions of LSA codes with model BM+WTI+HX with non-linear analysis are discussed in next chapter.

6.4. Concluding remarks

In this chapter, an LSA model considering distributed internal heat generation throughout the loop has been derived with assumption of negligible neutronics effect. This model has been validated with theoretical predictions available in literature for a special case. Later, it has been applied to MSNCL. The main conclusions derived are,

1. Distributed internal heat generation causes an increase in unstable zone for a typical NCL when wall thermal inertia etc. stabilizing effects are not present (or negligible).

2. Wall thermal inertia can cause significant stabilization to loop dynamics even in case of IHG/DH. MSNCL loop is stable in all operating conditions studied, in case of uniform internal heat generation of 0 – 10% of heater power.

CHAPTER 7

Nonlinear Stability Analysis – Insights into Observations So Far

As introduced in chapter 1, time domain analysis involves solution of governing partial differential equations of natural circulation to assess the stability of NCL at given operating conditions. This method complements the stability analysis of NCLs to better understand the loop dynamics which lead to instabilities. In the current work, time domain analysis (referred as NLSA hereafter) is utilized to understand the role of wall heat capacity on stabilization of NCL and to validate the stability maps generated by linear stability analysis methods in chapter 5 and 6.

7.1. Formulation

7.1.1. Governing equations

The governing equations for natural circulation have been derived in chapter 5 and chapter 6 for SHF/LH and IHG/DH cases respectively. Due to flexibility in accounting for both the cases with single set of governing equations, NLSA formulation has been obtained directly by combining suitable equations derived earlier.

Continuity and momentum equations are same for both the cases and they are given by Eq. 5.3 and 5.10. For fluid energy equation, Eq. 6.5 is considered to account for distributed internal heat generation. Conservation equation for energy of inner shell of wall is same for both cases and given by Eq. 5.16. The energy conservation for outer shell of wall is taken from Eq. 5.19 to account for surface heat flux at heater. All the above mentioned equations are reproduced here for easy reference in further derivation. It should be noted that T_{wi} and T_{wo} are aliased hereafter as T_1 and T_2 respectively to avoid crowded representation with lot of superscripts and subscripts.

$$\frac{\partial(w)}{\partial s} = 0 \tag{7.1}$$

$$\frac{L_t}{A}\frac{\partial w}{\partial t} = -\rho_0 g\beta \oint T.sin(\gamma).ds - \left(\frac{fL_t}{D} + K\right)\frac{w^2}{2\rho_0 A^2} \tag{7.2}$$

$$\frac{\partial(T)}{\partial t} = -\frac{w}{\rho A}\frac{\partial w}{\partial s} + \frac{1}{\rho C_p}\frac{\partial}{\partial s}\left(k\frac{\partial T}{\partial s}\right) + \frac{h_i P(T_{wi}-T)}{\rho A C_p} \tag{7.3}$$

$$\frac{\partial(T_{wi})}{\partial t} = \frac{1}{\rho_w C_{pw}}\frac{\partial}{\partial s}\left(k_w\frac{\partial T_{wi}}{\partial s}\right) - \frac{h_i P(T_{wi}-T)}{A_1\rho_w C_{pw}} + \frac{T_{wo}-T_{wi}}{R_w\rho_w C_{pw}A_1} \tag{7.4}$$

$$\frac{\partial(T_{wo})}{\partial t} = \frac{1}{\rho_w C_{pw}}\frac{\partial}{\partial s}\left(k_w\frac{\partial T_{wo}}{\partial s}\right) - \frac{T_{wo}-T_{wi}}{R_w\rho_w C_{pw}A_2} + \frac{Q_b}{A_2\rho_w C_{pw}} \tag{7.5}$$

where,

$$Q_b = \begin{cases} h_o(T_{amb}-T_{wo})P_2 + qP_2 & Heater \\ h_o(T_{amb}-T_{wo})P_2 & piping \\ h_o(T_s-T_{wo})P_2 & cooler \end{cases} \tag{7.6}$$

From adaptation of the same equations as used for linear stability analysis, it is evident that the underlying assumptions are same except with two exemptions. In NLSA, the axial heat conduction in fluid and wall are considered in analysis and no linearization is employed for any term.

7.1.2. Numerical solution of governing equations

The equations 7.1 to 7.5 are solved numerically. The solution procedure involves discretization of the partial differential equations by finite difference method to obtain algebraic equations and then solving them with suitable algorithm to obtain the solution at each location in the loop for consecutive time steps.

Diffusion terms have been discretized with central difference scheme [34] and convective terms have been discretized with first order (linear) upwind scheme [34]. Time derivatives in

energy equations have been discretized with explicit differencing scheme [34] whereas that of momentum equation has been discretized with implicit differencing scheme [34].

Fig. 7.1 shows a typical segment of NCL divided by nodes *j-1, j, j+1 ...* with spacing $\Delta s_j, \Delta s_{j+1}$ ... Discretization of governing equations is performed for a general case of variable spacing between the nodes i.e. $\Delta s_j \neq \Delta s_{j+1}$.

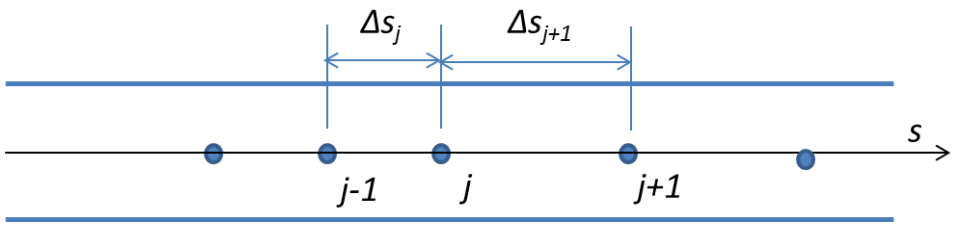

Fig. 7.1 Schematic showing a typical segment of NCL discretized by nodes with variable spacing between them

The discretized momentum equation at a typical node *j* is given as

$$\frac{w^{n+1}-w^n}{\Delta t} = -\frac{p\mu^b}{2\rho D^{1+b}A^{(1-b)}}.w^{n+1}|w^{n+1}|^{1-b} - \frac{K}{2\rho AL_t}w^{n+1}|w^{n+1}| + \frac{\rho g\beta_f A}{L_t}\oint T.\sin(\gamma).ds \tag{7.7}$$

After rearrangement of terms, it can be written as

$$x.w^{n+1}|w^{n+1}|^{1-b} + y.w^{n+1}|w^{n+1}| + w^{n+1} - z = 0 \tag{7.8}$$

where,

$$x = \frac{p\mu^b\Delta t}{2\rho D^{1+b}A^{(1-b)}};\ y = \frac{K\Delta t}{2\rho AL_t};\ z = \frac{\rho g\beta_f A\Delta t}{L_t}\oint T.\sin(\gamma).ds + w^n \tag{7.9}$$

The energy equation of fluid (Eq. 7.3) is discretized at a typical node *j* as follows

$$\frac{T_j^{n+1}-T_j^n}{\Delta t} + \frac{|w|}{\rho A}.\frac{T_j^n-T_x^n}{\Delta s_x} = \frac{\alpha}{\Delta s}.\frac{\left(\Delta s_j\left(T_{j+1}^n-T_j^n\right)-\Delta s_{j+1}\left(T_j^n-T_{j-1}^n\right)\right)}{\Delta s_j.\Delta s_{j+1}} + \frac{h_i P}{\rho C_p A}\left(T_{1j}^{n+1}-T_j^n\right) + \frac{q'''}{\rho C_p} \tag{7.10}$$

where,

$T_x = \begin{cases} T_{j-1} & \text{for } w > 0 \\ T_{j+1} & \text{for } w < 0 \end{cases}$ and $\Delta s_x = \begin{cases} \Delta s_j & w > 0 \\ \Delta s_{j+1} & w < 0 \end{cases}$ according to first order upwind scheme

and $\Delta s = 0.5\left(\Delta s_j + \Delta s_{j+1}\right)$

After rearrangement of terms, Eq. 7.10 can be written in standard explicit form as

$$T_j^{n+1} = a_{j-1}T_{j-1}^n + a_j T_j^n + a_{j+1}T_{j+1}^n + b_j \tag{7.11}$$

Where,

$$a_j = 1 - \frac{|w|\Delta t}{\rho A \Delta s_x} - \frac{2\alpha\Delta t}{\Delta s_{j+1}\Delta s_j} - \frac{h_i P \Delta t}{\rho C_p A} \tag{7.12a}$$

$$a_{j-1} = \begin{cases} \frac{|w|\Delta t}{\rho A \Delta s_j} + \frac{\alpha\Delta t}{\Delta s.\Delta s_j} & \text{for } w > 0 \\ \frac{\alpha\Delta t}{\Delta s.\Delta s_j} & \text{for } w < 0 \end{cases} \tag{7.12b}$$

$$a_{j+1} = \begin{cases} \frac{\alpha\Delta t}{\Delta s.\Delta s_{j+1}} & \text{for } w > 0 \\ \frac{|w|\Delta t}{\rho A \Delta s_{j+1}} + \frac{\alpha\Delta t}{\Delta s.\Delta s_{j+1}} & \text{for } w < 0 \end{cases} \tag{7.12c}$$

$$b_j = \frac{h_i P \Delta t}{\rho C_p A}.T_{1j}^{n+1} + \frac{q'''}{\rho C_p} \tag{7.12d}$$

Discretized form of the energy equations of inner and outer shells at a typical node *j* are

$$\frac{T_{1,j}^{n+1} - T_{1,j}^n}{\Delta t} = \frac{\alpha_w}{\Delta s} \frac{\left(\Delta s_j\left(T_{1,j+1}^n - T_{1,j}^n\right) - \Delta s_{j+1}\left(T_{1,j}^n - T_{1,j-1}^n\right)\right)}{\Delta s_j.\Delta s_{j+1}} - \frac{h_i P}{\left(\rho C_p\right)_w A_1}\left(T_{1,j}^n - T_j^n\right) + \frac{T_{2,j}^{n+1} - T_{1,j}^n}{\left(\rho C_p\right)_w A_1 R_w} \tag{7.13}$$

$$\frac{T_{2,j}^{n+1} - T_{2,j}^n}{\Delta t} = \frac{\alpha_w}{\Delta s} \frac{\left(\Delta s_j\left(T_{2,j+1}^n - T_{2,j}^n\right) - \Delta s_{j+1}\left(T_{2,j}^n - T_{2,j-1}^n\right)\right)}{\Delta s_j.\Delta s_{j+1}} - \frac{T_{2,j}^n - T_{1,j}^n}{\left(\rho C_p\right)_w A_2 R_w} + \frac{Q_b}{\left(\rho C_p\right)_w A_2} \tag{7.14}$$

Where,

$$Q_b = \begin{cases} q''P_2 + h_o P_2\left(T_{amb} - T_{2j}^n\right) & \text{heater} \\ h_o P_2\left(T_s - T_{2j}^n\right) & \text{cooler} \\ h_o P_2\left(T_{amb} - T_{2j}^n\right) & \text{otherwise} \end{cases} \quad (7.15)$$

After rearrangement into explicit form Eq. 7.13 and 7.14 can be written as

$$T_{1,j}^{n+1} = a_{1,j-1}T_{1,j-1}^n + a_{1,j}T_{1,j}^n + a_{1,j+1}T_{1,j+1}^n + b_{1,j} \quad (7.16)$$

Where,

$$a_{1,j} = 1 - \frac{2\alpha_w \Delta t}{\Delta s_{j+1}\Delta s_j} - \frac{h_i P \Delta t}{(\rho C_p)_w A_1} - \frac{\Delta t}{(\rho C_p)_w A_1 R_w} \quad (7.17a)$$

$$a_{1,j-1} = \frac{\alpha_w \Delta t}{\Delta s.\Delta s_j} \quad (7.17b)$$

$$a_{1,j+1} = \frac{\alpha_w \Delta t}{\Delta s.\Delta s_{j+1}} \quad (7.17c)$$

$$b_{1,j} = \frac{h_i P \Delta t}{(\rho C_p)_w A_1}.T_j^n + \frac{T_{2,j}^{n+1}\Delta t}{(\rho C_p)_w A_1 R_w} \quad (7.17d)$$

$$T_{2,j}^{n+1} = a_{2,j-1}T_{2,j-1}^n + a_{2,j}T_{2,j}^n + a_{2,j+1}T_{2,j+1}^n + b_{2,j} \quad (7.18)$$

Where,

$$a_{2,j} = 1 - \frac{2\alpha_w \Delta t}{\Delta s_{j+1}\Delta s_j} - \frac{h_o P_2 \Delta t}{(\rho C_p)_w A_2} - \frac{\Delta t}{(\rho C_p)_w A_2 R_w} \quad (7.19a)$$

$$a_{2,j-1} = \frac{\alpha_w \Delta t}{\Delta s.\Delta s_j} \quad (7.19b)$$

$$a_{2,j+1} = \frac{\alpha_w \Delta t}{\Delta s.\Delta s_{j+1}} \quad (7.19c)$$

$$b_{2,j} = \frac{T_{1,j}^n \Delta t}{(\rho C_p)_w A_2 R_w} + \frac{\Delta t}{(\rho C_p)_w A_2}.\begin{cases} q''P_2 + h_o P_2 T_{amb} & \text{heater} \\ h_o P_2 T_s & \text{cooler} \\ h_o P_2 T_{amb} & \text{otherwise} \end{cases} \quad (7.19d)$$

To satisfy the rule of positive coefficients, a_j (Eq. 7.12a), $a_{1,j}$ (Eq. 7.17a) and $a_{2,j}$ (Eq. 7.19a) are to be maintained positive. This renders a maximum limit on the time step for given operating conditions, geometry and node size. So, time step is kept as internal solution parameter which is determined as minimum of the maximum possible time step for each of these coefficients. Mathematically,

$$\Delta t = \min\left(\Delta t_f, \Delta t_{wi}, \Delta t_{wo}\right) \tag{7.20}$$

Where,

$$\Delta t_f = \left(\frac{|w|}{\rho A \Delta s_x} + \frac{2\alpha}{\Delta s_{j+1}\Delta s_j} + \frac{h_i P}{\rho C_p A}\right)^{-1} \tag{7.21}$$

$$\Delta t_{wi} = \left(\frac{2\alpha_w}{\Delta s_{j+1}\Delta s_j} + \frac{h_i P}{(\rho C_p)_w A_1} + \frac{1}{(\rho C_p)_w A_1 R_w}\right)^{-1} \tag{7.22}$$

$$\Delta t_{wo} = \left(\frac{2\alpha_w}{\Delta s_{j+1}\Delta s_j} + \frac{h_o P_2}{(\rho C_p)_w A_2} + \frac{1}{(\rho C_p)_w A_2 R_w}\right)^{-1} \tag{7.23}$$

Solution procedure:

Initially, the solution is initialized to given flow rate and temperature distribution. Time step is calculated by Eq. 7.20 with suitable under relaxation. With this time step, the temperature distribution of wall outer shell is determined throughout the loop and then using the updated outer shell temperatures, the inner shell temperatures are determined. These updated inner shell temperatures are in turn used to determine the fluid temperatures. Once the fluid temperatures are updated at current time step, the integral in the discretized momentum equation (Eq. 7.8) is determined numerically. With all the coefficients determined, the mass flow rate is updated by solving the Eq. 7.8 iteratively by Newton-Raphson method. Under relaxation and tolerances are employed, as per the usage experience, to their optimum values. This whole procedure has been implemented as a computer code.

Validation studies:

The computer code implemented here is named and referred hereafter as NLSA code. The formulation, solution methodology and solution parameters of NLSA code have been verified by comparing its steady state flow rate predictions with those of LSA codes (LSA codes determine steady state conditions before performing stability analysis). LSA codes have been chosen for this task because of their analytical way of predicting the steady state flow rates. Except the axial heat conduction, all the details of the loop that are simulated by NLSA are present in the formulation of LINSTA. Analysis has been performed for MSNCL geometry in HHHC orientation considering its material of construction and working fluid. A secondary side heat transfer coefficient of 100 W/m^2K and Prandtl number of 5 have been used. Analysis has been performed for the case of heat loss also. The results are shown in fig. 7.2.

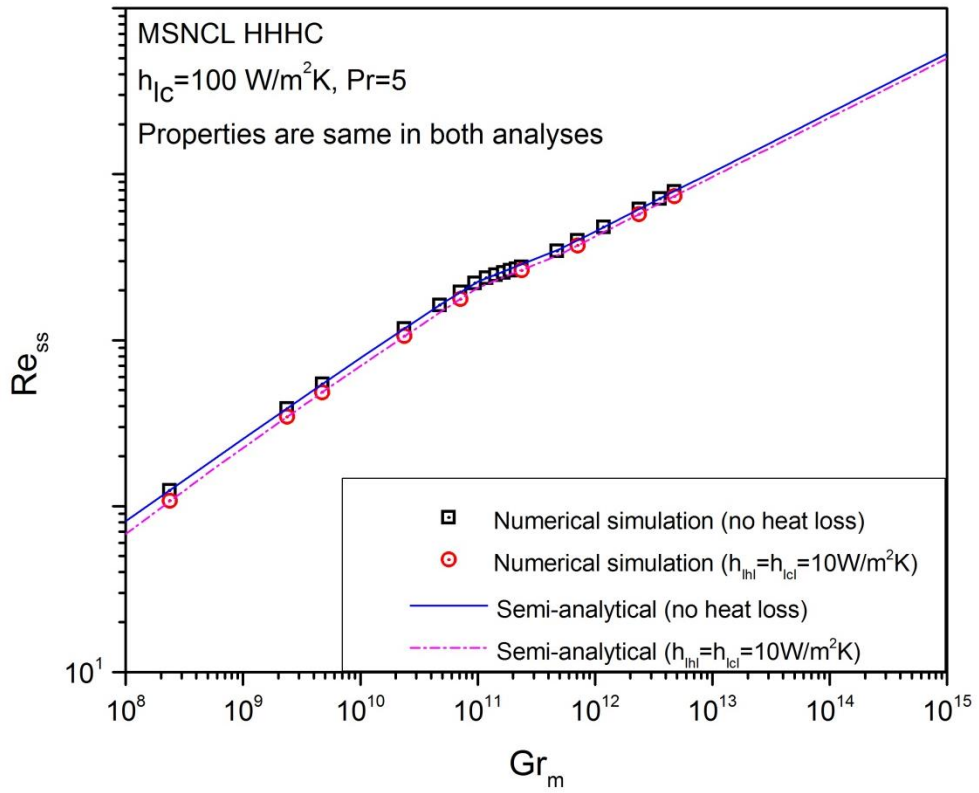

Fig. 7.2 Comparison of analytical and numerical predictions of steady state flow rates

For this study, SHF/LH case has been considered. For heat loss case, a heat loss coefficient of 10 W/m^{2}K has been taken for hot leg and cold leg. NLSA code has been proven to predict the steady state behaviour of the loop to the accuracy of semi-analytical LSA models with and without heat losses. The maximum deviation from analytical model is < 5%. Excluding the transition zone, the maximum error observed is < 1%.

7.2. Application of NLSA code

The NLSA code has been applied initially to study the phenomenon of stabilization of NCL by increased wall heat capacity. Later, NLSA code has been applied for validating the stability maps generated by LSA codes for different cases.

7.2.1. Stabilization of NCL by increased wall heat capacity

In literature it was quoted [25, 29, 30] that wall thermal inertia (represented by heat capacity, $\rho C_p V$ of wall) has stabilizing effect on NCL thermal hydraulics. In current study, LSA codes predicted the same with both MSNCL and the loop of Swapnalee and Vijayan [24] (Section 5.8). To study this phenomenon, a case has been considered in which a given NCL would be unstable at lower heat capacity and stable at higher heat capacity. The difference in the loop behaviour in these cases has been expected to give evidence for understanding the phenomenon of current interest.

For this analysis, NCL of Swapnalee and Vijayan [24] has been considered at a power of 1600 W and secondary heat transfer coefficient corresponding to $h_{oc}D_2 = 1.588$ W/mK (ensures same cooling rate for all cases). Prandtl number in this analysis is taken as 2. Simulations with NLSA code have been performed considering piping wall thicknesses 1 mm, 2 mm and 3.73 mm. Initially a steady state is established with 10 % higher flow rate than that calculated theoretically. This excess flow rate helps as a perturbation at the time the

flow rate starts getting updated according to momentum equation (Eq. 7.8). The variation of flow rate and temperatures are plotted in figs. 7.3 and 7.4. Fig. 7.3 shows the variation of mass flow rate with time and the variation of temperature of fluid with time at four different locations *viz.* near to the outlet of heater, in the middle of hot leg, near to the outlet of cooler and in the middle of cold leg. Fig. 7.4 shows the variation of fluid and outer shell temperatures at the beginning and ending of hot leg of NCL with time.

From fig. 7.3, it is evident that NCL is unstable at this operating condition for a wall thickness of 1 mm. This is in agreement with prediction of LSA. The sequence of events leading to instability is observed to be same as proposed by Welander [9] and is summarized with help of fig. 7.3 as follows. The initial flow rate for which steady state is forcibly established cannot be sustained by buoyancy. So, there is a drop in the flow rate at t = 20000 s (arbitrarily chosen starting point). This drop in the flow rate leads to increase (decrease) in the temperature of hot (cold) fluid coming from heater (cooler). This hotter (cooler) fluid is called warm (cold) pocket. A warm (cold) pocket can be identified by a peak (trough) in the fluid temperature in heater (cooler) and hot (cold) leg in fig. 7.3. Once the warm (cold) pocket enters the hot (cold) leg, buoyancy increases to a higher value than earlier and leads to an increase in the flow rate (fig. 7.3). Due to higher flow rate, the warm (cold) pocket cannot be cooled (heated) effectively in cooler (heater). So, the fluid emerges from cooler (heater) is hotter (colder) than earlier as evident from fig. 7.3. As soon as the warm (cold) pocket enters cold (hot) leg, buoyancy reduces leading to a reduction in the flow rate (fig. 7.3). Reduction in flow rate helps in further increment (decrement) in the temperature of warm (cold) pocket. This cycle repeats indefinitely. A typical cycle of warm pocket movement in NCL is depicted as 1-2-3-4-1 using black arrows in fig. 7.3.

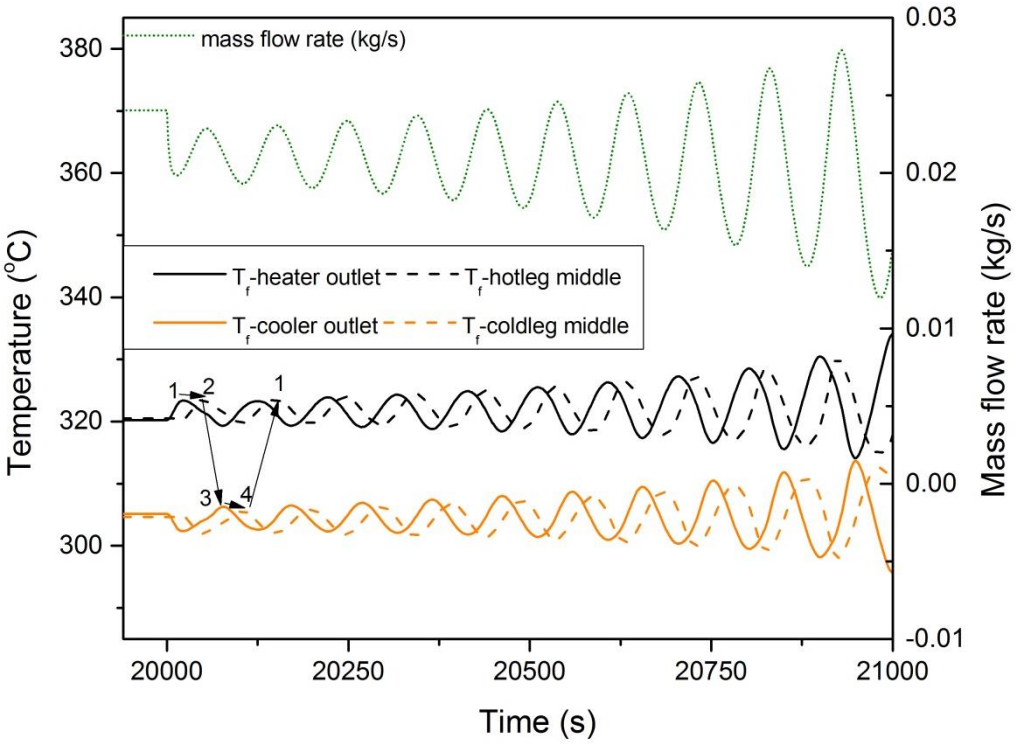

Fig. 7.3 Flow rate and fluid temperature variation with time for a wall thickness of 1 mm (power = 1600 W, $h_{oc}D_2 = 1.588$ W/mK)

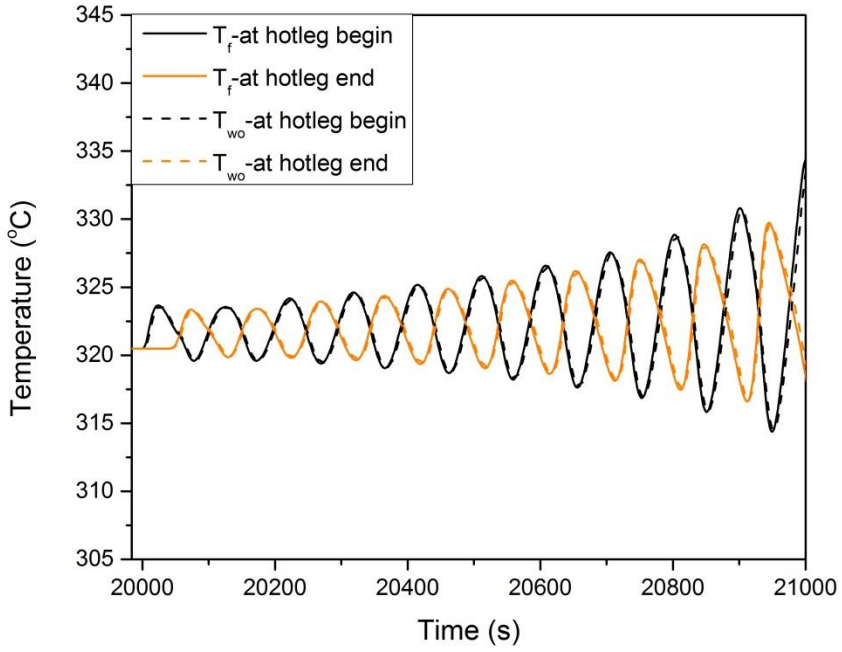

Fig. 7.4 Fluid and wall temperature variation with time at different locations for a wall thickness of 1 mm (power = 1600 W, $h_{oc}D_2 = 1.588$ W/mK)

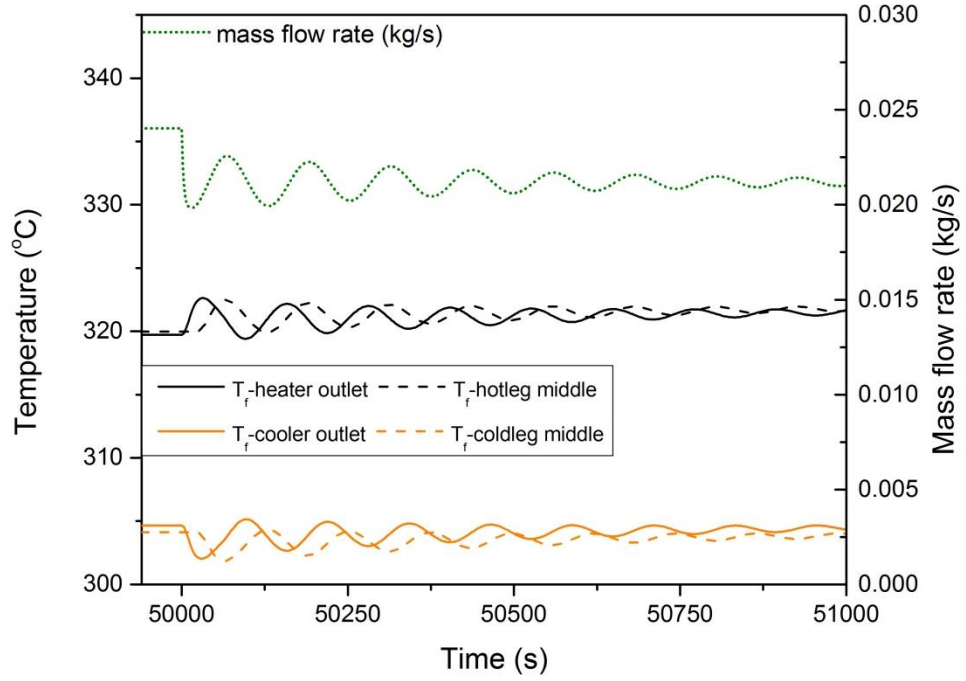

Fig.. 7.5 Flow rate and fluid temperature variation with time for a wall thickness of 2 mm (power = 1600 W, $h_{oc}D_2 = 1.588$ W/mK)

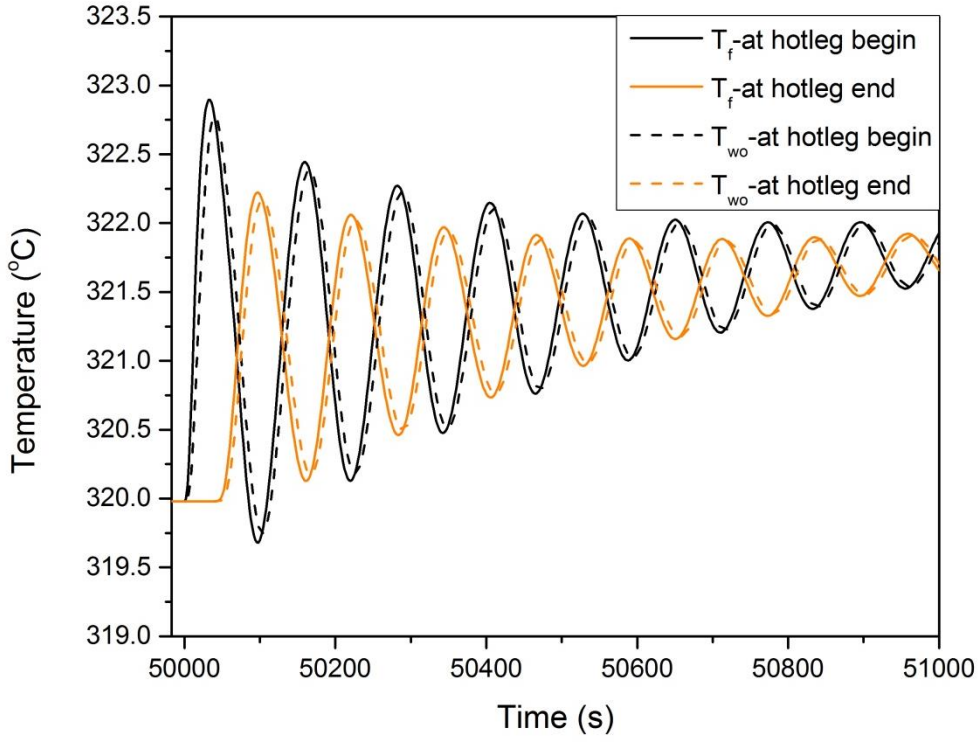

Fig. 7.6 Fluid and wall temperature variation with time at different locations for a wall thickness of 2 mm (power = 1600 W, $h_{oc}D_2 = 1.588$ W/mK)

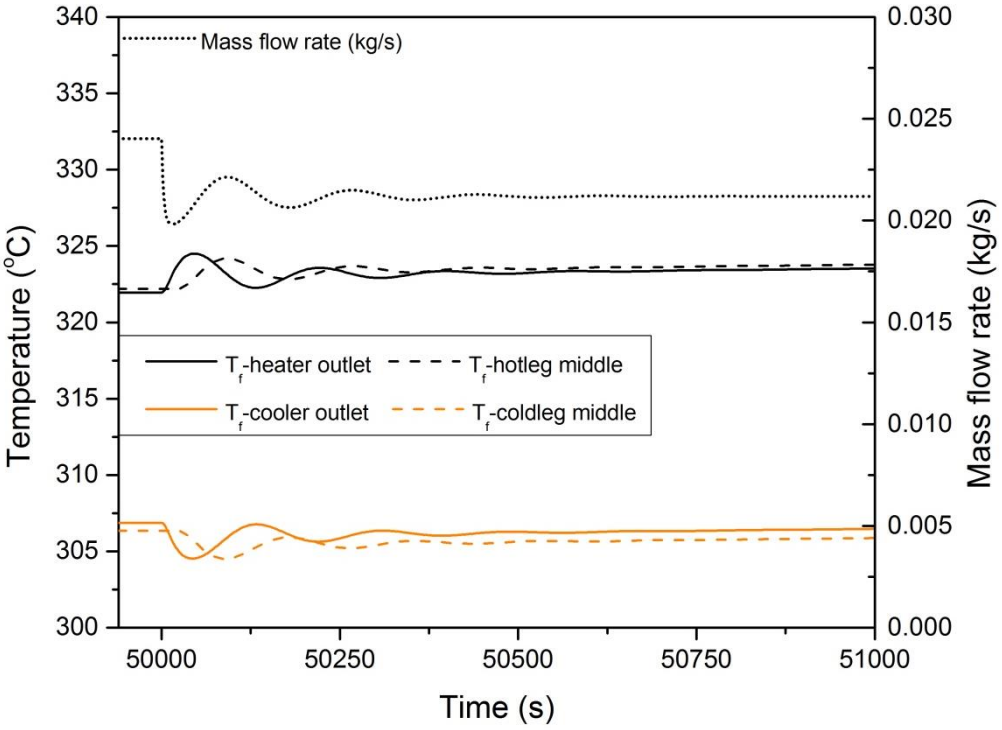

Fig.. 7.7 Flow rate and fluid temperature variation with time for a wall thickness of 3.73 mm (power = 1600 W, $h_{oc}D_2 = 1.588$ W/mK)

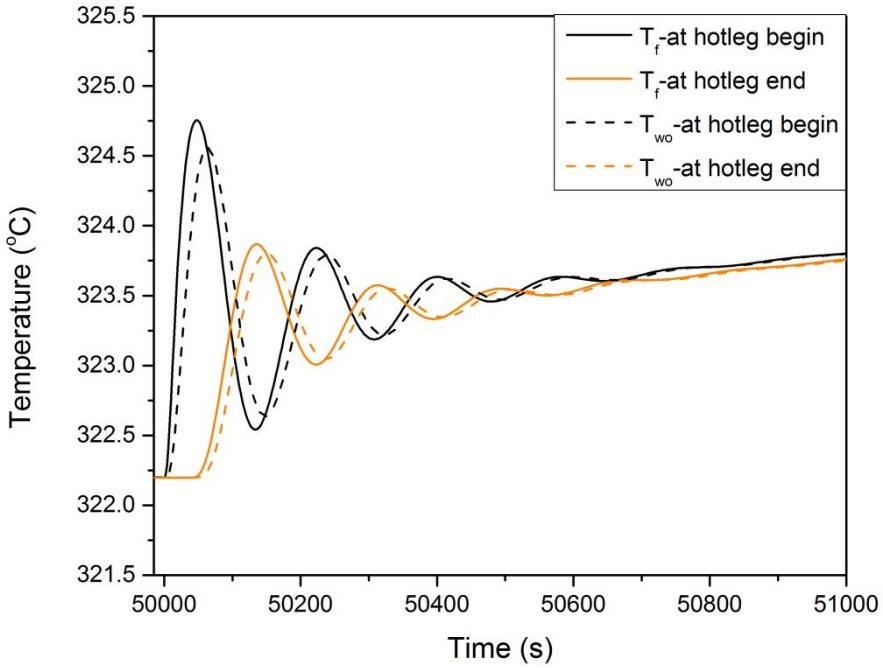

Fig. 7.8 Fluid and wall temperature variation with time at different locations for a wall thickness of 3.73 mm (power = 1600 W, $h_{oc}D_2 = 1.588$ W/mK)

It can be observed from fig. 7.4 that the wall is getting heated as fast as the warm pocket traverses through that location. It is a manifestation of lower heat capacity of the wall (due to low volume). Further investigation on fig. 7.4 will be done after putting forward the results of simulations with 2 mm and 3.73 mm wall thickness.

The same simulation procedure described above is followed with 2 mm and 3.73 mm wall thickness and the corresponding observations are plotted in figs. 7.5 – 7.8. Some quantitative details of the simulations are given in table 7.1. From figs. 7.5 and 7.7, it is evident that NCL is stable at this operating condition for wall thickness 2 mm and 3.73 mm. This is also in agreement with predictions of LSA code. While every other parameter is kept constant, the increase in the thickness of wall solely stabilized the loop dynamics. When the sequence of events which led to instability in case of 1 mm thick wall is revisited for 2 mm case, it is evident that these events do happen in this case also, but for a finite time. The difference can be observed by comparison of figs. 7.4 and 7.6. Wall temperature increases (decreases) due to heat exchange with warm (cold) pocket traversing by. The amount of heat exchange depends on temperature difference between fluid and wall and heat transfer coefficient. The temperature difference between wall and fluid depends on the heat capacity. If wall heat capacity is high, raise in its temperature is low thus able to get more heat from warm pocket. Coming to the observations, the increase in wall temperature (due to heat exchange with warm pocket) is quicker in case of 1 mm thickness due to its low heat capacity, thus amount of heat exchange is lower. So, the reduction in the intensity (represented by hotness (coldness)) of warm (cold) pocket while it is traversing through hot (cold) leg is lower in this case (difference in the first and second peaks in fluid temperature in fig. 7.4 is smaller than that in fig. 7.6. refer table 7.1 also). Thus in case of higher thickness, the buoyancy increment is lower leading to lower shoot up in the flow rate. This in turn leads to better cooling (heating) of warm (cold) pocket. In this way, wall is able to diminish the thermal anomalies

(warm and cold pockets) that arise in the fluid. These phenomena can be observed with much clarity in the case of 3.73 mm thick wall where stabilization is much faster.

It can be observed from table 7.1 that first warm pocket intensity is highest in case of low thickness. It can be explained as follows. When the flow rate suddenly drops, the heat transfer resistance between fluid and wall inner surface will increase. But, the heat flux is kept constant. So, the imbalance in the heat given by heater and heat delivered to fluid helps in increasing the wall temperature which in turn facilitate complete heat transfer to fluid. The more the heat capacity of the wall, the more will be the lag in this phenomena leading to low intensity warm pocket.

Table 7.1: Some quantitative results of simulation studies on wall effect

Thickness (mm)	**Steady state temperature at heater outlet (T_{ss} ^oC)**	**First warm pocket temperature (^oC)**		**T_1-T_{ss}**	**T_1-T_2**
		At hot leg begin (T_1)	**At hot leg end (T_2)**		
1	320.49	323.66	323.34	3.17	0.32
2	319.97	322.89	322.221	2.92	0.669
3.73	322.19	324.75	323.86	2.56	0.89

It should be noted here that solely increasing the thickness of wall or selecting a material of high heat capacity may not guarantee the stability unless the material has sufficient thermal conductivity. If the material has insufficient thermal conductivity, the temperature transient may not be able to travel to full thickness provided, due to thermal resistance, rendering the outermost volume of wall ineffective in stabilizing the NCL dynamics. Even if the loop dynamics gets stabilized with low thermal conductivity, it would take more number of oscillations before reaching steady state.

In the turbulent region, the stabilization due to wall may get enhanced due to increase in heat transfer coefficient with flow rate.

7.2.2. Validation of LSA predictions

The stability maps generated by LSA code for the cases of SHF/LH and IHG/DH have been validated with either published or experimental data in chapter 5. However, a detailed validation of the predictions of LSA model developed in current work could not be done due to lack of sufficient experimental data. Due to approximations involved in linearization process, some inaccuracy is expected to creep into predictions. So, a further and detailed investigation on the accuracy of the predictions of LSA codes has been performed using the code NLSA. It is achieved by simulating the concerned NCL at different operating conditions and observing its stability behaviour. In this respect, the scope of NLSA code has been limited to confirm the predictions of LSA code, instead of simulating the experimentally observed transient behaviours.

SHF/LH case

NLSA code can simulate the transient behaviour equivalent to the models BM+WTI+HX and BM+WTI+HX+HL with an additional feature of considering axial heat conduction in fluid and wall. So, the validation studies have been performed for the predictions of model BM+WTI+HX for the NCL of Vijayan *et al.* [22] (fig. 5.6) and for MSNCL (fig. 5.9). In each simulation, an operating power and secondary side heat transfer coefficient for cooler have been chosen. All the thermo-physical properties and conditions have been kept the same as taken for LSA. Simulation at each operating condition has been started from theoretical steady state conditions and a perturbation has been given at reference time t = 0 s. The evolution of mass flow rate has been observed. Successive amplification or recurrence of perturbation has been considered as unstable state; otherwise, the loop has been taken as

stable. The observations for loop of Vijayan *et al.* [22] and MSNCL are given in figs. 7.9 & 7.10.

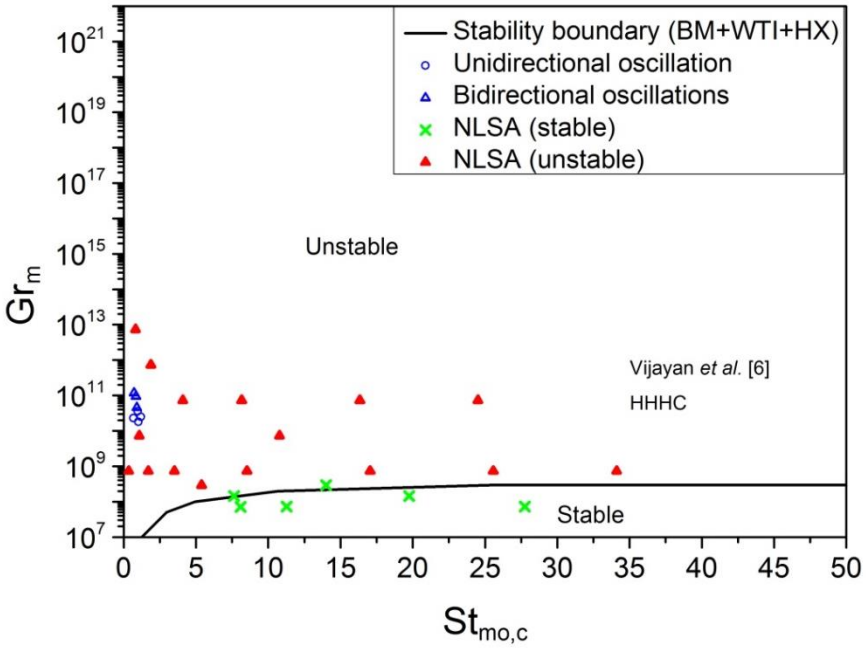

Fig. 7.9 Validation of LSA (model BM+WTI+HX) predictions for NCL of Vijayan *et al.* [22] with NLSA

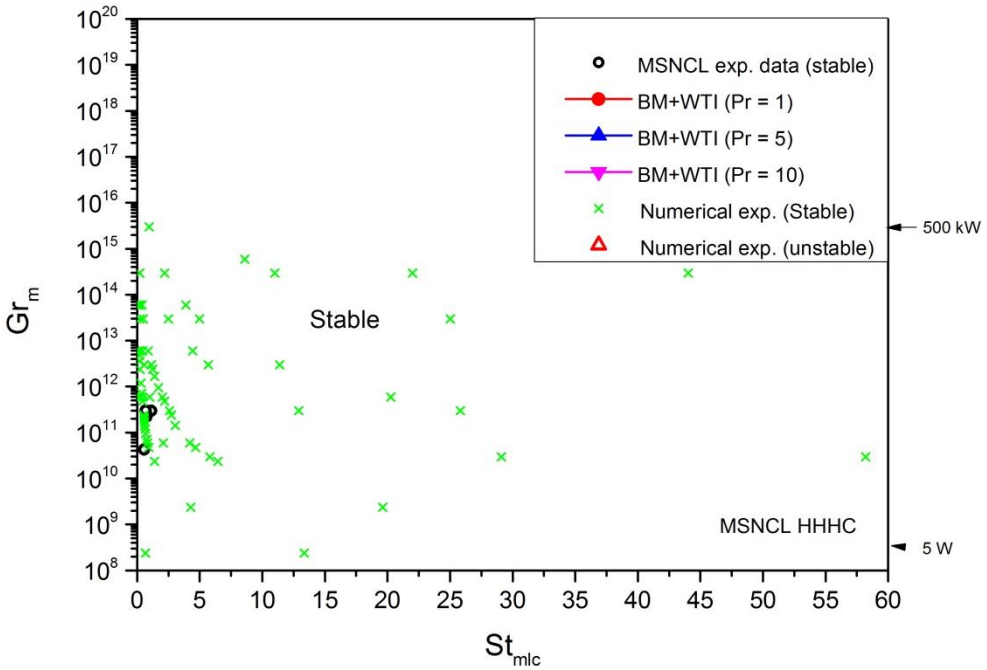

Fig. 7.10 Validation of LSA (model BM+WTI+HX) predictions for MSNCL with NLSA

In both the figs. 7.9 and 7.10 experimental data are also shown. Numerical simulations performed covering the major portion of the stability map for both NCLs have proved the accuracy of predictions of LSA, especially in case of NCL of Vijayan *et al.* [22] in which a distinct boundary between stable and unstable regions exists. To reconfirm the stable points obtained, further simulations have been performed by start up from rest, power rise and power step back transients. It is important since there is a possibility of conditional stability or hysteresis (path dependent stability) in NCLs as discussed by Vijayan *et al.* [13, 14]. As a conclusion, all the points which are denoted as 'stable' are unconditionally stable and all the points which are denoted as 'unstable' are conditionally or unconditionally unstable. It is to be noted once again at this juncture that LSA demarcates the stability by the same philosophy [13].

IHG/DH case

The predictions for stability behaviour of MSNCL have been done by LSA (model BM+WTI+HX) for the cases of 0% ($\Lambda_j = 0; j = hl, cl, c$), 5% ()$\Lambda_j = 0.05; j = hl, cl, c$ and 10% ($\Lambda_j = 0.10; j = hl, cl, c$) as discussed in section 6.__. It has been found that MSNCL is stable in all operating conditions in these cases. For validating these predictions, numerical simulations have been performed in this case for 10% ($\Lambda_j = 0.10; j = hl, cl, c$) IHG distributed in loop outside the heater portion of MSNCL in HHHC orientation. All thermo-physical properties have been taken the same as LSA. Simulation strategy to assess the stability has been same as mentioned for the SHF/LH case earlier. The observations are given in fig. 7.11.

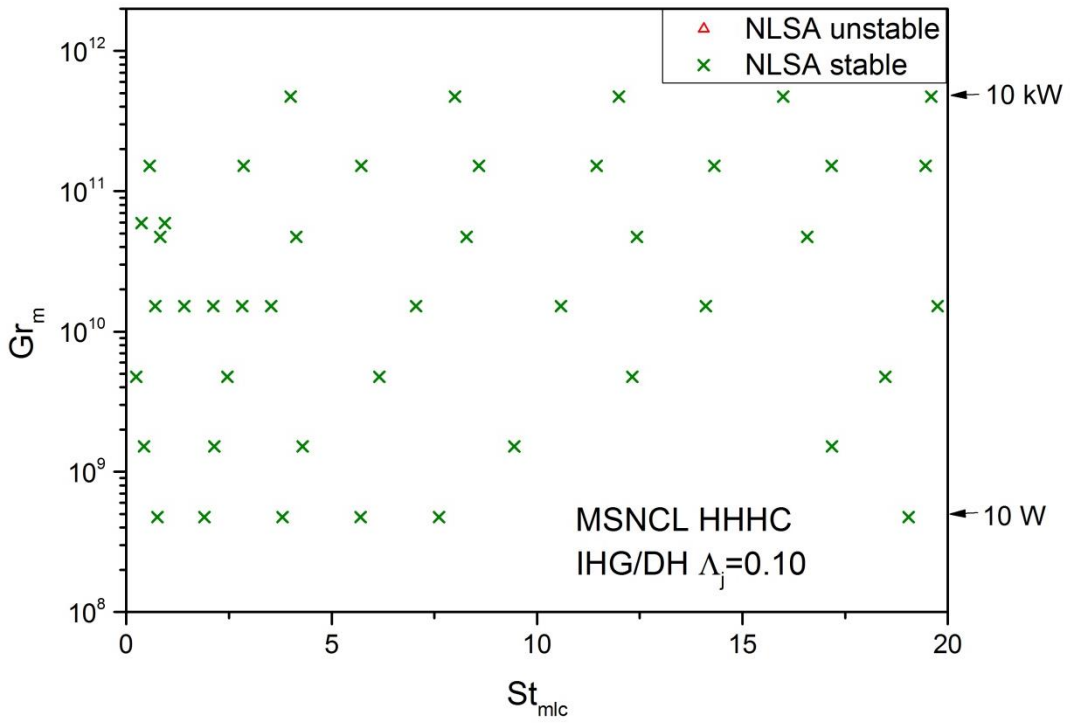

Fig. 7.11 Validation of LSA (model BM+WTI+HX) predictions for MSNCL in IHG/DH case $(\Lambda_j = 0.10; j = hl, cl, c)$ with NLSA

From the observations in figs. 7.9-7.11, it is evident that the linearization employed in LSA may not misinterpret the stability behaviour.

7.3. Code integration – SiPhN

All the three computer codes developed under this project are integrated and named as SiPhN (**Si**ngle **Ph**ase **N**atural circulation). The generic name is derived from the fact that all three kinds of analyses *viz.* steady state, transient and stability pertaining to single phase natural circulation loops can be performed by a set of these three codes for both SHF/LH and IHG/DH cases. A user interface has been created in SiPhN to facilitate the ease of giving inputs and getting outputs from the code. A provision for incorporating user defined friction factor correlations and internal heat transfer coefficient correlations has been given.

7.4. Concluding remarks

In this chapter, nonlinear (or transient) analysis formulation considering both SHF/LH and IHG/DH cases has been derived and implemented as computer code. Validating the code for steady state predictions against analytical results, it has been applied for a detailed investigation on wall thermal inertia effect. Later, it has been applied to validate the prediction of LSA obtained in chapter 5 and 6. Main conclusions are,

1. The instability in single phase natural circulation loops can be accurately explained by Welander's [11] warm pocket theory.

2. Piping wall can stabilize the NCL dynamic behaviour by absorbing the thermal anomalies those arise in the working fluid. A loop piping with good thermal conductivity and heat capacity is ideal for stabilization of loop dynamics.

3. Despite the approximations involved in linearization process, LSA can predict the stability behaviour with sufficient accuracy.

CHAPTER 8

Conclusions and Future Scope

8.1. Conclusions

In the current study, formulation and computer code development for linear and nonlinear stability analysis of molten salt based rectangular natural circulation loops have been pursued in the context of research and development program for IMSBR. It includes stability analysis of natural circulation loops in which working fluid is heated locally by surface heat flux (SHF/LH) or by distributed internal heat generation (IHG/DH).

Existing formulation for linear stability analysis for SHF/LH case has been improved to consider effect of wall, variable internal heat transfer coefficient, finite cooling rate on secondary side of cooler and heat losses (important for high temperature systems). A computer code has been developed based on this formulation and validated to be accurate in predictions with experimental observations from two water based NCLs and MSNCL.

Formulation for linear stability analysis for IHG/DH case has been developed and implemented in another computer code. All the phenomena considered for SHF/LH case have also been considered. Code has been validated with theoretical predictions published in literature and then applied to MSNCL with and without wall.

To confirm the accuracy of stability predictions obtained from LSA, which has some inherent approximations, a transient analysis code has been developed including all the phenomena considered in LSA and axial heat conduction in wall and working fluid too. It can simulate both SHF/LH and IHG/DH cases. Numerous simulations have been performed at various operating conditions to validate the stability boundary predicted by LSA for different cases. Further, simulations have been performed for NCL of Swapnalee and Vijayan [24] with

different thickness of wall to study the phenomena of stabilization induced by wall heat capacity.

The main conclusions derived from current work are:

1. The balance between buoyancy and frictional force in NCLs can be made stable by increasing the effectiveness of cooling to a minimum required value (achieving this minimum cooling rate may or may not be practically feasible for a given loop at given operating conditions)

2. The local pressure drops (e.g. pressure drop at elbows, orifices etc.) can stabilize the dynamics of NCL in laminar as well as turbulent regime. However, when analysis has been done without considering wall effect, destabilization of NCL has been observed at Reynolds numbers higher than ~10^6 – 10^7 (Corresponds to Gr_m of ~10^{18}) for both MSNCL and the loop of Vijayan *et al.* [22].

3. The variation of internal heat transfer coefficient with flow rate of working fluid induces a stabilization effect on NCL dynamics. This helps in reducing the minimum cooling rate required for stabilization (as mentioned in point 1), especially in turbulent flow regime.

4. The heat exchange between working fluid and piping material reduces the magnitude of thermal anomalies arise in the working fluid due to various reasons. The higher the heat capacity of piping the better the stabilization of NCL dynamics. It can be possible to stabilize an NCL at a given operating condition by employing suitable thickness of piping with high heat capacity. A sufficient thermal conductivity is also required to utilize the total thickness of the piping in effective absorption of thermal anomaly.

5. As far as there is no heating outside the heater portion, the stability of NCL is not affected by the mode of heating of working fluid (surface heat flux or internal heat generation).

6. The stability of NCL with HHHC orientation of heater and cooler reduces with increased uniform internal heat generation outside the heater region.

7. Representation of stability maps in Gr_m-St_{moc} (represents power input and secondary side heat transfer coefficient) is proposed based on the philosophy of representing only the feasible operating conditions on stability map. It is thought to be more realistic and intuitive in used compared to the parameter spaces employed so far in literature (Gr_m-St_m or Re-St_m).

8. Consideration of local pressure losses, variable internal heat transfer phenomena and wall effect in stability analysis leads to a more accurate stability map compared to the highly conservative predictions obtained from the models which do not consider these phenomena.

8.2. Future scope

1. Application of linear stability analysis models to other molten salt based natural circulation loops and for other type of coolants like water and liquid metals.

2. Experiments for the case of distributed internal heat generation to validate the predictions of stability analysis models presented in current work.

3. Coupling of thermal hydraulics with neutronics, to consider neutronic feedback in both SHF/LH and IHG/DH cases.

4. Improving NLSA code to simulate the start-up conditions of natural circulation loops.

5. Performing 3D CFD analysis for detailed study of stability behaviour of NCLs.

6. Extending the improved LSA model, based on homogeneous equilibrium model, to two phase flow natural circulation loops.

7. Extending the model to study instabilities like parallel channel instability relevant to reactor conditions.

REFERENCES

1. Vijayan P. K., Shivakumar V., Basu S., Sinha R.K., 2017, Role of thorium in the Indian nuclear power programme, Progress in Nuclear Energy 101, 43-52.
2. Dulera, I.V., Vijayan, P.K., Sinha, R.K., 2013, Indian Programme on Molten Salt Cooled Nuclear Reactor, Conference on Molten Salts in Nuclear Technology, 9-11 January, 2013, Bhabha Atomic Research Centre, Mumbai.
3. Vijayan P.K., Basak A., Dulera I.V., Vaze K.K., Basu S., Sinha R.K., 2015 Conceptual design of Indian molten salt breeder reactor. Pramana 85, 539-554.
4. Rakesh Chouhan, Borgohain A., Shrivastava A.K., Maheshwari N.K. and Vijayan P.K., 2015, CFD analysis of molten fluoride salt natural circulation in a rectangular loop, Thorium Energy Conference (ThEC15), October 12-15, 2015, Mumbai, India.
5. Srivastava A.K., Kudariyawar J.Y., Borgohain A., Jana S.S, Maheshwari N.K., Vijayan P.K., 2016, Experimental and theoretical studies on the natural circulation behaviour of molten salt loop, Applied Thermal Engineering 98, 513–521.
6. Gorman M., Widmann P.J., Robbins K.A., 1986, Nonlinear dynamics of a convection loop: a quantitative comparison of experiment with theory, Physica 19d, 255-267.
7. Churchill, S.W., 1977, "Friction-factor equation spans all fluid-flow regimes." Chemical engineering 84(24), 91-92.
8. Don W. Green, Robert H. Perry, Perry’s Chemical Engineers’ handbook, 8 Ed, McGraw-Hill.
9. Welander Pierre, 1965, Steady and oscillatory motions of a differentially heated fluid loop, Technical report, Woods Hole Oceanographic Institute, Woods Hole, Mass.
10. Keller Joseph B., 1966, Periodic oscillations in a model of thermal convection, Journal of Fluid Mechanics 26 (3), 599-606.

11. Welander Pierre, 1967, On the oscillatory instability of a differentially heated fluid loop, Journal of Fluid Mechanics 29(1), 17-30.
12. Creveling H. F., De Paz J. F., Baladi J. Y. and Schoenhals R. J., 1975, Stability characteristics of a single-phase free convection loop, Journal of Fluid Mechanics 67(1), 65-84.
13. Vijayan P.K. and Date A.W., 1992, The limits of conditional stability for single-phase natural circulation with throughflow in a figure-of-eight loop, Nuclear Engineering and Design 136, 361-380.
14. Vijayan P.K., Austregesilo H., 1994, Scaling laws for single-phase natural circulation loops, Nuclear Engineering and Design 152, 331-347.
15. Vijayan P.K., Austregesilo H., Teschendorff V., 1995, Simulation of the unstable oscillatory behaviour of single-phase natural circulation with repetitive flow reversals in a rectangular loop using the computer code ATHLET, Nuclear Engineering and Design 155, 623 641.
16. Misale Mario and Frogheri Monica, 1999, Influence of pressure drops on the behaviour of a single-phase natural circulation loop: preliminary results, International Communications in Heat and Mass Transfer 26 (5), 597-606.
17. Misale M., Ruffino P. and Frogheri M., 2000, The influence of the wall thermal capacity and axial conduction over a single-phase natural circulation loop: 2D numerical study, Heat and mass transfer 36, 533-539.
18. Misale M. and Frogheri M., 2001, Stabilization of a single phase natural circulation loop by pressure drops, Experimental Thermal and Fluid science 25, 277-282.
19. Vijayan P.K., 2002, Experimental observations on the general trends of the steady state and stability behaviour of single-phase natural circulation loops, Nuclear engineering and design 215, 139-152.

20. Jiang Y.Y. and Shoji M., 2003, Flow stability in a natural circulation loop: influences of wall thermal conductivity, Nuclear Engineering and Design 222, 16–28.
21. Misale Mario, Devia Francesco, and Garibaldi Pietro, 2005, Some considerations on the interaction between the fluid and wall tube during experiments in a single-phase natural circulation loops, Proceedings of the 3rd IASME/WSEAS International Conference on heat transfer, August 20-22, 2005, Thermal engineering and environment, Corfu, Greece, 128-133.
22. Vijayan P. K., Sharma M. and Saha D., 2007, Steady state and stability characteristics of single-phase natural circulation in a rectangular loop with different heater and cooler orientations, Experimental Thermal and Fluid Science 31, 925–945.
23. Misale M., Garibaldia P., Tarozzib L. and Barozzib G.S., 2011, Influence of thermal boundary conditions on the dynamic behaviour of a rectangular single-phase natural circulation loop, International Journal of Heat and Fluid Flow 32(2), 413-423.
24. Swapnalee B.T., Vijayan P.K., 2011, A generalized flow equation for single phase natural circulation loops obeying multiple friction laws, International Journal of Heat and Mass Transfer 54, 2618–2629.
25. Muralidhara Rao Nakka, Komal Pawar and Pradip Kshirsagar, 2013, The Influence of Core Capacitance on the Dynamic Performance of a Single-Phase Natural Circulation Loop With End Heat Exchangers, Heat Transfer Engineering 34(4), 323-337.
26. Kudariyawar J.Y., Vaidya A.M., Maheshwari N.K., Satyamurthy P., 2016, Computational study of instabilities in a rectangular natural circulation loop using 3D CFD simulation, International Journal of Thermal Sciences 101,193-206.
27. Ruiz D. E, Cammi A., Luzzi L., 2015, Dynamic stability of natural circulation loops for single phase fluids with internal heat generation, Chemical Engineering Science 126, 573–583.

28. Pini A., Cammi A., Luzzi L, 2016, Analytical and numerical investigation of the heat exchange effect on the dynamic behaviour of natural circulation with internally heated fluids, Chemical Engineering Science 145, 108–125.
29. Incropera F., De Witt D., Bergam T., Lavine A., 2011, Fundamentals of Heat and Mass Transfer, John Wiley & Sons, Inc., 111 River Street, Hoboken, NJ, United States.
30. Cammi A., Luzzi L., Pini A., 2016, The influence of the wall thermal inertia over a single –phase natural convection loop with internally heated fluids, Chemical Engineering Science 153, 411–433.
31. Luzzi L., Misale M., Devia F., Pini A., Cauzzi M.T., Fanale F. and Cammi A., 2017, Assessment of analytical and numerical models on experimental data for the study of single-phase natural circulation dynamics in a vertical loop, Chemical Engineering Science 162, 262–283.
32. Ogata Katsuhiko, 2010, Modern Control Engineering, 5 Ed, Pearson Publications.
33. Zhangpeng Guo, Jianjun Zhou, Dalin Zhang, Khurrum Saleem, Chaudri, Wenxi Tian, Guanghui Su and Suizheng Qiu, 2013, Coupled neutronics/thermal-hydraulics for analysis of molten salt reactor Nuclear Engineering and Design 258, 144–156.
34. Patankar Suhas V., 2014, Numerical heat transfer and fluid flow, Taylor & Francis.